The Role of Micellar Nanowires in Diagnosing Tropical Diseases

Hubbe, H.M.K.

Important note
To cite this publication, please use the final published version (if applicable).
Please check the document version above.
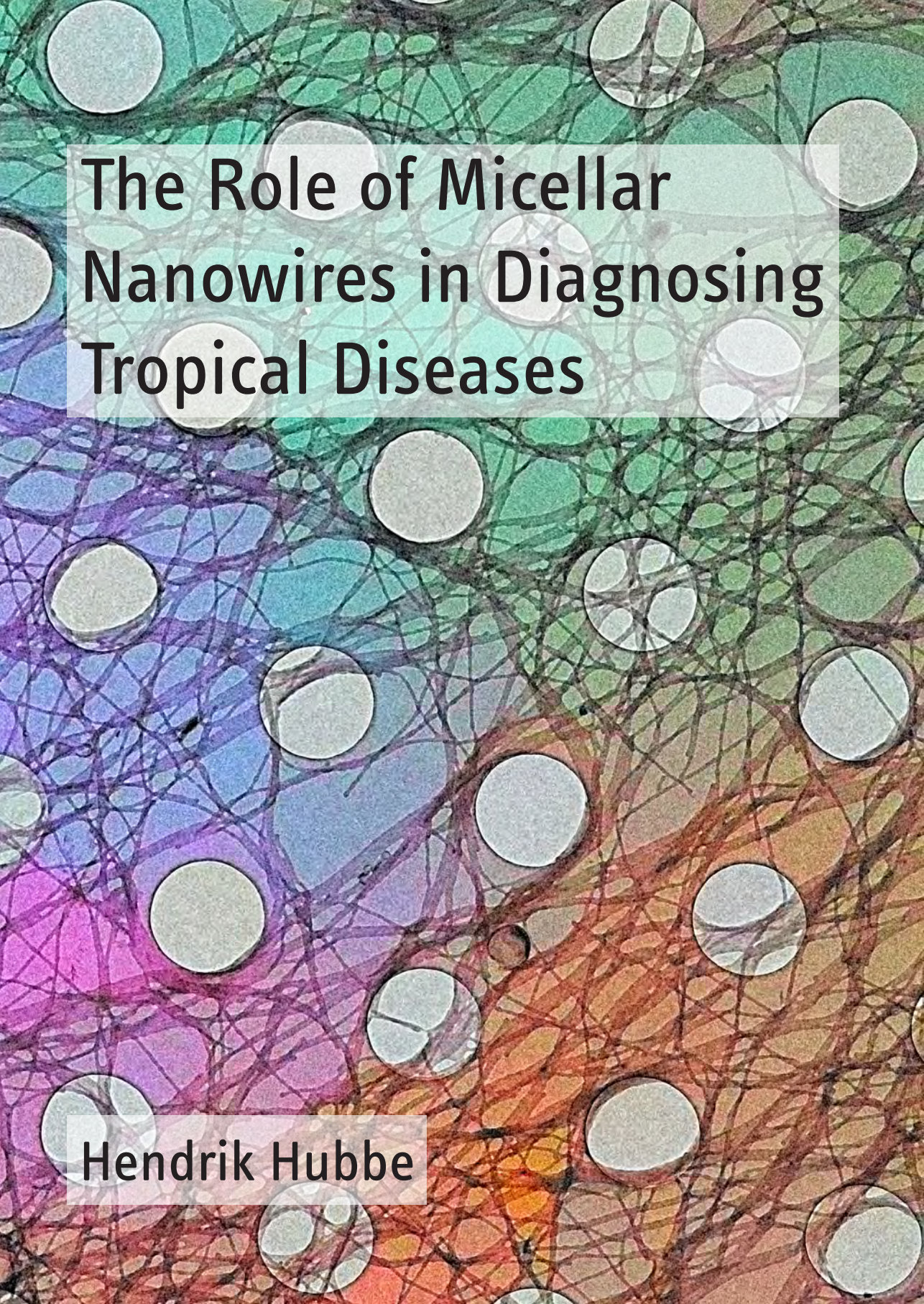
The Role of Micellar Nanowires in Diagnosing Tropical Diseases

Hendrik Hubbe

THE ROLE OF MICELLAR NANOWIRES IN DIAGNOSING TROPICAL DISEASES

THE ROLE OF MICELLAR NANOWIRES IN DIAGNOSING TROPICAL DISEASES

Proefschrift

ter verkrijging van de graad van doctor
aan de Technische Universiteit Delft,
op gezag van de Rector Magnificus prof. dr. ir. T.H.J.J. van der Hagen,
voorzitter van het College voor Promoties,
in het openbaar te verdedigen op *vrijdag, 6 oktober 2023 om 12:30 uur*

door

Hendrik Marc Konstantin HUBBE

Master of Science in Microsystems Engineering,
Albert-Ludwigs-Universität, Freiburg, Duitsland,
geboren te Konstanz, Duitsland.

Dit proefschrift is goedgekeurd door de promotoren.

Samenstelling promotiecommissie:

Rector Magnificus	voorzitter
Dr. habil. E. Mendes	Technische Universiteit Delft, promotor
Dr. P. E. Boukany	Technische Universiteit Delft, promotor
Prof. dr. U. Staufer	Technische Universiteit Delft, promotor

Onafhankelijke leden:

Prof. dr. R. Luttge	Technische Universiteit Eindhoven
Prof. dr.ir. A.G. Denkova	Technische Universiteit Delft
Prof. dr. P.G. Steeneken	Technische Universiteit Delft
Prof. dr. C. Marques	École Normale Supérieure de Lyon, Frankrijk
Prof. dr.ir. S.J. Picken	Technische Universiteit Delft

Cover:	Colorized transmission electron microscopy picture of self-assembled polymeric micellar nanowires on a carbon film support grid.

An electronic version of this dissertation is available at
http://repository.tudelft.nl/.

Wissen und nichts tun ist wie nichts wissen.
Weten en niets doen is als niets weten.
Possessing knowledge without acting on it, is like not knowing at all.

Dalai Lama

CONTENTS

SUMMARY

The tropical mosquito-transferred virus diseases Dengue, Zika and Chikungunya are causing hundreds of millions infections worldwide every year. Their occurrences are often linked, also due to their common transfer vector – the mosquito – thus they are of interest as a group together. Areas of prevalence include vast rural areas of low to middle income countries such as Indonesia, often with sub-optimal access to medical facilities. An affordable, reliable and easy-to-use point-of-care test would assist monitoring outbreaks, allowing earlier countermeasures such as mosquito extermination or setup of temporary on-site medical aid, as well as help allowing timely treatment in the often far-away hospitals.

However, while laboratory testing is very advanced, it is often not available where needed. And devices which are point-of-need capable, do not exhibit a very good specificity and sensitivity so far. Thus new methods of detection are desirable and nanowires represent a promising approach. Polymeric nanowires are especially interesting, due to the vast number of available modifications and the flexibility that organic chemistry offers. The first chapter of this thesis provides an overview of the situation in Indonesia taken as a case study, the viral diseases in question and a literature review of detection methods, polymeric nanowires and detection strategies.

Self-assembled micellar polymeric nanowires were chosen as basis for a new detection method. Chapter 2 describes the development of a multifunctional micellar nanowire, as a platform of a flexible nanowire based assay. They can be stretched and contact printed using microstructured PDMS stamps, creating arrays of well-localized nanowires in a simple dewetting step. Chemical bifunctionality is a minimum requirement, such that fixation of the nanowires on a substrate and fixation of binding moieties specific to pathogens can occur. The result is a modular design, allowing easy mix of constituents and expansion to other functionalities. The choice of azide as functional endgroups on the polymer is shown not to interfere with micellar self-assembly, and allows use of the well-established click-chemistry. The binding sites availability on self-assembled nanowires is demonstrated with the use of fluorophores and both classic CuAAC reactions between azide and alkyne as well as copper-free spAAC reaction of azide and dibenzo-cyclooctyne. Further successful functionalization using biotin and streptavidin is also described, allowing for binding of $2\,\mu m$ diameter microbeads.

In chapter 3 the testing of the novel bifunctional nanowires was extended to larger biologically relevant entities: giant unilamellar vesicles were used to model eukaryotic cells, but proved to be too instable for reliable binding, at least when a typical washing procedure was used. Binding could be observed in some cases, however quantified analysis of this behaviour proved too difficult, owing to the large size and inherent instability of non-reinforced giant unilamellar vesicles (GUVs). In contrast, when a bacteriophage as a model virus was used, binding to self-assembled nanowires was successful, the limits of which are described in chapter 3.

The fourth chapter exhibits and discusses micromanufacturing strategies used in creating microstructures for the dewetting technique and other applications in cooperation research projects.

In conclusion, this work presents results on new technical approaches of diagnostics using versatile, self-assembled polymeric nanowires for an important group of tropical diseases. Such novel approach to pathogen detection using multifunctional micellar nanowire assemblies is described in detail. The developed nanowires can be used as a modular system with a variety of different linker groups. Such modularity makes this system very flexible and in combination with simple contact printing, a versatile platform for many applications in diagnostics and biology in general is provided.

SAMENVATTING

De tropische door muggen overgedragen virusziekten Dengue, Zika en Chikungunya veroorzaken jaarlijks wereldwijd honderden miljoenen infecties. Hun voorkomen hangt vaak samen, mede door hun gemeenschappelijke overbrengingsvector – de mug – zodat zij als groep samen van belang zijn. Tot de prevalentiegebieden behoren uitgestrekte plattelandsgebieden in landen met een laag tot gemiddeld inkomen, zoals Indonesië, waar de toegang tot medische voorzieningen vaak niet optimaal is. Een betaalbare, betrouwbare en gemakkelijk te gebruiken point-of-care test zou helpen bij het monitoren van uitbraken, waardoor eerder tegenmaatregelen genomen kunnen worden zoals het verdelgen van muggen of het opzetten van tijdelijke medische hulp ter plaatse, en een tijdige behandeling in de vaak verafgelegen ziekenhuizen mogelijk wordt.

Maar hoewel laboratoriumtests zeer geavanceerd zijn, zijn ze vaak niet beschikbaar waar ze nodig zijn. En apparaten die op de plaats van bestemming kunnen worden gebruikt, zijn niet erg specifiek en gevoelig. Nieuwe detectiemethoden zijn dus wenselijk en nanodraden vormen een veelbelovende benadering. Vooral polymere nanodraden zijn interessant vanwege het grote aantal beschikbare modificaties en de flexibiliteit die de organische chemie biedt. Het eerste hoofdstuk geeft een overzicht van de situatie in Indonesië, de betrokken virusziekten en een literatuuroverzicht van detectiemethoden, polymere nanodraden en detectiestrategieën.

Micellaire polymere nanodraden werden gekozen als basis voor een nieuwe detectiemethode en hoofdstuk 2 beschrijft de ontwikkeling van een multifunctionele micellaire nanodraad, waarmee een assay op basis van nanodraden kan worden gemaakt. Ze kunnen worden uitgerekt en met behulp van microgestructureerde PDMS-stempels worden bedrukt, waardoor arrays van goed gelokaliseerde nanodraden ontstaan in een eenvoudige ontwateringsstap. Bifunctionaliteit is een minimum, zodat zowel fixatie van de nanodraden op een substraat als fixatie van bindingsmoleculen specifiek voor het pathogeen kan plaatsvinden. Het resultaat is een modulair ontwerp, waardoor de bestanddelen gemakkelijk kunnen worden gemengd en uitgebreid naar andere functionaliteiten. De keuze van azide als functionele eindgroep op het polymeer verstoort de micellaire zelfassemblage niet, en maakt gebruik van de beproefde click-chemie mogelijk. De beschikbaarheid van bindingsplaatsen wordt aangetoond met behulp van fluoroforen en zowel klassieke CuAAC-reacties tussen azide en alkyne als koperloze spAAC-reactie van azide en dibenzocyclooctyne. Verdere succesvolle functionalisering met biotine en streptavidine wordt beschreven, waardoor binding van microkorrels met een diameter van ongeveer 2 micrometer mogelijk wordt.

In hoofdstuk 3 werd het testen van de nieuwe bifunctionele nanodraden uitgebreid tot grotere biologisch relevante entiteiten: giant unilamellar vesicles werden gebruikt om eukaryote cellen te modelleren, maar bleken te instabiel voor betrouwbare binding, althans met behulp van een wasstap. Binding kon in sommige gevallen worden waargenomen, maar analyse van dit gedrag bleek te moeilijk, vanwege de grote omvang en

de inherente instabiliteit van niet-versterkte GUVs. Daarentegen waren de tests met een bacteriofaag als modelvirus succesvol, het systeem bleek levensvatbaar voor het gebruik van bacteriofagen. Het leek waarschijnlijk dat virale deeltjes kunnen worden gevangen op de nanodraden, maar het was onbekend of er sprake is van onspecifieke binding aan de micellaire draad.

Het vierde hoofdstuk toont en bespreekt microfabricagestrategieën die worden gebruikt bij het maken van microstructuren voor de ontwateringstechniek en andere toepassingen in partnerprojecten.

Concluderend kan worden gesteld dat in dit werk onderzoek is verricht naar belangrijke tropische koortsziekten en technische benaderingen van de diagnostiek. Er wordt een nieuwe aanpak beschreven voor de detectie van pathogenen met behulp van multifunctionele micellaire nanodraden. De voorgestelde nanodraden kunnen worden gebruikt als een modulair systeem met verschillende linkergroepen. De modulariteit maakt dit systeem zeer flexibel en in combinatie met eenvoudige contactafdrukken een veelzijdig platform voor vele toepassingen in de diagnostiek en de biologie in het algemeen.

PREFACE

With this thesis I present my work on "The role of micellar nanowires in diagnosing tropical diseases". My work aims to contribute to advancements in global point-of-care diagnostics outside of a clinical setting. Several research questions arise from this motivation and are presented in the following chapters.

The basic question of this research was, if polymeric nanowires can provide diagnostic support for tropical virus fevers. **Chapter 1** introduces into this complex thematic. The focus of the project was Indonesia, a middle- to low-income country with vast rural areas. Three major viral diseases – Dengue, Zika and Chikungunya – transmitted by the same mosquitoes were identified as relevant research objects, due to their pervasiveness, linked occurrence and the possible severe symptoms. Field research was conducted, which showed a need for a more reliable and affordable quick test. Virus biology, established detection methods and state-of-the-art of polymeric nanowires were reviewed.

Choosing polymeric micellar nanowires as a focus of this research, more detailed questions were tackled in **chapter 2.** How can micellar nanowires be integrated in biological assays? To capture biomolecules, they needed to be functionalized. A suitable biochemical linker had to be identified, advantageously a widely-used biochemical linker to be compatible with established commercial products e.g. antibodies. Functionality with click chemistry and biotin-streptavidin interaction were evaluated using fluorescent molecules and functionalized microbeads. With streptavidin, a first protein could also be tested using this assembly.

Biological components are complex. To further test compatibility with biorelevant entities, **chapter 3** looked into capture of viral particles and large cell-like objects. To provide proof-of-concept for virus detection, a bacteriophage model virus was used. The nanowires were able to capture these viral particles. Additionally, giant unilamellar vesicles were employed to research the nanowire's ability to capture cells.

Microfabrication was an important aspect of this work and the projects of collaborating partners. Different techniques were tested and summarized in **chapter 4:** How do common microfabrication tools compare in perspective of microtopography and microfluidic manufacturing in the biomedical field? The one dimensional character of the wires was utilized by stretching, aligning and printing them using microgrid dewetting techniques described in literature. New approaches to the creation of these micro structures were taken and synergies were achieved, supporting partner projects and collaborating on interesting additional applications benefiting from the structures developed. A comparison is made, also regarding user-friendliness and effort.

Hendrik Hubbe
Delft, August 31, 2023

LIST OF ACRONYMS AND ABBREVIATIONS

2PP	two photon polymerization
AAGB	alternating amphiphilic glycopolypeptide brushes
ADE	antibody/dependant enhancement
Az	azide
BSA	bovine serum albumin
BSL-1	biosafety level 1
CAD	computer-aided design
CDE	chemical dry etching
cDNA	complementary deoxynucleic acid
CHIKV	Chikungunya virus, family of *Togaviridae*
CNC	computer numerical control
CNT	carbon nanotube
CTC	circulating tumor cell
CuAAC	copper(I)-catalyzed Azide-Alkyne Cycloaddition
DBCO	dibenzocyclooctyne
DENV	Dengue virus
DiI	1,1'-dioctadecyl-3,3,3',3'-tetramethylindocarbocyanine perchlorate
DiLL	dip-in laser lithography
DMF	dimethylformamide
DNA	deoxynucleic acid
DOPC	1,2-dioleoyl-sn-glycero-3-phospholine
DRIE	deep reactive ion etching
E. coli	*Escherichia coli*
EDC	1-ethyl-3- (-3-dimethylaminopropyl) carbodiimide hydrochloride
ELISA	enzyme-linked immunosorbent assay
EpCAM	epithelial cell adhesion and activating molecule
FITC	fluorescein isothiocyanate
FT-IR	fourier-transform infrared spectroscopy
GUV	giant unilamellar vesicle
HMBC	heteronuclear multiple bond correlation
HRP	horseradish peroxidase
ICP	inductively coupled plasma
IgA	immunoglobulin A
IgG	immunoglobulin G
IgM	immunoglobulin M
IPA	isopropanol

LAP	lithium phenyl-2,5,6 trimethyl benzoyl phosphite
LIP	laser interference patterning
MA	methacrylate
MEMS	microelectromechanical systems
MIBK	methyl isobutyl ketone
NHS	N-hydroxysuccinimidyl
NMR	nuclear magnetic resonance
NS1	non-structural protein NS1 of Dengue virus
PANI	polyaniline
PBS	phosphate-buffered saline
PDMS	polydimethylsiloxane
PECVD	plasma-enhanced chemical vapor deposition
PEDOT	poly(3,4-ethylenedioxythiophene)
PEG	polyethylene glycol
PEO	polyethylene oxide
PFU	plaque-forming unit
PLA	polylactic acid
PMMA	poly(methyl methaacrylate)
PPy	polypyrrole
PS-PSMA	polystyrene-poly(styrene-co-maleic anhydride)
PS-b-PEO	polystyrene-polyethylene oxide block-copolymer
PSS	polystyrene sulfonate
PTFE	polytetrafluoroethylene
PRNT	plaque reduction neutralization test
PVF	polyvinyl formal
RIE	reactive ion etching
RNA	ribonucleic acid
RT-LAMP	reverse transcriptase loop-mediated isothermal amplification
RT-PCR	real-time polymerase chain reaction
SCCM	standard cubic centimetres per minute
SEM	scanning electron microscope
spAAC	strain promoted alkyne azide cycloaddition
SU-8	bisphenol A novolac epoxy based negative photoresist
TBA	anti-thrombin aptamer
TEM	transmission electron microscopy
THF	tetrahydrofuran
UV	ultraviolet
YFP	yellow fluorescent protein
ZIKV	Zika virus

1

INTRODUCTION

Human interaction is not just a lack of able machinery,

but a fundamental part of sane diagnostics.

1

This chapter provides background to the different fields and techniques involved in this work. Disease situation in the field is reviewed and the state-of-the-art point-of-care testing. The project evolved on the basis of tropical fever diagnostic (Dengue, Zika, Chikungunya), motivated by the current situation in Indonesia, approaching the question of most adequate support for healthcare from technological side.

Polymer nanowires were chosen for research of a better platform for detecting pathogens. More specifically, micellar nanowires, as they bring both the one dimensional feature of a wire and the process of self-assembly from mixed monomers, allowing for interesting possibilities in wire composition and functionality.

1.1. DENGUE, ZIKA, CHIKUNGUNYA: SITUATION IN INDONESIA 2018

Indonesia is a low to middle income country and in many rural areas, the access to healthcare is limited. The number of Dengue cases each year is in the 100 000, with a large number of suspected unreported cases [3]. Chikungunya is considered endemic, and there have been reports of confirmed Zika cases. Diagnosis is often only done through classical anamnesis, as the available biochemical virus tests are not affordable for many. A blood platelet count is often preferred. It is cheaper and offers the doctor insight into the condition of the patient. But it can not indicate a Dengue infection at an early stage and is additionally often not interpretable by the midwifes and nurses, that usually provide the only accessible local medical aid in rural parts of the country. Also it does not help the differential diagnosis, which is still considered a big challenge, especially for *Flaviviruses* such as Dengue virus (DENV) and Zika virus (ZIKV) [4]. The field study in 2017 showed the need for an affordable diagnostic tool. Especially the small nurseries in rural areas, remote and of lower income, would benefit from an early diagnostic. Personnel is often not qualified to perform a clinical diagnosis. Uncertainties in severe fever cases are life-threatening, as transport to intensive care units in cities takes much time and the progression of the fever can be very fast. Interest was also shown by health officials. The health care system as a whole would benefit. More frequent testing would enable monitoring of outbreaks and coordination of counter measures e.g. against the mosquito population. A thorough monitoring would help to follow-up on the recent occurrence of ZIKV in Indonesia, which is mostly neglected by conventional anamnesis.

1.2. VIRUS BIOLOGY AND PATHOGENESIS

In this section, the biology of the target viruses and the pathogenesis of the connected diseases are summarized. All Zika, Dengue and Chikungunya are caused by viruses, that

belong to the artificial group of arboviruses, an acronym for arthropod-born viruses [5]. From the large group of arboviruses, the medically most relevant stem from the families *Togaviridae, Flaviviridae* and *Bunyaviridae* [6].

All three viruses are single-stranded, positive sense ribonucleic acid (RNA) viruses, (+)ssRNA. While Chikungunya virus, family of *Togaviridae* (CHIKV) belongs to the family of *Togaviridae*, DENV and ZIKV belong to the same family of *Flaviviridae*, as Yellow fever virus (lat. flavus "yellow") and West Nile virus. The similarity of DENV and ZIKV lead to frequent cross-reactivities of antibody assays in diagnostics, as to be discussed in the following chapter. They are of similar size with roughly 50 nm – 70 nm diameter. [7]

All three viruses are mainly transferred by mosquitoes of the *Aedes* family, *Ae. aegypti* and *Ae. albopictus* in particular. The mosquitoes are highly adapted to urban areas: small stagnant waters are sufficient as a breeding ground for larvae, the adult insect (imago) is day-active and also bites during day time, feeding mostly on humans. For flaviviruses, transmission from mosquito to egg is possible. Viremiae in humans are high enough for a transfer human-arthropod-human without the need for an intermediate non-human host [8, 9].

The case numbers are high. Dengue was reported to show 390 mill. infections per annum worldwide [10]. ZIKV infection numbers of the recent outbreak in the Americas 2015 are suspected to have been as high as 1.3 mill. [11, 12]. Chikungunya also showed 1.1 mill. reported cases 2014 in the Americas alone [13].

The joint occurrence of the viruses in countries worldwide (see Figure 1.1), creates additional complication through contemporaneous multiple virus infections and it shows the importance of addressing these diseases in a combined monitoring and diagnostic tool [14, p.493].

This consideration is backed by Bisanzio et al. [16], who showed a strong spatio-temporal coherence of Dengue, ZIKV and CHIKV in Merida, Mexico. And if the survival of the mosquito as the principal vector is possible, there is a risk of these diseases spreading
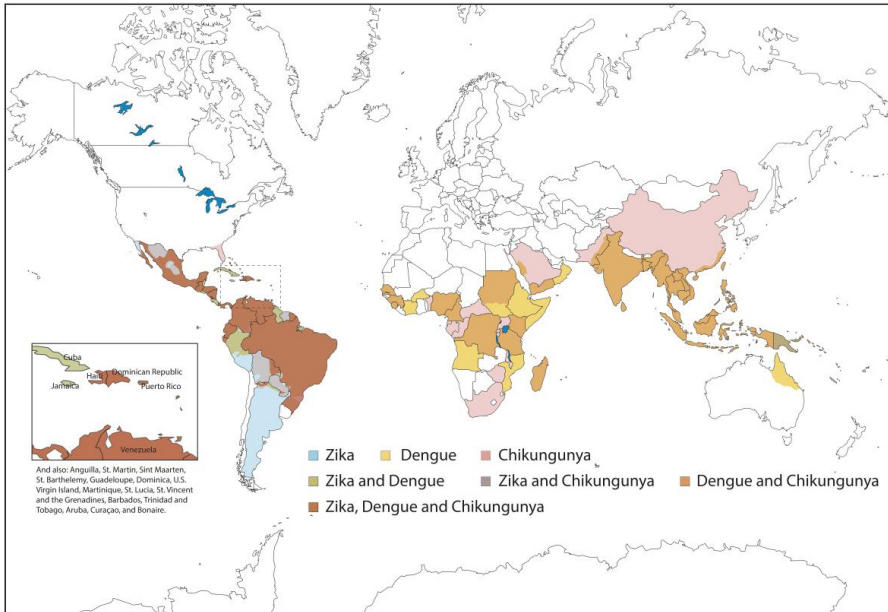
Figure 1.1: Worldwide distribution of Dengue, Zika and Chikungunya (figure by Patterson et al. [15] licensed under CC BY 4.0)

into a new area [17, 18]. Transmission occurs between 18 °C – 34 °C for all three viruses, as shown by models and human case data. A peak of transmission is found around 26 °C – 29 °C [19]. A manifestation of this risk has recently been observed in European countries, with outbreaks of Dengue and Chikungunya in mainland France, Italy, Croatia and Madeira [20]. West Nile virus – also a flavivirus transmitted by mosquitoes – is now frequently detected in birds, horses and humans in south/south-east Europe with massive outbreaks in 2018 since its first occurrence in Hungary 2004 [21]. As shown in Figure 1.2, *Aedes albopictus* have also been detected in parts of the Netherlands, most likely having arrived in bamboo imports from China [22].

Clinical presentation: Most cases are suspected to stay undetected, as asymptomatic progression is very common (DENV 75 %, ZIKV 80 %, CHIKV up to 28 %). The signs and symptoms of the diseases are very alike, including fever, rash, itch, severe muscle aches, headache or vomiting, and thus not very specific even compared to further possible

1
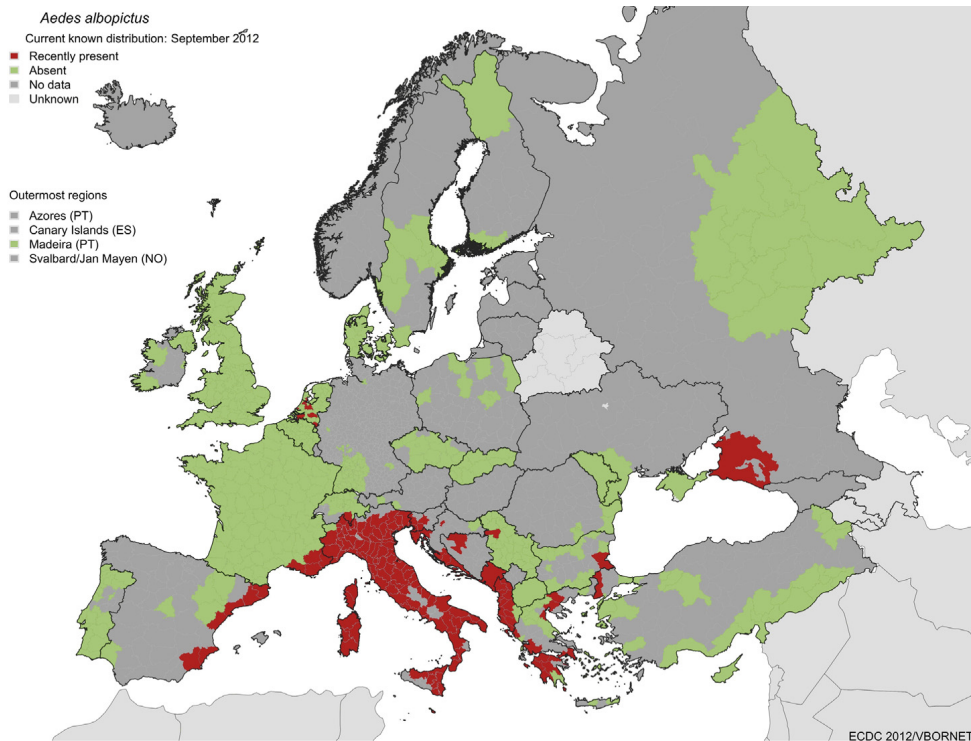
Figure 1.2: Distribution of *Aedes albopictus* mosquito in Europe as of September 2012. Red areas have recently shown presence, green confirmed absence (figure reprinted from Tomasello et al. [20], copyright (2013), with permission from Elsevier)

infections (e.g. measles, malaria, leptospriosis, adenovirus, other leviviruses) or conditions (postinfectious arthritis, rheumatologic conditions). Diagnosis under optimal conditions thus usually includes an assessment of all symptoms together with a travel history. Subsequent laboratory testing of serum is used to confirm the clinical diagnosis. However, the respective incubation times have to be taken into account. It is important, to keep in mind the possibility of multiple contemporaneous infections and to always view laboratory-analyzed findings under consideration of the specific context. [13, 23–26]

For Chikungunya, the incubation period is usually 3 – 7 days. Patients can develop sudden and high fever, and severe, often debilitating joint pain.[1] Further serious complications have been reported, but rarely. Fatalities are also seldom. Literature shows

---

[1]Chikungunya translates as "that which bends up" in the Makonde language

varying percentages (5 % – 80 %) of patients with persistent joint pain that can last months or even years. A transmission to the fetus by the infected mother is very rare, but infection can occur during birth (intrapartum) and result in neurological symptoms among other things. [13]

In the case of Zika, incubation period is suspected to be between 3 – 14 days. Most commonly patients develop a rash, itch, prostration (extreme exhaustion) and muscle pain. Fever is usually reported low and short, but high fever occurred in some cases. Fatalities are seldom, but there are reports of fetal losses and microcephaly, of which ZIKV infections of the pregnant women are meanwhile accepted as causation [11, 12, 27]. A study in 2019 with 219 children born after a ZIKV infection of the mother during pregnancy showed ~70 % of children exhibit a normal neurological development [28]. A unique problem with ZIKV in this group of viruses is the reported sexual transmission due to high concentrations of viral particles in semen, even two weeks after the onset of symptoms and potentially even longer [27, 29].

Dengue incubation is stated with 5 – 7 days, with most common symptoms being rash, muscle pain, headaches and fever. 5 % of patients develop severe Dengue, resulting in internal bleeding and dangerously low blood pressure [25]. This special complication is usually connected to a secondary DENV infection and explained with the antibody/dependant enhancement (ADE) of infection: Four subtypes of DENV are known and the body develops antibodies against the first DENV subtype it is infected with. If the secondary infection occurs with a different subtype, the antibodies bind to these viruses, but without deactivating the virus, as the fit is not perfect. The marked but active virus-antibody complexes are then taken up by immune cells, resulting in a high number of infected cells producing large numbers of viral particles [30]. The World Health Organization explicitly emphasizes the importance of monitoring in case of Dengue for early curtailing of the transmission vector and the early diagnosis for appropriate patient management to reduce deaths in severe cases [26].

1.3. AVAILABLE DETECTION METHODS

General detection methods are summarized in the following, before specific solutions for polymeric nanowires and their application in test devices are presented in a later section 1.5. A basic consideration of the target molecule used in a detection can be deducted from Figure 1.3. The different analytes largely vary in concentration over time, limiting the time scope in which a certain test can identify an infection.
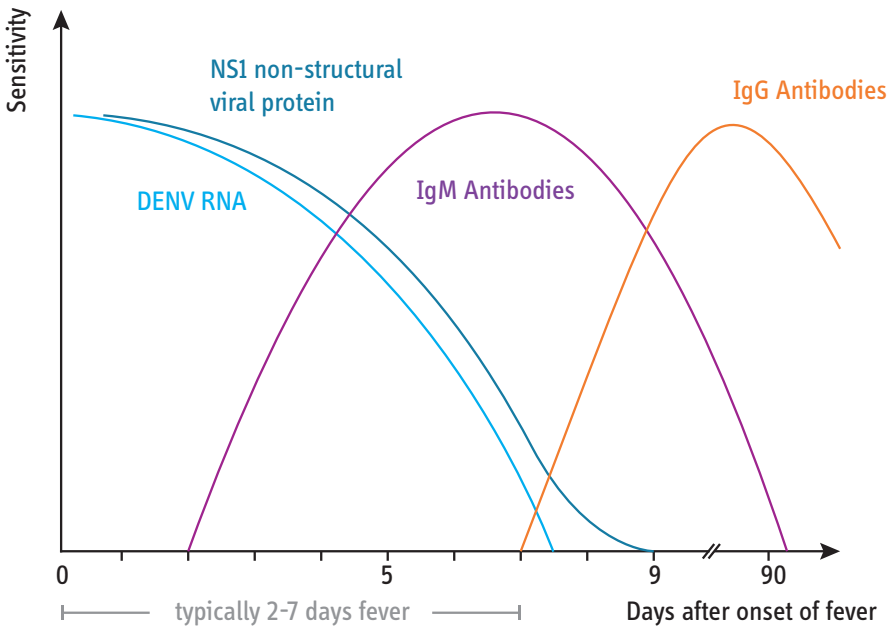
Figure 1.3: Variation in analyte concentration of different target molecules in case of Dengue serum samples. The choice of analyte molecule strongly influences the sensitivity of the diagnostic test in correlation to days after onset of fever (redraw with adaption based on [31, 32])

1

1.3.1. DIRECT VIRUS DETECTION

These methods directly detect the virus or parts of it.

DIRECT VIRUS ISOLATION

A conventional method of virus detection is the direct virus isolation. An appropriate eucaryotic cell culture is mixed with the sample fluid and incubated; alternatively an infant mouse brain is infected [33]. The viruses – if contained – will infect the cells, multiply and can then be visualized directly through electron microscopy.

This technique is not possible without a highly specialized biosafety laboratory and is thus very expensive [34]. Additionally the process can take 48 hours and more [35]. Especially in the case of Zika, where the duration of a higher virus concentration is short, testing can be very difficult and yield false negatives [4]. It is not suitable as a fast and affordable point-of-care test.

IMMUNOASSAYS ANTIGENS

In this case testing is performed for specific molecular features (antigens) of the virus. A substrate is coated with antibodies specific for an antigen of the virus. The sample is added and the antigens of the virus – if present – bind to the antibodies. A washing step assures removal of any unspecific binding, before an enzyme-linked antibody is added and binds to the immobilised antigens. After another washing step, a subsequent color change reaction catalyzed through the enzyme yields information about the presence and concentration of antigens in the patients sample. ([36, p. 111], compare Figure 1.4)

For DENV, the NS1 protein is frequently used. The advantage is, that infected cells release this viral glycoprotein and it is freely circulating [37]. For ZIKV and CHIKV, a commonly used antigen is not available, immunoassay testing is done for antibodies [38, 39].
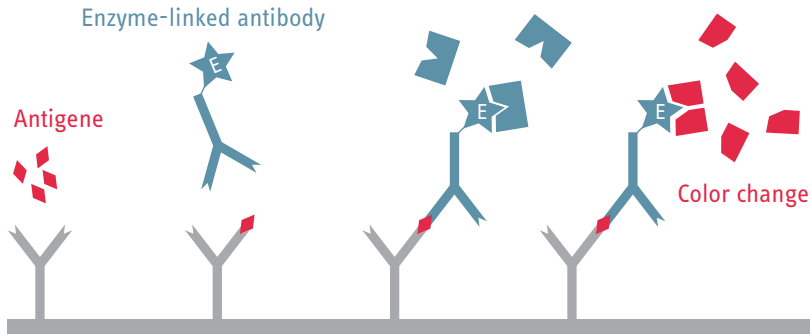
Figure 1.4: Working principle of enzyme-linked immunosorbent assay (ELISA): Antigens are captured from the analyte by specific immobilized antibodies. Enzyme-linked antibodies bind to the captured antigens and washing steps remove all non-specifically bound residues. Enzyme catalyzes color change reaction.

NUCLEIC-ACID BASED

Detection of viruses can also be performed on basis of their individual RNA sequences. Most common and established technique is the real-time polymerase chain reaction (RT-PCR), depicted in Figure 1.5 [40]. It uses polymerase enzymes to exponentially copy parts of deoxynucleic acid (DNA) strands, only if a pair of short oligonucleotide (the forward and reverse primer) specific only to the target species binds to the DNA. A third oligonucleotide (the probe), outfitted with a fluorophore-quencher set and specific to a region of the species DNA in between the primers, is cleaved and activates its fluorescence as it is cleaved by the polymerase during the copy process. The fluorescence signal allows for quantitative calculation of the original DNA concentration. In case of RNA targets, a reverse transcription step is added to yield complementary deoxynucleic acid (cDNA) that is compatible with the polymerase.

RT-PCR is sometimes preferred over serology, as it is not prone to cross reactivity and can also distinguish DENV subtypes. It is very sensitive, but it relies on acute samples, as the amount of circulating RNA drops fast during the first week [11, 14, 41, 42]. But the method is not able to determine if the virus belonging to the RNA signal is still infectious or not [39]. The most significant problem for point-of-care testing through RT-PCR is the

1
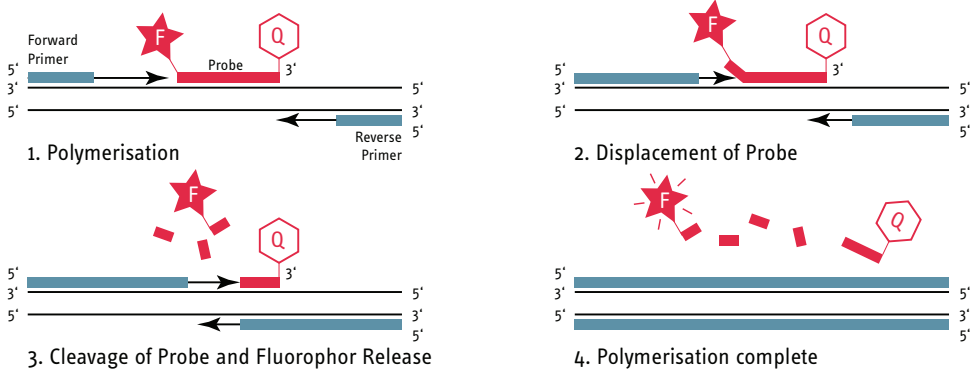
Figure 1.5: Working principle of RT-PCR: 1. A primer/probe set is engineered to a genetic sequence specific for the target species. The proximity of fluorophore F and quencher Q inhibit the fluorescent signal. The polymerase is activated by the primer/DNA binding complexes and starts polymerisation of complementary strands. 2.-3. During polymerization, the probe is cleaved and F released. 4. F is no longer quenched and signal becomes detectable. The DNA amount has doubled and the process can start over, yielding in theory exponentially growing numbers of the specific DNA strands and activated fluorophore (based on [40])

demanding temperature control. Lab-on-chip solutions for RT-PCR are not affordable in the setting of this project. More recently emerging isothermal nucleic-acid based methods such as reverse transcriptase loop-mediated isothermal amplification (RT-LAMP) are promising, but have a lower sensitivity [43–45].

1.3.2. Indirect Virus Detection

These tests differ from the previous, in that they do not directly detect the virus itself, but the immune response of the patient. As a result of the virus infection, the body produces specific antibodies of different kinds against the viral antigens. Their presence indicates contact of the immune system to the virus.

Plaque Reduction Neutralization Test (PRNT)

The serum sample of the patient is mixed with a standard solution of the virus in question and plated on cell culture susceptible for the virus infection. The viruses become visible as plaques of dead cells in the cell layer, but the presence of virus-specific antibodies in the patients sample will neutralize a proportion of the viruses and reduce this effect.

1

The occurrence of these spots in comparison to a standard of known concentrations, yield information about the concentration of the antibodies [46]. It should be taken into consideration, that early response immunoglobulin M (IgM) antibodies sometimes do not have a neutralizing effect. Thus a control with an immunoassay, as discussed in the next paragraph, can be insightful and should not be declared a false-positive without further consideration, only because plaque reduction neutralization test (PRNT) testing is negative [6]. Although very time consuming, PRNT is still considered a clinical gold standard for arbovirus detection and used as a confirmation of IgM assays, which are discussed in the next paragraph [4]. Shan et al. state the standard turnaround time of this method to be more than a week [4]. They present a new method for PRNT with a turnover time of two days. But even with the largely reduced duration, the method suffers of the same deficits as direct virus isolation and is not suitable for the aforementioned regions of Indonesia.

IMMUNOASSAY ANTIBODIES

The previously introduced antibodies can also be identified using ELISA, as introduced earlier for viral antigens. The test surface is then coated with the antigen of the virus in question. The sample is added and the patients virus-specific antibodies – if present – bind to the antigens. A washing step assures removal of any unspecific binding, before an anti-human enzyme-linked antibody is added and binds to any immobilised antibodies of human origin, which in this case can only be the patients virus-specific antibodies. A subsequent color change reaction catalyzed through the enzyme yields information about the presence and concentration of the patients antibodies. [36, p. 111]

Testing for specific IgM antibodies is currently recommended for suspected Arbovirus infections [13]. But a subsequent PRNT is also recommended to confirm a positive result, as IgM testing is prone to cross-reactivities inside the Flavivirus family, e.g. ZIKV, DENV or West Nile fever [47, p. 605]. Alternatively, a combination with a test for non-structural viral proteins can enhance the specificity [48].

Theoretically, one could also test for the immunoglobulin G (IgG) antibodies. But as vaccination or previous infection can give a lifetime signal of IgG, it is not very useful for diagnostic purposes [31]. Although, the ratio of IgM and IgG can yield information over a possible previous infection, which helps to identify high risk patients in case of DENV infections (IgM/IgG ratio >1.7 indicates primary infection) [41]. Figure 1.6 shows an overview of the immunoglobulin concentrations expected in Dengue patients. Testing including immunoglobulin A (IgA) and IgM has been shown and might also be a valuable option for enhancing the sensitivity [49].
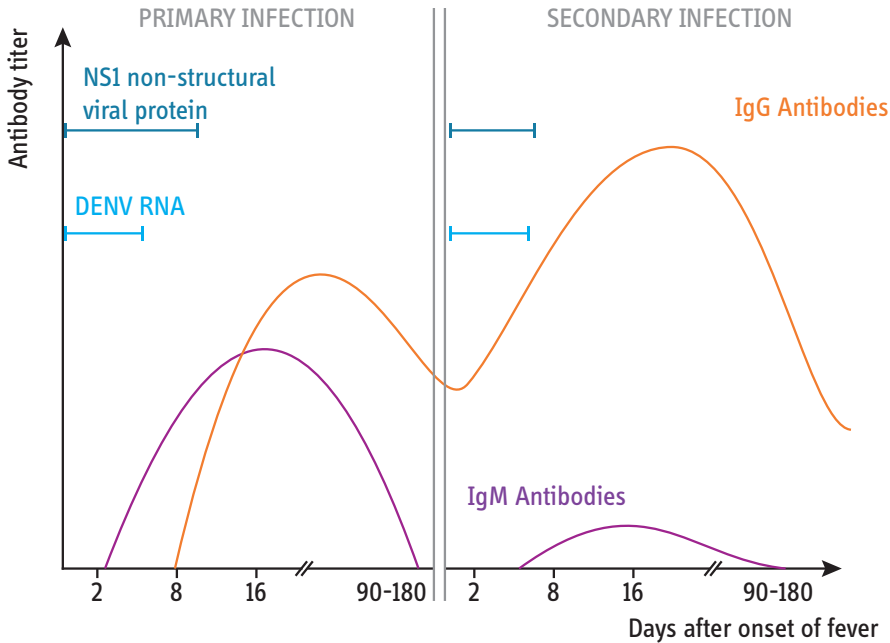
Figure 1.6: Antibody titer of IgM and IgG in Dengue patients. After a primary infection, the IgG titer can stay positive for a lifetime. Secondary infections show much lower, sometimes undetectable IgM titer, posing a challenge to the sensitivity of the method but offering information on a possible previous infection through comparison of IgG and IgM titers. (redraw with adaption from [32, 34])

1

1.3.3. CONCLUSION FOR POINT-OF-CARE TESTING INDONESIA

Of the described common detection techniques, only the immunoassays and nucleic-acid based methods appear to be adaptable to a point-of-care device in principle. But as mentioned before, handling of RT-PCR protocols needs complex devices, that are too expensive for use in a remote country side situation, even if they would be available in handheld size. There are promising less complex methods such as isothermal LAMP amplification, but the detection limit is 100 to 1000-fold lower than reported RT-PCR and sensitivity with clinical samples should be evaluated [39, 44].

Most promising techniques are the immunoassays. When integrated on a paper-based lateral flow assay (as the standard issue pregnancy test), they represent the least complex device available (see Figure 1.7). But issues with sensitivity should be addressed and strategies to tackle problems of cross-reactivity. Our field research showed, that a price of 15 USD is not considered affordable, as further tests are necessary to confirm the result and no further advantage is offered. The use of suspended nanowires for antibody immobilization could enhance sensitivity, as literature shows effects reducing the affinity of antibodies immobilized to surfaces [50]. Antibodies on suspended nanowires might keep the higher affinity of free-floating ones, but with the possibility for washing steps, controlled sample flow and spatial definition of the signal. A combination of different antigens and antibody targets in a single, low volume multiplex device will further enhance the quality of the result and add a monitoring function as additional benefit.

1.4. POLYMERIC NANOWIRES

Polymer nanowire-related research has shown considerable progress over the last decade.[2] The wide variety of materials and the multitude of well-established chemical modifications have made polymer nanowires interesting as a functional part of a diagnostic biosensing device. This review provides an overview of relevant publications addressing

---

[2]The following sections of this chapter have already been published by us [1]
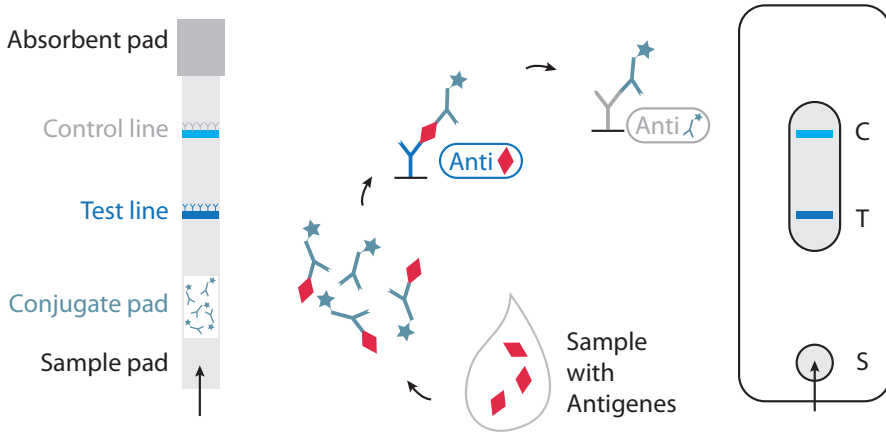
Figure 1.7: Schematics of a lateral flow assay for detection of an antigene. No actuated parts are involved, the technique equals the well established consumer pregnancy test. A nitrocellulose membrane is prepared with a dried conjugate of a signalling antibody specific to the antigene. The liquid sample spreads on the membrane, mixing with the conjugate. Antigene specific antibodies on the test line will capture the antigene-signalling antibody conjugates and the line will become visible if sufficient antigene was present (usually a chemical signal enhancement takes place). The control line employs antibodies capturing the conjugate antibodies to confirm their presence and enhance the reliability of the test.

the needs for a nanowire-based sensor for biomolecules. Working our way towards the detection methods itself, we review different nanowire fabrication methods and materials. Especially for an electrical signal read-out, the nanowire should persist in a single-wire configuration with well-defined positioning. Thus, the possibility of the alignment of nanowires is discussed. While some fabrication methods immanently yield an aligned single wire, other methods result in disordered structures and have to be manipulated into the desired configuration.

One-dimensional nanostructured materials, namely nanowires, have a strong potential to provide a valuable platform for sensing of biomolecules and pathogens when integrated in affordable devices. To date, the search for one-dimensional nanostructures of high quality materials with control of the diameter, length, composition, and phase has enabled some strong advances with their incorporation as functional parts of integrated devices [51–55]. While this review focuses on polymeric nanowires, the interested reader will find detailed information on silicon nanowires [51, 52, 54–56], III-nitride

1

semiconductor nanowires [57], and carbon nanotubes [52, 58, 59] in the cited literature.

From all possible materials that can be used for diagnostic purposes, polymeric nanowires are promising candidates. Ease of formulation, biocompatibility, their suitability for decoration with biomolecules, and the availability of electrically-conductive materials are advantages that can be utilized due to the highly precise chemistry of synthetic polymers, which is very well established by now [60, 61]. Conductive properties of polymers, however, differ strongly from other typical materials used in system integration electronics, such as metals and semiconductors. Examining the literature of nanowire system integration, it appears that the a priori lower conductive properties of polymers in relation to typical materials used in integrated electronics has left polymer nanowires underinvestigated for such purposes. In the search for new solutions and approaches, resistance measurements (or impedance measurements) with conductive polymers must be considered in addition to the usual optical readout methods.

1.4.1. RANDOMLY-ALIGNED NANOWIRES

Polymeric wires are composed of long molecules, and the systems are flexible and elastic. If not confined in any way, the nature of the material will lead to disorder of the nanowire structure [62, 63]. This section presents nanowires of interest for a diagnostic application, which are randomly oriented after synthesis. Strategies for alignment are discussed in a later section.

ELECTROSPINNING

Electrospinning is an old technique, long established in the textile industry and with recent advances into the biomedical field. Interest in electrospinning arises from the huge variety of materials that can be spun into fibers, with diameters in the nanoscale well possible. Intensive reviewing of the various possibilities including hierarchically-structured fibers, but exceeding our review's scope have been discussed in the review of Yang et al. [64].

Researchers made composite materials from this simple method, producing conductive nanofibers. Recently, Lee et al. [65] presented a highly-conductive electrospun polyethylene oxide (PEO) nanowire carbon nanotube (CNT) composite, using poly(styrene sulfonic acid graft aniline) (PSS-g-ANI) as an amphiphilic surfactant to create a stable solution of the CNT and the polymer. High electrical conductivity (1570 S/m) was reported, comparing well to the intrinsic conductivity of conductive polymers varying from 1×10^{-14} S/cm – 1×10^2 S/cm [66].
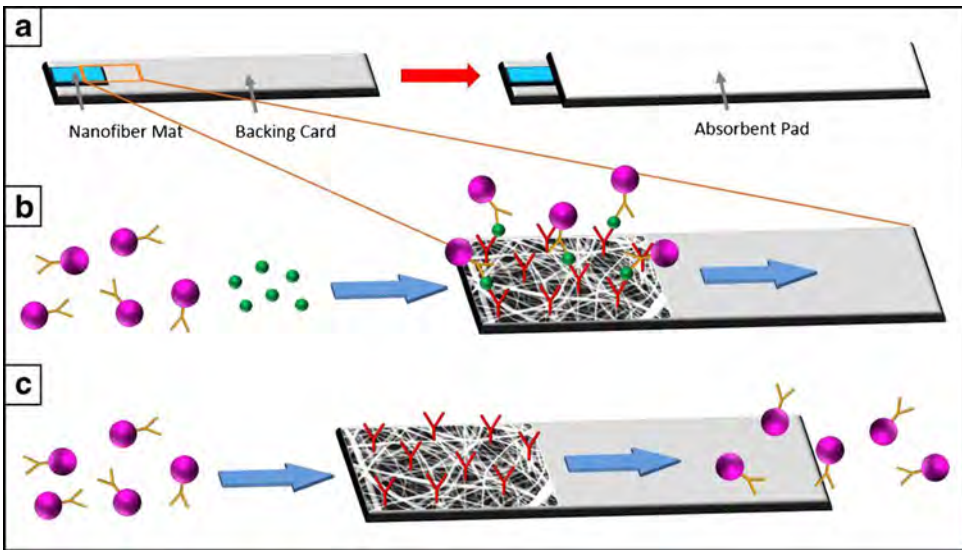
Figure 1.8: Illustration of a lateral flow assay using an electrospun nanofiber mat instead of the classic nitrocellulose membrane: (a) sample flows through the mat into the absorbent pad; (b) *Escherichia coli (E. coli)* (green) are captured by the antibodies (red) on the mat, and following horseradish peroxidase (HRP), linked antibodies (pink/orange) are immobilized, catalyzing a colorimetric signal in place when the HRP substrate is added; (c) if *E. coli* is not present in the sample, no binding of the secondary antibody can occur, and the enzyme is transferred to the absorbent pad. Figure by Reinholt et al. [67] reproduced with permission from Springer Nature

Reinholt et al. [67] showed that an electrospun polylactic acid-polyethylene glycol (PLA-PEG) mat without further advancements is comparable in use as a lateral flow assay to a classic nitrocellulose membrane (Figure 1.8). They demonstrated its use as a matrix in an antibody-based *E. coli* immunoassay, achieving a limit of detection of 3.8×10^6 CFU/mL, which is comparable to those seen in the literature for nitrocellulose

membranes [68, 69].

Aiming at hormone/protein detection, Lee et al. [70] could demonstrate the feasibility of outfitting electrospun polystyrene-poly(styrene-co-maleic anhydride) (PS-PSMA) with aptamers (Figure 1.9). This is of special interest, as the maleic acid contained in the spun wire comprises a bioconjugation compatible linker. Although more of a microfiber in diameter, reduced sizes might well be achieved in the future or not even necessary for the envisaged diagnostic application. Lee et al. had it react with streptavidin in a simple buffer solution overnight and attached the primary biotin-linked aptamer in the next step. In the presented aptamer sandwich immunoassay, the group was able to achieve thrombin detection down to a concentration of 10 pM, using secondary aptamers conjugated to quantum dots.
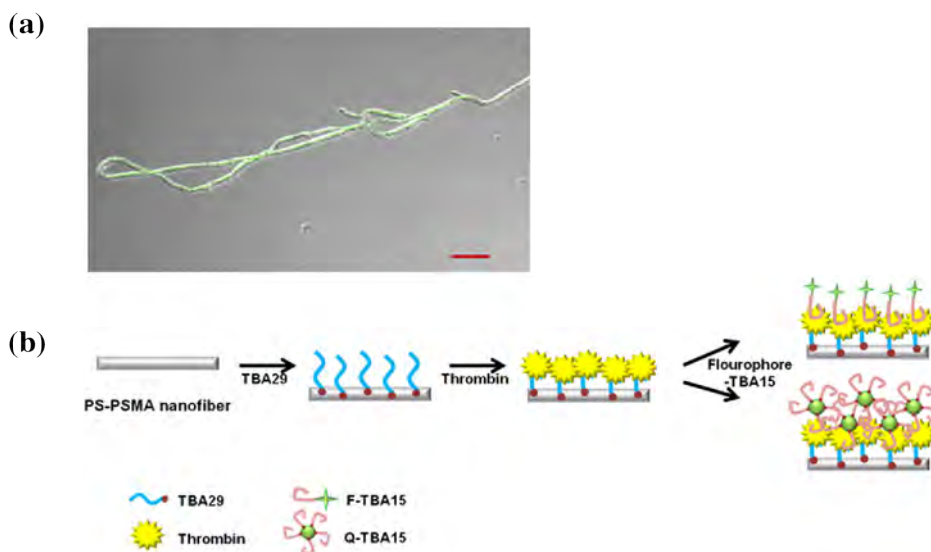
Figure 1.9: (a) Composite microscope picture combining the brightfield and fluorescence of anti-thrombin aptamer (TBA) sandwich on nanofiber with a quantum dot-labeled secondary aptamer (scale bar: 20 μm); (b) schematic of the nanowire-based anti-thrombin sandwich assay. (figure reprinted from Lee et al. [70], copyright (2012), with permission from Elsevier)

The process of electrospinning does not yield oriented wires. New setups tried to overcome this disadvantage, such as aligning the wire to a magnetic field while still flying [71]

or reducing the whipping motion by adjusting the electrical field to a lower strength and higher uniformity and mechanically pulling the wire towards the collector [72]. Although a linear pattern of wires can be created, this process is not able to define the position of each single wire precisely. Without any further processing, the result is still that of randomly-placed wires with a common orientation and mean density.

A unique strategy for creating aligned wires was shown by Thiha et al. [73] (Figure 1.10). bisphenol A novolac epoxy based negative photoresist (SU-8) photoresist was electrospun onto an electrode structure, creating an area of randomly-distributed wires as typical for electrospinning. They illuminated the small gap in between the electrodes with ultraviolet (UV) light, so that only a part of a wire spanning this gap was cured. Any neighboring wires were dissolved in the following development step. The authors reported that in five repetitions with sets of 24 electrode structures each, 80 % showed 1–3 suspended wires, 20 % of these resulting in a single-wire configuration. Perhaps this rate can be improved, if the electrospinning is combined with an alignment technique such as the aforementioned magnetic field induction [71]. As both the electrode and wire are carbonized in a furnace afterwards, this process results in an electrical contact of a conductive (then) carbon nanowire.

Overall, electrospinning has shown a high variety of materials and possibilities to combine them in composites, making it a promising process for the production of polymeric nanowires. Reliable processes for decoration of the wires have to be established. A functionalization of the respective polymer that is easily compatible with a standard bioconjugation method such as N-hydroxysuccinimidyl (NHS) esters or a bioorthogonal strategy such as copper(I)-catalyzed Azide-Alkyne Cycloaddition (CuAAC) "click-chemistry", which were intensively reviewed by Zheng et al. [74], is desirable. The main issue remains the alignment: extra steps are needed to align or remove the usually random fibers. Figure 1.4.2 will discuss a possible method for alignment of such fibers.
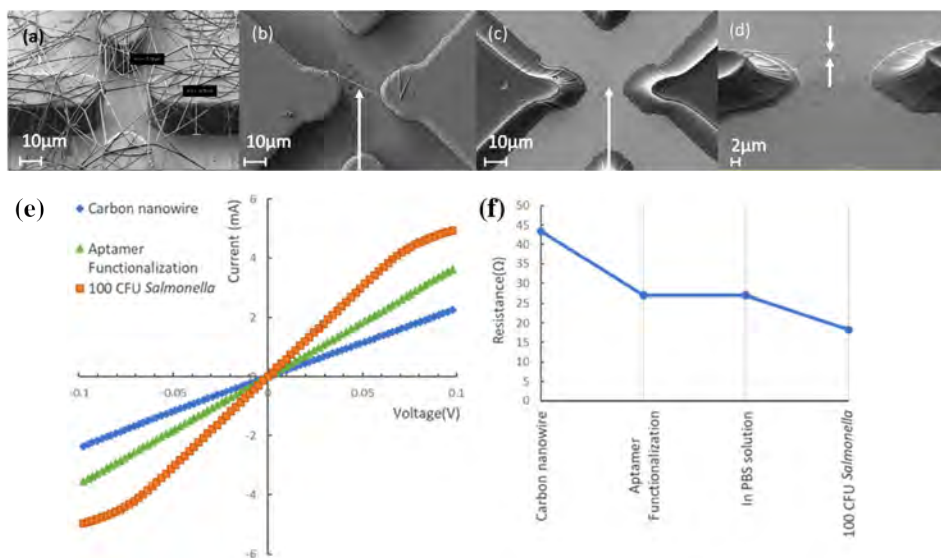
Figure 1.10: (a) SU-8 photoresist electrode structure with electrodeposited SU-8 photoresist nanowires, (b) after UV curing and development, and (c,d) finally carbonized in a furnace; (e,f) resistance changes measured in the nanowire after decoration with the aptamer and addition of *Salmonella* bacteria. Figure reprinted from Thiha et al. [73], copyright 2018, with permission from Elsevier.

Self-Assembly of Micelles

An elegant way of producing nanowires of well-defined diameter and chemical properties is self-assembly of worm-like micelles. In contrast to spherical micelles, the choice of polymer favors the assembly of molecules in the cylindrical body in lieu of a spherical end-cap, resulting in the growth of a micellar wire (further details and examples of stimuli-responsive worm-like micelles were given in [75]). Polymeric micelles are strong candidates for nanowires, as long as they can be either quenched or assembled during the dewetting process, exhibiting in both cases hundreds of microns in length [76]. So far, only quenched micelles grown out of equilibrium exhibit such dimensions. Furthermore, it has been shown that quenched micelles, containing a glassy core, exhibit such a length without branching. Zhang et al. [77] presented such micelles, with lengths of up to 250 µm. The amphiphilic nature of the building blocks opens up many options when it comes to integration of different molecules into the core while keeping the solubility in a solvent

unimpeded. Another advantage is that once the monomers are available, processes for forming the wires are rather facile.

Liu et al. [78] presented a library of alternating amphiphilic glycopolypeptide brushes (AAGB), where varying ratios of sugar and amino acid units lead to self-assembly of micelles, nanoribbons, or nanowires. Figure 1.11 depicts an example of a glycopolypeptide configuration resulting in nanowire self-assembly. The material seems to be a very promising candidate for good biocompatibility due to the building blocks naturally occurring in the body. Biofunctionalization would have to be investigated.
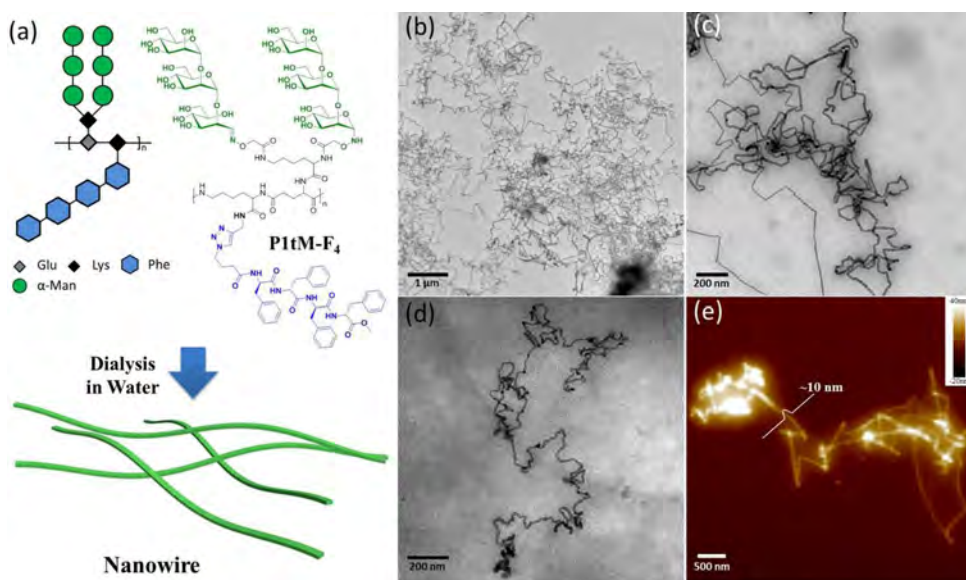
Figure 1.11: One variant of self-assembled micelle nanowires (P1tM-F_4) created from AAGB in water. (a) Chemical structure and illustration of nanowires, (b,c) transmission electron microscopy (TEM) images in different magnifications, (d) cryo-TEM image and (e) AFM image; as no alignment is performed on the nanowires, they deposit in a random configuration of disorder. Figure reprinted from Liu et al. [78] with permission from ACS. All rights reserved.

Glazer et al. [79] showed a polystyrene-polyethylene oxide block-copolymer (PS-b-PEO) micelle nanowire that self-assembles using an immiscible solvent process, as previously introduced by Zhu et al. [80]: the polymer is dissolved in chloroform, and droplets of the solution are added to water, leading to a rearrangement of the molecules to form a stable micelle nanowire in the water phase, once the chloroform evaporates. The resulting

nanowires have a hydrophilic corona and hydrophobic core, showing lengths of hundreds of micrometers with a diameter of approximately 60 nm. They mention the incorporation of a hydrophobic dye 1,1'-dioctadecyl-3,3,3',3'-tetramethylindocarbocyanine perchlorate (DiI) inside the micelles, showing an example for using the unique amphiphilic nature of micelle-based nanowires. Without further processing, the nanowires are disordered (see section 1.4.2).

Another example of micelle functionalization was demonstrated by Nie et al. [81]. They incorporated CdS nanorods into PS-b-PEO worm-like micelles by using a surfactant (hexadecyl trimethyl ammonium bromide).

The interested reader will find further information in comprehensive reviews covering the recent advances in self-assembly of amphiphilic block and graft copolymers and their biomedical applications in [82–87].

1.4.2. ALIGNED NANOWIRES

Developing low-cost strategies to order, assemble, and align macromolecules (polymeric chains) is a challenging task, due to the random conformation of polymeric chains in solution. However, if the advantages of single-wire configurations are desired for sensing applications, alignment is crucial. The main advantage of the single-wire configuration is the possibility of electrical contacting and better defined signal density. Alignment in this sense can mean two things: the change of orientation of a given wire, but also the direct creation of a wire structure in the preferred orientation and place. Many techniques have been thoroughly reviewed by Su et al. [88, 89]. The following sections focus on vertical nanowires, micropillar dewetting, and electrosynthesizing.

VERTICAL NANOWIRES

Vertical nanowires represent an ideal variant of aligned nanowires. A major advantage for diagnostic applications can be the very high surface area achievable with the dense packing possible in such geometry.

A top-down approach to achieve vertical polymer wires was demonstrated by Fang et al. [90]. They created vertical nanowire arrays in UV-transparent and UV-absorbent polymers through laser interference patterning (LIP) and inductively coupled plasma (ICP) etching. Diameters increase with the pattern periodicity and vary from 100 nm with a 500 nm period up to 500 nm for the 2.5 µm period array. Aspect ratio and height are not explicitly discussed, although the authors claimed that elongated ICP etching would not change the LIP pattern and so increase the aspect ratio. The group previously presented ICP-based etching of nanowires into diverse organic materials, achieving wire lengths of several micrometers [91, 92].

A vertical architecture can be challenging if it comes to electrical contacting, as connecting the top end of a free-standing wire is not a trivial procedure in these dimensions. Vlad et al. [93] showed the vertical growth of polyaniline (PANI) nanowires, using a poly(methyl methaacrylate) (PMMA) template (see Figure 1.12). Using this template, they could also facilitate electrical contact on top of the wires. The nanowire height was 500 nm for cross bar latched arrays with top and bottom metal electrode contacts.

Polypyrrole (PPy) nanowires appear suitable for work with cells, due to their property of swelling on application of electrical fields, potentially allowing controlled release of substances incorporated into the wire, but also the triggered detachment of cells adhered to it [94]. This has been used by the same group in Hong et al. [95] to demonstrate circulating tumor cell (CTC) capture and release using vertical PPy nanowire arrays (see section 1.5.2). As a sample usually contains only low concentrations of the targeted cells, capturing them on a small surface area enhances the signal of a subsequent detection, allowing here a very low detection limit of 10 cells/mL. To facilitate binding of the capture antibody, disulfide-biotin was incorporated into the PPy nanowires during electrochemical deposition of the pyrrole. It allowed for ligation of the biotinylated capture antibody through streptavidin addition and offered a second option for detaching captured cells by cleaving the sulfide bond using glutathione instead of applying a voltage.

1
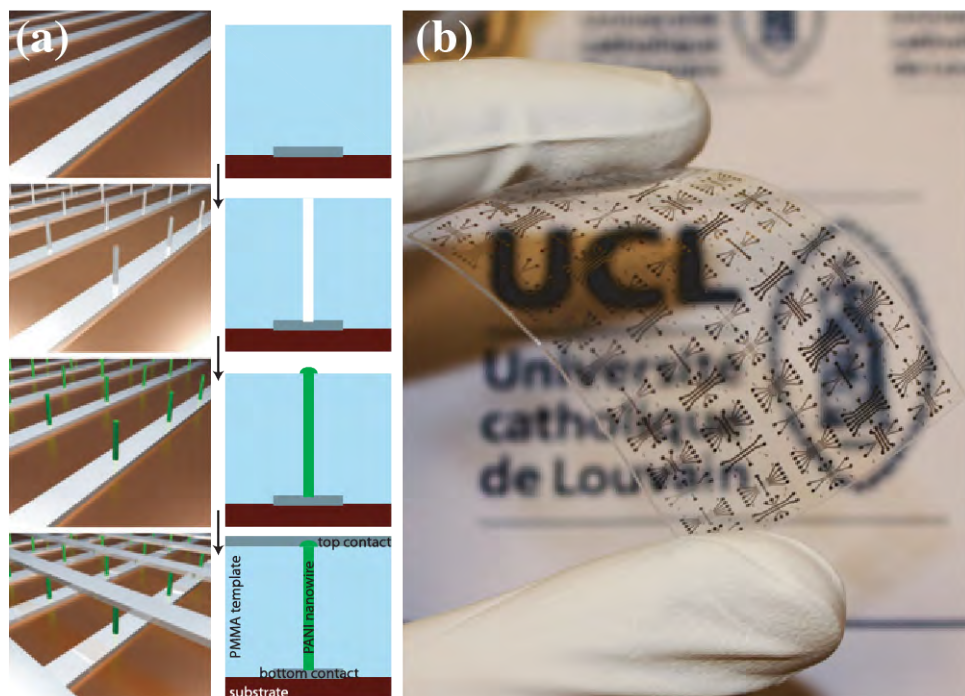
Figure 1.12: (a) Production process of vertical polymeric nanowires with electrical contact on both ends of the wire using a PMMA template and metal strips (b) Realization on a flexible, transparent Teflon substrate. Figure by Vlad et al. [93], ©IOP Publishing. Reproduced with permission. All rights reserved

MICROPILLAR DEWETTING

Wetting is a common phenomenon that can often be found in our everyday life activity from swimming on a beach to effects in ion transport. The dewetting process of liquids, containing macromolecules on micro-patterned substrates, has become an effective strategy to form large arrays of polymeric nanowires. Various types of polymeric nanowires including DNA, polyvinyl formal (PVF), and PS-b-PEO worm-like micelles have been successfully formed. The techniques yield large arrays of oriented wires out of polymer solutions by retracting the solution drop from micro-patterned surfaces. This has been shown in different ways (see Figure 1.13): Guan et al. [96] and Lin et al. [97] used a solution of DNA wires, enclosing the droplet between the structured stamp and a plain surface and carefully separating the planes. Glazer et al. [79] created worm-like micelles with

a PS-b-PEO block copolymer and dewetted the structured stamp removing the liquid with the tip of a tissue. Su et al. [98] created the dewetting effect by moving a droplet of dissolved polyvinyl formal over the structure with a pipette, forcing the dissolved polymer to entangle and form wires, while the solvent retracted. In a different publication, Su et al. [99] employed the same strategy for calcein, but using gravity by tilting the substrate.
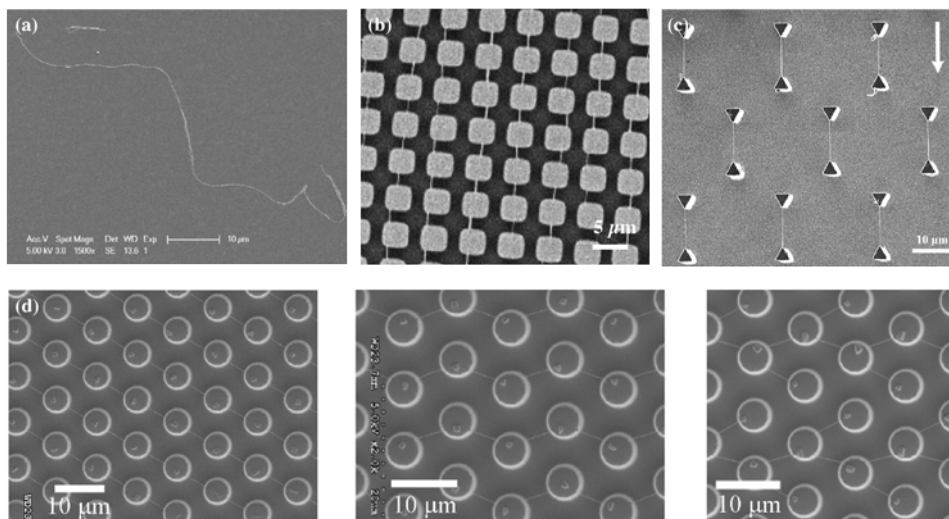
Figure 1.13: (a) Disordered deposition of a micellar nanowire on an unstructured surface, compared to (b) aligned nanowires after dewetting of microstructures (square pillars of 3.5 μm in width, 2 μm in gap, and 3 μm in height); figure by Glazer et al. [79]. (c) Variation of the microstructure geometry yields different nanowire formations; figure by Su et al. [98], also seen in (d), where a different flow direction angle of receding fluid in each picture additionally influenced the layout of resulting nanowires; figure by Lin et al. [97]. (a-c) reprinted from [79, 98] with permission from Wiley; (d) reprinted from [97] with permission of AIP publishing.

Many different dewetting structures have been shown to yield various patterns of aligned wires [100]. In general, this method seems applicable to alignment of any randomly-produced nanowires available in solution. Furthermore, it has been shown that this method can be employed to hold in restraint *S. aureus* bacterial colonies and shape the architecture of their growth for biological investigations [101]. Furthermore, electrical contacting should be feasible, but has yet to be shown.

ELECTROSYNTHESIZING

The process of electrosynthesizing is of interest, as it combines synthesis, alignment, and electrical contacting in one step. Different materials and processes have been presented in the past. Kannan et al. [102] showed the electrosynthesizing of a single poly(3,4-ethylenedioxythiophene) (PEDOT) wire in between two gold electrodes. They decorated it with DNA oligonucleotides specific to ovarian and breast cancer cells (Figure 1.14). A mixture of the monomer EDOT/EDOT-COOH, $LiClO_4$, and polystyrene sulfonate (PSS) in acetonitrile was placed on the electrode gap and exposed to a square wave electric field (± 7 V at 25 kHz). The resulting wires were not exactly straight and showed a high roughness, but spanned a distance of 11 µm (Figure 1.15).
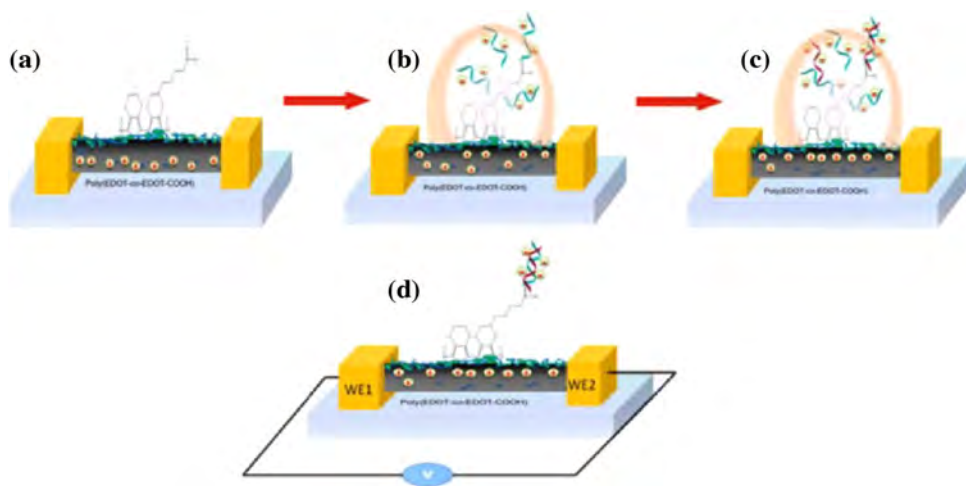
Figure 1.14: (a) Schematic of electrosynthesized nanowire with -COOH end groups for conjugation (b) with oligonucleotides (ODN) through EDC/NHS chemistry, (c) hybridization of target ODN, and (d) resistance measurement after drying of the wire. Reprinted from Kannan et al. [102], copyright 2012, with permission from Elsevier.

To overcome the random fluctuations in electrogrown wires, Hu et al. [103] confined the wire growth inside a PMMA nanochannel (height 100 nm, channel diameter 100 nm) flanking the direct connection between the two electrodes (Figure 1.15). They showed a combined sensor chip, using electrically-conductive polymer, ZnO, and palladium wires for gas sensing (hydrogen, methanol, carbon monoxide, and nitrogen dioxide). Both a

PPy and a PANI nanowire were grown through electrochemical deposition in between two Ti/Au electrodes. Owing to the channel confinement, the shown wires spanning the 5 μm distance were straight. Measured widths of the wires were 126 nm for PPy and 104 nm for PANI.
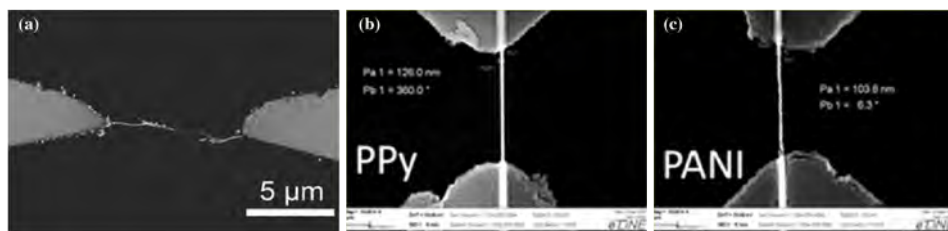
Figure 1.15: Comparison of resulting electrosynthesized wires: (a) PEDOT nanowire grown in between two gold electrodes [102] and (b,c) PPy and PANI nanowires grown in a confining PMMA nanochannel [103]. Reprinted from Kannan et al. [102], copyright 2012 and Hu et al. [103], copyright 2013, with permission from Elsevier.

A very uncommon, yet intriguing composite of an electrodeposited polymer with integrated bacteriophages has been shown by Arter et al. [104]. Nickel electrodes were used to create thin initial layers of PEDOT through electrodeposition, facilitating the following co-deposition of PEDOT and M13 bacteriophages (see Figure 1.16). The nickel was removed and the resulting nanowires contacted with silver paste. The authors demonstrated the functionality of the bacteriophage surface by attaching fluorescing anti-M13 antibodies. However, most importantly, they showed significant resistance changes of the wire arrays on administration of the binding antibody, as compared to the negative control (Figure 1.16 c). The future idea is that viruses can be modified to carry specifically-engineered binding sites on the outside, thus allowing the buildup of different diagnostic assays. This could allow label-free detection of analytes using libraries of virus variants.

1.5. DETECTION STRATEGIES AND OPPORTUNITIES

With all previously-mentioned nanowire materials and alignment methods, the key point towards a diagnostic device is the detection strategy employed to address healthcare-
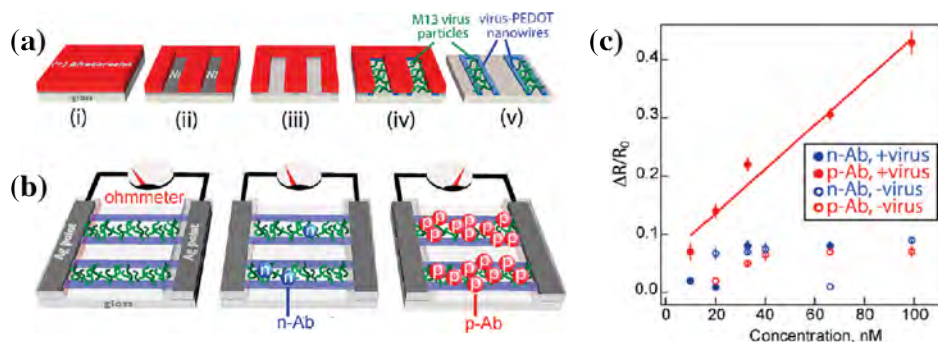
Figure 1.16: (a) Illustration of the synthesis of virus-containing PEDOT nanowires through lithographically-patterned nanowire electrodeposition (LPNE). (b) Schematic of the resulting nanowires in the final configuration; relatively low ohmic resistance when bare, also after addition of non-binding control antibodies (n-Ab), but significant rise of resistance after applying virus-binding antibodies (p-Ab). (c) Resistance changes for combinations of virus containing/free and binding/non-binding antibodies to demonstrate the selectivity. Reprinted with permission from Arter et al. [104]. Copyright 2010 American Chemical Society.

relevant device needs. This last section focuses on strategies for use of polymer nanowires in detection applications. Findings are summarized in Table 1.1. Some considerations concerning packaging are given in the last section.

1.5.1. OPTICAL

Polymeric fibers can be decorated with biofunctional molecules such as antibodies, aptamers, or oligonucleotides. In the most basic approach, a detection is then possible using a label such as a fluorophore or an enzyme, catalyzing a color change reaction.

An approach using enzyme has been shown by Reinholt et al. [67], as previously mentioned. They created a lateral flow assay using an electrospun mat of polylactic acid (PLA)-polyethylene glycol (PEG) wires to perform a sandwich immunoassay detecting *E. coli*. The labeling secondary antibody was linked to HRP, a commonly-used enzyme in immunoassays, catalyzing a color change with an added substrate. The wicking and washing time of the assay were not stated, the duration of the final color reaction was 10 min.

A fluorophore-based setup was demonstrated by Lee et al. [70]. Instead of antibodies, aptamers were used to detect the protein thrombin. Especially interesting in this setup is that the decoration of the PS-PSMA nanowire occurred using the intrinsic reactivity of the maleic anhydride part of the wire towards streptavidin. Decoration with biotin-linked aptamers can follow thereafter. The immobilization of the streptavidin on the wire surface took place in aqueous buffer solution. The approach should easily allow for any other biotin-tagged biomolecule to be used in this assay. Incubation time and washing steps amounted to ~1.5 h.

Aptamers are similar to antibodies, in that they bind specifically to the target molecule with a high specificity. They are made of sequences of either RNA or DNA. Advantages compared to protein-based antibodies are numerous. Target specificity and affinity can be selected in vitro, allowing a broader variety of targets: culturing of antitoxin antibodies for example is difficult, as it involves application of the toxin to the animal or animal cells producing the antibody. In some cases, the DNA aptamer is more stable than the antibody protein. Synthesis happens chemically with little to no batch variations and a higher shelf life. Finally, the aptamer often changes conformation when binding, an effect that can be detected with an integrated sensor. This was discussed by Lee et al. [105] and Song et al [105], where further information can also be found.

Garcia-Cruz et al. [106] presented a nanocontact printed PPy nanowire, decorated with antibodies to detect the protein interleukin-10. They could show the specific binding to the nanowire using secondary fluorophore-linked antibodies. The optical-based proof-of-principle testing took 2 h. As PPy is a conductive polymer, it will be interesting to see future applications of electrical read-outs using this setup.

1

Table 1.1: Overview of relevant diagnostic setups and their range of detection.

Publication	Target	Sensor	Read-Out	Range of Detection
Thiha et al. [73]	*Salmonella* bacteria	Aptamer on carbon wire	Resistance change while wet	10 CFU/mL
Reinholt et al. [67]	*E. coli* bacteria	Antibody on nanowire mat	Colorimetric	3.8×10^6 cells/mL
Hong et al. [95]	Circulating tumor cells	Antibody on PPy	Amperometric	10 cells/mL
Kannan et al. [102]	DNA oligo	DNA oligo on PEDOT	Resistance change after drying	0.1 fM
Garcia-Cruz et al. [106]	Interleukin-10 protein	Antibody on PPy	Fluorescence (for proof-of-concept)	250 ng/mL
Lee et al. [70]	Thrombin protein	Aptamer on PS-PSMA	Fluorescence	10 pM with QD
Zhu et al. [107]	Estradiol protein	DNA aptamer on Py-co-PAA membrane	Electrochemical impedance spectroscopy	1 fM

1.5.2. ELECTRICAL

The already introduced work of Hong et al. [95] used an array of vertical PPy nanowires to capture CTCs using anti-epithelial cell adhesion and activating molecule (EpCAM) antibodies (see Figure 1.17). They concluded a nine-fold higher capture of cells as compared to a flat PPy surface and were able to demonstrate a limit of detection down to 10 cells/mL using antibody-linked HRP, performing amperometric measurements. Although based on silicon nanowires, we also recommend for further reading the work of Wang et al. [108] and Lu et al. [109]. The application of microfluidics to this field has been reviewed by Chen et al. [110].

Additionally interesting in this regard is the use of vertical nanowires for sample preparation such as cell lysis, which would have to precede a detection, if the target is contained inside the cell rather than on the cell surface. An example was shown by Kim et al. [111], using vertical ZnO nanowires to lyse cells for release of contained proteins and nucleic acids. Further background on the challenges of microfluidic cell lysis was provided by Nan et al. [112].

In some cases, changes in a nanowire's electrical resistance are measurable if the composition of the matter in the close proximity of a nanowire changes. This enables the direct detection of target molecules, as they bind to a functionalized decoration of the conductive nanowire. An additional molecular label as discussed for the optical detection methods or the electrochemical detection is not necessary.

In the previously introduced work of Kannan et al. [102], a PEDOT nanowire was decorated with oligonucleotides, which hybridize with their targeted counterparts, if contained in the sample. They proposed that the close proximity of the negatively-charged backbone of the hybridized oligonucleotide leads to an increase in immobile, surface-trapped electron holes. This results in a decrease of the wires' conductivity. In the presented work, the wire had to be dried after application of the sample droplet and 1 h of incubation time at 42 °C, before an electrical measurement was started.

1

The drying process was not necessary in the setup of Thiha et al. [73] and was performed with the wire submerged in the buffered sample solution after 5 min of incubation time. The nanowire and electrodes were integrated into a microfluidic channel. In their case, the polymer nanowire was transformed into a pure carbon wire using a furnace and high temperatures. Decorated with an aptamer, *Salmonella* bacteria were captured on the wire, and a decrease in electrical resistance can be measured directly while the wire is covered with buffer solution. The Gram-negative nature of the bacteria accounts for a high concentration of lipopolysaccharides in its membrane, creating a negative membrane charge. Bound in close distance to the wire on the aptamer, the charges induce electron holes in the carbon wire, lowering the resistance.

Zhu et al. demonstrated a different method of electrical read-out using electrochemical impedance spectroscopy, but using a flat, nanoporous electrode of a conductive polymer [107]. For this, a potential was applied to the electrochemical system, and the frequency dependence of the impedance was analyzed. This frequency dependence is especially sensitive to surface interactions. In this setup, the folding of the immobilized aptamer when binding to the target protein (estradiol) leads to a charge redistribution. The range of detection was as low as 1 fM, and the incubation time was 20 min. It will be interesting to see if this measurement method can be adapted to conductive polymer nanowire systems.

A common problem in sensing biomolecules is unspecific binding, leading to false positive signals and a higher limit of detection. Two effective approaches to optimize this aspect were developed. In the work previously discussed, Reinholt et al. [67] presented a second PLA mat, which included additions of antifouling polymer in the electrospin solution. It reduced nonspecific binding beyond detection limits, showing a possible advantage of using electrospun wires over nitrocellulose. A second example of interest was presented by Chang et al. [113]. They used In_2O_3 nanowires, decorated with antibodies against a tumor marker, and passivated the nanowire against unspecific binding by

attaching Tween-20 molecules to the nanowire. It is an amphiphatic molecule commonly used in classical immunoassays for this purpose and should be applicable to polymeric wires as well.
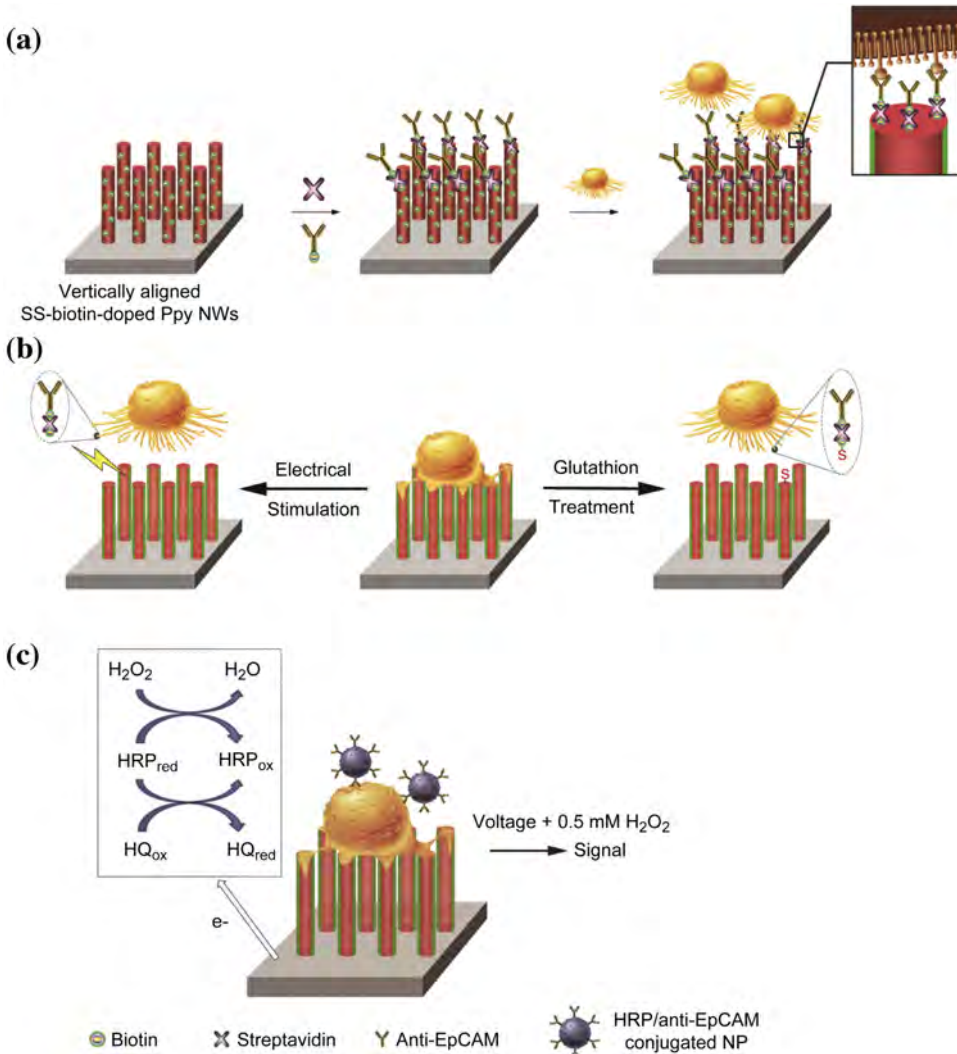
Figure 1.17: (a) Composition of the cell capture array: disulfide-biotin has been doped into the vertical PPy nanowires during electrochemical polymerization and linked to the biotin-linked anti-EpCAM antibodies through addition of streptavidin. (b) Captured cells can be released either by applying a voltage swelling the PPy or the addition of glutathione for cleavage of the disulfide bond. (c) Electrochemical detection after labeling of captured cells with HRP-nanoparticle-linked antibodies. Reprinted from Hong et al. [95], copyright 2014, with permission from Elsevier.

1.5.3. PACKAGING

Even the most advanced detection method might never make the step out of a research lab into the application world without a reliable, user-friendly packaging. Depending on the sensor type, it has to be tightly sealed, and electrical, fluidical, and optical connections have to be made to connect peripheries such as reservoirs, pumps, or electronics; this still poses several challenges in manufacturing and reliability (compare Figure 1.18) [114–117]. While in the lab, tinkering with connections can be a viable option to allow focus on the sensor technology, but even the early stage development will gain much from reliable integration. Van den Driesche et al. [118] developed a platform suitable for the sensor development phase of a microfluidic chip. It provides reliable fluidical and electrical connections to interchangeable microfluidic chips and can be useful as a development platform, even if it is not a consumer device. Temiz et al. [115] presented an in-depth review of sealing and fluidical/electrical interconnection of microfluidic devices in general. They concluded that manifold techniques are available, but still, there is a persistent gap between the preferences of the academic researcher and mass production compatibility considerations of the industry. The most prominent example of this is the widespread use of PDMS in research labs as opposed to injection-moldable thermoplastics preferred in industry. For apparent reasons, decisions about materials used in research are often made on the basis of availability of the material and machinery, but also practical demands of the ongoing research work, such as the demand to be able to view the processes optically with a microscope. These approaches often result in a carefully optimized technology, which is not compatible with the scale-up demands of industrial companies. Early consideration of these limitations is helpful, if application in the field is desired. New fast-prototyping technologies and low-cost materials offer suitable starting points for research groups, avoiding the costly and not easily available clean room techniques [114, 119]. For detailed critical discussion of 3D-printing techniques from the perspectives of microfluidics, read Waheed et al. [120].
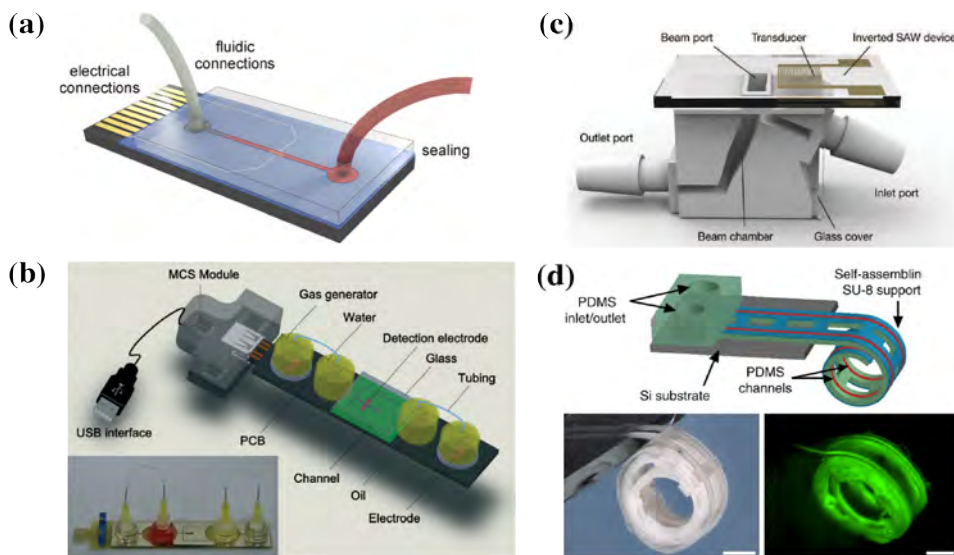
Figure 1.18: (a) Schematic of a microfluidic chip with sealed fluidic channels and microfluidic and electrical connections [115]. (b) Complex integrated microfluidic device, including reservoirs, pumps, and USB interface electronics [116]. (c) 3D-printed fluidic accessory [119]. (d) Self-assembling microfluidic channels show one of many possibilities to rethink packaging in new directions [121]. (a) reprinted from Temiz et al. [115], copyright 2015, with permission from Elsevier; (b,c) republished with permission from Royal Society of Chemistry, from Li et al. [116] and Dentry et al. [119], Copyright 2014; (d) Jamal et al. [121], reproduced with permission from Springer Nature.

1.6. Conclusions

During the last few decades, the field of nanowires witnessed numerous novel techniques and materials that have been developed from both the synthesis (chemistry) and processing (fabrication, manipulation, and alignment) points of view, providing a sustained advance, especially for polymer-based nanowires. However, fabrication of the nanowire, synthesis of the material composing it, and their manipulation (alignment) are imposing constraints on each other. Material properties, nanowire dimensions, and final alignment on a given substrate are therefore often interdependent.

In terms of polymer-based nanowire processing, electrospinning appears to offer the highest diversity of materials. Mixed materials, for instance, polymer blends or composites using carbon nanotubes, have been obtained, allowing for tuning of parameters such

as electrical conductivity or affinity to biomolecules. Diameters down to hundreds of nanometers were demonstrated. An alternative approach is the self-assembly of micellar wires, because of the relative ease of production. This process spontaneously results in nanowires of a well-defined diameter, exhibiting lengths of several hundreds of micrometers. The amphiphilic structure of such nanowires allows for the incorporation of substances or nanoparticles into the core of the micelle in addition to possible chemical modification or binding of biomolecules to the corona. Both synthetic polymers and sugar/peptide-based materials have been used to create such structures.

Single nanowires are desired as opposed to a random mat, which is usually obtained by electrospinning. The single wire configuration is necessary either for precise electrical read-out or to guarantee a certain signal density when these are integrated into a device. To overcome this, electrosynthesizing produces wires in between two electrodes, following the direction of the applied field. In this case, alignment is an immanent component of the production process. A strong drawback, however, is the limited lengths of these wires that are only up to tens of micrometers. Furthermore, the growth process is prone to a certain degree of unevenness, which can be controlled using confined growth channels. Incorporation of viruses into these wires during the growth process is possible, greatly enhancing the potential of this technique for diagnostic assays, as viruses can be engineered to exhibit different surface structures, e.g. specific antigens.

Another promising method of nanowire alignment is the dewetting of solutions on microstructured surfaces. This can either happen with a polymer solution forming nanowires connecting the microstructures during the process of dewetting or using a solution of already prepared nanowires, which then align into the desired pattern on the microstructure during dewetting. Of special interest would be a combination of this mass alignment dewetting process and the numerous possible materials to be gained from electrospinning: while electrospinning lacks a reliable single-wire alignment, it offers access to very promising materials, composites, and blends. In combination, both

techniques could well achieve a single nanowire configuration with possible electrical contacting.

For detection of biomolecules and microorganisms, approaches rely on the use of antibodies, aptamers (their synthetic equivalent), or DNA oligonucleotides. The strategy of incorporating specific viruses into the wire should also be mentioned in this context. The read-out of sensing setups often takes place in a two-step approach: adding a secondary antibody (label), which attaches to any bound target molecules and carries a fluorophore or an enzyme to catalyze a color reaction (known as sandwich immunoassay). Finally, it has been demonstrated that molecules or particles attached to the capture probes on the polymer-based nanowire are detectable using electrical conductivity readouts. Analyzing the frequency behavior (impedance spectroscopy), further advancements in terms of sensitivity might also be possible, but these aspects still remain to be investigated for polymeric nanowires. Further effort has to be made for evaluating the long-term stability of polymer nanowire-based sensors in the sense of shelf-life and storage.

REFERENCES

[1] H. Hubbe, E. Mendes, and P. E. Boukany, *Polymeric nanowires for diagnostic applications,* Micromachines **10** (2019).

[2] V. Z. Hardikurnia, *Detecting Mosquitoes-Borne Diseases in Indonesia: Opportunity Mapping & Strategic Roadmap Development for Nanowires-Based Diagnostic Tools,* Master's thesis, TU Delft (2017).

[3] D. S. Shepard, E. A. Undurraga, and Y. A. Halasa, *Economic and Disease Burden of Dengue in Southeast Asia,* PLoS Neglected Tropical Diseases **7**, e2055 (2013).

[4] C. Shan, X. Xie, P. Ren, M. J. Loeffelholz, Y. Yang, A. Furuya, A. P. Dupuis, L. D. Kramer, S. J. Wong, and P. Y. Shi, *A Rapid Zika Diagnostic Assay to Measure Neutralizing Antibodies in Patients,* EBioMedicine **17**, 157 (2017).

1

[5] O. Lupi, *Mosquito-Borne Hemorrhagic Fevers,* Dermatologic Clinics **29**, 33 (2011).

[6] D. A. Martin, D. A. Muth, T. Brown, A. J. Johnson, N. Karabatsos, and J. T. Roehrig, *Standardization of immunoglobulin M capture enzyme-linked immunosorbent assays for routine diagnosis of arboviral infections.* Journal of clinical microbiology **38**, 1823 (2000).

[7] J. Louten, *Virus structure and classification,* in *Essential Human Virology*, edited by J. Louten (Elsevier, 2016) pp. 19–29.

[8] S. M. Best, *Flaviviruses,* Current Biology **26**, R1258 (2016).

[9] A. C. Fredericks and A. Fernandez-Sesma, *The burden of dengue and Chikungunya worldwide: Implications for the Southern United States and California,* Annals of Global Health **80**, 466 (2014).

[10] S. Bhatt, P. W. Gething, O. J. Brady, J. P. Messina, A. W. Farlow, C. L. Moyes, J. M. Drake, J. S. Brownstein, A. G. Hoen, O. Sankoh, M. F. Myers, D. B. George, T. Jaenisch, G. R. W. Wint, C. P. Simmons, T. W. Scott, J. J. Farrar, and S. I. Hay, *The global distribution and burden of dengue,* Nature **496**, 504 (2013).

[11] G. A. Calvet, F. B. dos Santos, and P. C. Sequeira, *Zika virus infection,* Current Opinion in Infectious Diseases **29**, 459 (2016).

[12] L. R. Petersen, D. J. Jamieson, A. M. Powers, and M. A. Honein, *Zika Virus,* New England Journal of Medicine **374**, 1552 (2016).

[13] J. E. Staples, S. L. Hills, and A. M. Powers, *Chikungunya,* in *CDC Yellow Book 2018: Health Information for International Travel* (Oxford University Press, 2017).

[14] P. Shapshak, J. T. Sinnott, C. Somboonwit, and J. H. Kuhn, eds., *Global Virology I - Identifying and Investigating Viral Diseases* (Springer New York, New York, NY, 2015).

[15] J. Patterson, M. Sammon, and M. Garg, *Dengue, Zika and Chikungunya: Emerging Arboviruses in the New World,* Western Journal of Emergency Medicine **17**, 671 (2016).

[16] D. Bisanzio, F. Dzul-Manzanilla, H. Gomez-Dantés, N. Pavia-Ruz, T. J. Hladish, A. Lenhart, J. Palacio-Vargas, J. F. González Roldan, F. Correa-Morales, G. Sánchez-Tejeda, P. Kuri Morales, P. Manrique-Saide, I. M. Longini, M. E. Halloran, and G. M. Vazquez-Prokopec, *Spatio-temporal coherence of dengue, chikungunya and Zika outbreaks in Merida, Mexico,* PLOS Neglected Tropical Diseases **12**, e0006298 (2018).

[17] S. Leta, T. J. Beyene, E. M. De Clercq, K. Amenu, M. U. Kraemer, and C. W. Revie, *Global risk mapping for major diseases transmitted by Aedes aegypti and Aedes albopictus,* International Journal of Infectious Diseases **67**, 25 (2018).

[18] P. Horwood and P. Buchy, *Chikungunya,* Revue Scientifique et Technique de l'OIE **34**, 479 (2015).

[19] E. A. Mordecai, J. M. Cohen, M. V. Evans, P. Gudapati, L. R. Johnson, C. A. Lippi, K. Miazgowicz, C. C. Murdock, J. R. Rohr, S. J. Ryan, V. Savage, M. S. Shocket, A. S. Ibarra, M. B. Thomas, and D. P. Weikel, *Detecting the impact of temperature on transmission of zika, dengue, and chikungunya using mechanistic models,* PLOS Neglected Tropical Diseases **11**, e0005568 (2017).

[20] D. Tomasello and P. Schlagenhauf, *Chikungunya and dengue autochthonous cases in Europe, 2007-2012,* Travel Medicine and Infectious Disease **11**, 274 (2013).

[21] F. Bergmann, D. S. Trachsel, S. D. Stoeckle, J. B. Sierra, S. Lübke, M. H. Groschup, H. Gehlen, and U. Ziegler, *Seroepidemiological survey of west nile virus infections in horses from berlin/brandenburg and north rhine-westphalia, germany,* Viruses **14**, 243 (2022).

1

[22] E. J. Scholte, E. Dijkstra, H. Blok, A. De Vries, W. Takken, A. Hofhuis, M. Koopmans, A. De Boer, and C. B. Reusken, *Accidental importation of the mosquito Aedes albopictus into the Netherlands: A survey of mosquito distribution and the presence of dengue virus,* Medical and Veterinary Entomology **22**, 352 (2008).

[23] D. Paquet, L. Jung, H. Trawinski, S. Wendt, and C. Lübbert, *Fever in the returning traveler,* Deutsches Ärzteblatt international (2022).

[24] S. Beltrán-Silva, S. Chacón-Hernández, E. Moreno-Palacios, and J. Pereyra-Molina, *Clinical and differential diagnosis: Dengue, chikungunya and zika,* Revista Médica del Hospital General de México **81**, 146 (2018).

[25] M. C. Castro, M. E. Wilson, and D. E. Bloom, *Disease and economic burdens of dengue,* The Lancet Infectious Diseases **17**, e70 (2017).

[26] World Health Organization, *Special Programme for Research and Training in Tropical Diseases* (WHO, 2009) pp. x, 147.

[27] I. Mylonas, S. Dieterle, M. Hampl, U. B. Hoyme, J. Jückstock, W. Mendling, G. Neumann, and K. Friese, *Zika-Virus-Infektion in der Gynäkologie und Geburtshilfe,* Der Gynäkologe **49**, 786 (2016).

[28] K. Nielsen-Saines, P. Brasil, T. Kerin, Z. Vasconcelos, C. R. Gabaglia, L. Damasceno, M. Pone, L. M. A. de Carvalho, S. M. Pone, A. A. Zin, I. Tsui, T. R. S. Salles, D. C. da Cunha, R. P. Costa, J. Malacarne, A. B. Reis, R. H. Hasue, C. Y. P. Aizawa, F. F. Genovesi, C. Einspieler, P. B. Marschik, J. P. Pereira, S. L. Gaw, K. Adachi, J. D. Cherry, Z. Xu, G. Cheng, and M. E. Moreira, *Delayed childhood neurodevelopment and neurosensory alterations in the second year of life in a prospective cohort of ZIKV-exposed children,* Nature Medicine **25**, 1213 (2019).

[29] J. M. Mansuy, M. Dutertre, C. Mengelle, C. Fourcade, B. Marchou, P. Delobel,

J. Izopet, and G. Martin-Blondel, *Zika virus: high infectious viral load in semen, a new sexually transmitted pathogen?* The Lancet Infectious Diseases **16**, 405 (2016).

[30] M. G. Guzman, M. Alvarez, and S. B. Halstead, *Secondary infection as a risk factor for dengue hemorrhagic fever/dengue shock syndrome: an historical perspective and role of antibody-dependent enhancement of infection,* Archives of Virology **158**, 1445 (2013).

[31] K. M. Tomashek, T. M. Sharp, and H. S. Margolis, *Dengue,* in *CDC Yellow Book 2018: Health Information for International Travel* (Oxford University Press, 2017).

[32] S. D. Blacksell, *Commercial dengue rapid diagnostic tests for point-of-care application: Recent evaluations and future needs?* Journal of Biomedicine and Biotechnology **2012**, 1 (2012).

[33] N. H. Ahmed and S. Broor, *Comparison of NS1 antigen detection ELISA, real time RT-PCR and virus isolation for rapid diagnosis of dengue infection in acute phase.* Journal of vector borne diseases **51**, 194 (2014).

[34] C. Ohst, S. Saschenbrecker, K. Stiba, K. Steinhagen, C. Probst, C. Radzimski, E. Lattwein, L. Komorowski, W. Stöcker, and W. Schlumberger, *Reliable serological testing for the diagnosis of emerging infectious diseases,* in *Advances in Experimental Medicine and Biology*, Vol. 1062 (2018) pp. 19–43.

[35] Y.-c. Xia, Z.-h. Hu, Z.-j. Qiu, Z.-b. Ma, H.-l. Wang, and F. Deng, *An improved culture system for virus isolation and detection,* Virologica Sinica **23**, 345 (2008).

[36] W. Luttmann, K. Bratke, M. Küpper, and D. Myrtek, *Der Experimentator: Immunologie* (Springer Berlin Heidelberg, Berlin, Heidelberg, 2014).

[37] L. L. Hermann, B. Thaisomboonsuk, Y. Poolpanichupatam, R. G. Jarman, S. Kalayanarooj, A. Nisalak, I.-K. Yoon, and S. Fernandez, *Evaluation of a Dengue NS1 Antigen*

Detection Assay Sensitivity and Specificity for the Diagnosis of Acute Dengue Virus Infection, PLoS Neglected Tropical Diseases **8**, e3193 (2014).

[38] S. J. Wong, A. Furuya, J. Zou, X. Xie, A. P. Dupuis, L. D. Kramer, and P. Y. Shi, *A Multiplex Microsphere Immunoassay for Zika Virus Diagnosis*, EBioMedicine **16**, 136 (2017).

[39] S. Shukla, S.-Y. Hong, S. H. Chung, and M. Kim, *Rapid Detection Strategies for the Global Threat of Zika Virus: Current State, New Hypotheses, and Limitations*, Frontiers in Microbiology **7**, 1 (2016).

[40] K. J. Livak, S. J. Flood, J. Marmaro, W. Giusti, and K. Deetz, *Oligonucleotides with fluorescent dyes at opposite ends provide a quenched probe system useful for detecting PCR product and nucleic acid hybridization.* Genome Research **4**, 357 (1995).

[41] H.-P. Tsai, Y.-Y. Tsai, I.-T. Lin, P.-H. Kuo, K.-C. Chang, J.-C. Chen, W.-C. Ko, and J.-R. Wang, *Validation and Application of a Commercial Quantitative Real-Time Reverse Transcriptase- PCR Assay in Investigation of a Large Dengue Virus Outbreak in Southern Taiwan*, PLOS Neglected Tropical Diseases **10**, e0005036 (2016).

[42] T. Laue, P. Emmerich, and H. Schmitz, *Detection of dengue virus RNA in patients after primary or secondary dengue infection by using the TaqMan automated amplification system.* Journal of clinical microbiology **37**, 2543 (1999).

[43] A. E. Calvert, B. J. Biggerstaff, N. A. Tanner, M. Lauterbach, and R. S. Lanciotti, *Rapid colorimetric detection of Zika virus from serum and urine specimens by reverse transcription loop-mediated isothermal amplification (RT-LAMP)*, PLOS ONE **12**, e0185340 (2017).

[44] A. Priye, S. W. Bird, Y. K. Light, C. S. Ball, O. A. Negrete, and R. J. Meagher, *A smartphone-based diagnostic platform for rapid detection of Zika, chikungunya, and dengue viruses*, Scientific Reports **7**, 44778 (2017).

[45] M. M. Parida, S. R. Santhosh, P. K. Dash, N. K. Tripathi, V. Lakshmi, N. Mamidi, A. Shrivastva, N. Gupta, P. Saxena, J. P. Babu, P. V. L. Rao, and K. Morita, *Rapid and real-time detection of Chikungunya virus by reverse transcription loop-mediated isothermal amplification assay.* Journal of clinical microbiology **45**, 351 (2007).

[46] S. J. Thomas, A. Nisalak, K. B. Anderson, D. H. Libraty, S. Kalayanarooj, D. W. Vaughn, R. Putnak, R. V. Gibbons, R. Jarman, and T. P. Endy, *Dengue plaque reduction neutralization test (PRNT) in primary and secondary dengue virus infections: How alterations in assay conditions impact performance.* The American journal of tropical medicine and hygiene **81**, 825 (2009).

[47] L. C. Garfunkel, J. M. Kaczorowski, and C. Christy, *Pediatric Clinical Advisor* (Elsevier, 2007).

[48] P. Dussart, B. Labeau, P. Louis, M. R. T. Nunes, S. G. Rodrigues, R. Cesaire, J. Morvan, M. Flamand, and L. Baril, *Evaluation of an Enzyme Immunoassay for Detection of Dengue Virus NS1 Antigen in Human Serum,* Clinical and Vaccine Immunology **13**, 1185 (2006).

[49] K. Steinhagen, N. Wilhelm, J. M. Warnecke, and W. Schlumberger, *Testing anti-Zika virus NS1 IgA additionally to IgM increases sensitivity in acutely infected patients from regions endemic for flaviviruses,* in *Proceedings 8th International Congress on Infectious Diseases (ICID)*, March (Buenos Aires, 2018).

[50] L. Heinrich, N. Tissot, D. J. Hartmann, and R. Cohen, *Comparison of the results obtained by ELISA and surface plasmon resonance for the determination of antibody affinity,* Journal of Immunological Methods **352**, 13 (2010).

[51] Z. Wang, S. Lee, K. Koo, and K. Kim, *Nanowire-Based Sensors for Biological and Medical Applications,* IEEE Transactions on NanoBioscience **15**, 186 (2016).

[52] K. Zhang, P. J. Glazer, L. Jennings, S. Vedaraman, S. Oldenhof, Y. Wang, F. Schosseler, J. H. van Esch, and E. Mendes, *A facile approach for the fabrication of 2D supermicelle networks,* Chem. Commun. **52**, 12360 (2016).

[53] M. C. Roco, C. A. Mirkin, and M. C. Hersam, *Nanotechnology research directions for societal needs in 2020: summary of international study,* Journal of Nanoparticle Research **13**, 897 (2011).

[54] F. Patolsky, G. Zheng, and C. M. Lieber, *Nanowire sensors for medicine and the life sciences,* Nanomedicine **1**, 51 (2006).

[55] F. Patolsky, G. Zheng, and C. M. Lieber, *Nanowire-Based Biosensors,* Analytical Chemistry **78**, 4260 (2006).

[56] D. P. Tran, T. T. T. Pham, B. Wolfrum, A. Offenhäusser, and B. Thierry, *CMOS-compatible silicon nanowire field-effect transistor biosensor: Technology development toward commercialization,* Materials **11** (2018).

[57] V. Cimalla, *Label-Free Biosensors Based on III-Nitride Semiconductors,* in *Label-Free Biosensing,* 16, edited by M. Schöning and A. Poghossian (Springer, 2017) pp. 59–102.

[58] C.-M. Tîlmaciu and M. C. Morris, *Carbon nanotube biosensors,* Frontiers in Chemistry **3**, 1 (2015).

[59] N. Yang, X. Chen, T. Ren, P. Zhang, and D. Yang, *Carbon nanotube based biosensors,* Sensors and Actuators B: Chemical **207**, 690 (2015).

[60] S. Chen, Y. Tang, K. Zhan, D. Sun, and X. Hou, *Chemiresistive nanosensors with convex/concave structures,* Nano Today **20**, 84 (2018).

[61] M. H. Naveen, N. G. Gurudatt, and Y. B. Shim, *Applications of conducting polymer composites to electrochemical sensors: A review,* Applied Materials Today **9**, 419 (2017).

[62] L. Rems, D. Kawale, L. J. Lee, and P. E. Boukany, *Flow of DNA in micro/nanofluidics: From fundamentals to applications,* Biomicrofluidics **10**, 043403 (2016).

[63] M. Rubenstein and R. H. Colby, *Polymer physics* (Oxford University Press, Oxford, 2003).

[64] G. Yang, X. Li, Y. He, J. Ma, G. Ni, and S. Zhou, *From nano to micro to macro: Electrospun hierarchically structured polymeric fibers for biomedical applications,* Progress in Polymer Science **81**, 80 (2018).

[65] J. Y. Lee, T.-H. Kang, J. H. Choi, I.-S. Choi, and W.-R. Yu, *Improved electrical conductivity of poly(ethylene oxide) nanofibers using multi-walled carbon nanotubes,* AIP Advances **8**, 035024 (2018).

[66] B. D. Malhotra and M. A. Ali, *Biopolymeric Nanostructures,* in *Nanomaterials for Biosensors* (Elsevier, 2018) pp. 127–144.

[67] S. J. Reinholt, A. Sonnenfeldt, A. Naik, M. W. Frey, and A. J. Baeumner, *Developing new materials for paper-based diagnostics using electrospun nanofibers,* Analytical and Bioanalytical Chemistry **406**, 3297 (2013).

[68] D. Çam and H. A. Öktem, *Optimizations needed for lateral flow assay for rapid detection of pathogenic E. coli,* Turkish Journal of Biology **41**, 954 (2017).

[69] M. S. Suria, A. T. Mohd Afendy, M. Noor Azlina, and I. Zamri, *Lateral flow assay strip for detection of Escherichia coli O157:H7,* International Food Research Journal **22**, 2587 (2015).

[70] S. J. Lee, R. Tatavarty, and M. B. Gu, *Electrospun polystyrene–poly(styrene-co-maleic anhydride) nanofiber as a new aptasensor platform,* Biosensors and Bioelectronics **38**, 302 (2012).

[71] Y. Liu, X. Zhang, Y. Xia, and H. Yang, *Magnetic-Field-Assisted Electrospinning of Aligned Straight and Wavy Polymeric Nanofibers*, Advanced Materials **22**, 2454 (2010).

[72] P. Kiselev and J. Rosell-Llompart, *Highly aligned electrospun nanofibers by elimination of the whipping motion*, Journal of Applied Polymer Science **125**, 2433 (2012).

[73] A. Thiha, F. Ibrahim, S. Muniandy, I. J. Dinshaw, S. J. Teh, K. L. Thong, B. F. Leo, and M. Madou, *All-carbon suspended nanowire sensors as a rapid highly-sensitive label-free chemiresistive biosensing platform*, Biosensors and Bioelectronics **107**, 145 (2018).

[74] H. Zheng and X. Shen, *Design and control of a pneumatically actuated transtibial prosthesis*, Journal of Bionic Engineering **12**, 217 (2015).

[75] Q. Tian, C. Fei, H. Yin, and Y. Feng, *Stimuli-Responsive Polymer Wormlike Micelles*, Progress in Polymer Science (2018).

[76] L. Jennings, G. Waton, F. Schosseler, and E. Mendes, *Towards a rational morphology control of frozen copolymer aggregates*, Soft Matter **13**, 6090 (2017).

[77] K. Zhang, A. Suratkar, S. Vedaraman, V. Lakshminarayanan, L. Jennings, P. J. Glazer, J. H. van Esch, and E. Mendes, *Two Robust Strategies toward Hydrogels from Quenched Block Copolymer Nanofibrillar Micelles*, Macromolecules **51**, 5788 (2018).

[78] Y. Liu, Y. Zhang, Z. Wang, J. Wang, K. Wei, G. Chen, and M. Jiang, *Building Nanowires from Micelles: Hierarchical Self-Assembly of Alternating Amphiphilic Glycopolypeptide Brushes with Pendants of High-Mannose Glycodendron and Oligophenylalanine*, Journal of the American Chemical Society **138**, 12387 (2016).

[79] P. J. Glazer, L. Bergen, L. Jennings, A. J. Houtepen, E. Mendes, and P. E. Boukany,

Generating Aligned Micellar Nanowire Arrays by Dewetting of Micropatterned Surfaces, Small **10**, 1729 (2014).

[80] J. Zhu and R. C. Hayward, *Spontaneous Generation of Amphiphilic Block Copolymer Micelles with Multiple Morphologies through Interfacial Instabilities,* Journal of the American Chemical Society **130**, 7496 (2008).

[81] X. Nie, J. Cui, and W. Jiang, *Ultralong cylindrical micelles precisely located with semiconductor nanorods by solvent evaporation-driven self-assembly,* Soft Matter **10**, 8051 (2014).

[82] L. Atanase and G. Riess, *Self-Assembly of Block and Graft Copolymers in Organic Solvents: An Overview of Recent Advances,* Polymers **10**, 62 (2018).

[83] Z. Ahmad, A. Shah, M. Siddiq, and H.-B. Kraatz, *Polymeric micelles as drug delivery vehicles,* RSC Adv. **4**, 17028 (2014).

[84] W. Xu, P. Ling, and T. Zhang, *Polymeric Micelles, a Promising Drug Delivery System to Enhance Bioavailability of Poorly Water-Soluble Drugs,* Journal of Drug Delivery **2013**, 1 (2013).

[85] S. S. Kulthe, Y. M. Choudhari, N. N. Inamdar, and V. Mourya, *Polymeric micelles: authoritative aspects for drug delivery,* Designed Monomers and Polymers **15**, 465 (2012).

[86] H. K. Cho, I. W. Cheong, J. M. Lee, and J. H. Kim, *Polymeric nanoparticles, micelles and polymersomes from amphiphilic block copolymer,* Korean Journal of Chemical Engineering **27**, 731 (2010).

[87] K. Nakashima and P. Bahadur, *Aggregation of water-soluble block copolymers in aqueous solutions: Recent trends,* Advances in Colloid and Interface Science **123-126**, 75 (2006).

[88] B. Su, Y. Tian, and L. Jiang, *Bioinspired Interfaces with Superwettability: From Materials to Chemistry,* Journal of the American Chemical Society **138**, 1727 (2016).

[89] B. Su, Y. Wu, and L. Jiang, *The art of aligning one-dimensional (1D) nanostructures,* Chemical Society Reviews **41**, 7832 (2012).

[90] H. Fang, D. Yuan, R. Guo, S. Zhang, R. P. S. Han, S. Das, and Z. L. Wang, *Fabrication of Patterned Polymer Nanowire Arrays,* ACS Nano **5**, 1476 (2011).

[91] H. Fang, W. Wu, J. Song, and Z. L. Wang, *Controlled Growth of Aligned Polymer Nanowires,* The Journal of Physical Chemistry C **113**, 16571 (2009).

[92] J. R. Morber, X. Wang, J. Liu, R. L. Snyder, and Z. L. Wang, *Wafer-Level Patterned and Aligned Polymer Nanowire/Micro- and Nanotube Arrays on any Substrate,* Advanced Materials **21**, 2072 (2009).

[93] A. Vlad, C. A. Dutu, P. Jedrasik, U. Södervall, J. F. Gohy, and S. Melinte, *Vertical single nanowire devices based on conducting polymers,* Nanotechnology **23**, 025302 (2012).

[94] J.-W. Jeon, J.-H. Kim, J.-M. Lee, W.-H. Lee, D.-Y. Lee, and S.-H. Paek, *Rapid immuno-analytical system physically integrated with lens-free CMOS image sensor for food-borne pathogens.* Biosensors & bioelectronics **52**, 384 (2014).

[95] W. Y. Hong, S. H. Jeon, E. S. Lee, and Y. Cho, *An integrated multifunctional platform based on biotin-doped conducting polymer nanowires for cell capture, release, and electrochemical sensing,* Biomaterials **35**, 9573 (2014).

[96] J. Guan, B. Yu, and L. J. Lee, *Forming highly ordered arrays of functionalized polymer nanowires by dewetting on micropillars,* Advanced Materials **19**, 1212 (2007).

[97] C. H. Lin, J. Guan, S. W. Chau, S. C. Chen, and L. J. Lee, *Patterning nanowire and micro-/nanoparticle array on micropillar-structured surface: Experiment and modeling,* Biomicrofluidics **4**, 034103 (2010).

[98] B. Su, S. Wang, J. Ma, Y. Wu, X. Chen, Y. Song, and L. Jiang, *Elaborate Positioning of Nanowire Arrays Contributed by Highly Adhesive Superhydrophobic Pillar-Structured Substrates,* Advanced Materials **24**, 559 (2012).

[99] B. Su, S. Wang, Y. Wu, X. Chen, Y. Song, and L. Jiang, *Small molecular nanowire arrays assisted by superhydrophobic pillar-structured surfaces with high adhesion,* Advanced Materials **24**, 2780 (2012).

[100] P. J. Glazer, Q. Warringa, L. Bergen, and P. E. Boukany, *Affordable techniques for fabricating large array of functional nanowires: From DNA to micellar systems,* 2015 37th Annual International Conference of the IEEE Engineering in Medicine and Biology Society (EMBC) , 2187 (2015).

[101] Z. Jahed, H. Shahsavan, M. S. Verma, J. L. Rogowski, B. B. Seo, B. Zhao, T. Y. Tsui, F. X. Gu, and M. R. K. Mofrad, *Bacterial Networks on Hydrophobic Micropillars,* ACS Nano **11**, 675 (2017).

[102] B. Kannan, D. E. Williams, C. Laslau, and J. Travas-Sejdic, *A highly sensitive, label-free gene sensor based on a single conducting polymer nanowire,* Biosensors and Bioelectronics **35**, 258 (2012).

[103] Y. Hu, H. Lee, S. Kim, and M. Yun, *A highly selective chemical sensor array based on nanowire/nanostructure for gas identification,* Sensors and Actuators, B: Chemical **181**, 424 (2013).

[104] J. A. Arter, D. K. Taggart, T. M. McIntire, R. M. Penner, and G. A. Weiss, *Virus-PEDOT Nanowires for Biosensing,* Nano Letters **10**, 4858 (2010).

[105] J.-O. Lee, H.-M. So, E.-K. Jeon, H. Chang, K. Won, and Y. H. Kim, *Aptamers as molecular recognition elements for electrical nanobiosensors,* Analytical and Bioanalytical Chemistry **390**, 1023 (2008).

1

[106] A. Garcia-Cruz, M. Lee, N. Zine, M. Sigaud, P. Marote, M. Lopez, J. Bausells, N. Jaffrezic-Renault, and A. Errachid, *Biopatterning of antibodies on poly(pyrrole)-nanowires using nanocontact printing: Surface characterization,* Materials Science and Engineering: C **91**, 466 (2018).

[107] B. Zhu, O. A. Alsager, S. Kumar, J. M. Hodgkiss, and J. Travas-Sejdic, *Label-free electrochemical aptasensor for femtomolar detection of 17β-estradiol,* Biosensors and Bioelectronics **70**, 398 (2015).

[108] S. Wang, K. Liu, J. Liu, Z. T.-F. Yu, X. Xu, L. Zhao, T. Lee, E. K. Lee, J. Reiss, Y.-K. Lee, L. W. K. Chung, J. Huang, M. Rettig, D. Seligson, K. N. Duraiswamy, C. K.-F. Shen, and H.-R. Tseng, *Highly Efficient Capture of Circulating Tumor Cells by Using Nanostructured Silicon Substrates with Integrated Chaotic Micromixers,* Angewandte Chemie International Edition **50**, 3084 (2011).

[109] Y.-T. Lu, L. Zhao, Q. Shen, M. A. Garcia, D. Wu, S. Hou, M. Song, X. Xu, W.-H. OuYang, W. W.-L. OuYang, J. Lichterman, Z. Luo, X. Xuan, J. Huang, L. W. Chung, M. Rettig, H.-R. Tseng, C. Shao, and E. M. Posadas, *NanoVelcro Chip for CTC enumeration in prostate cancer patients,* Methods **64**, 144 (2013).

[110] J. Chen, J. Li, and Y. Sun, *Microfluidic approaches for cancer cell detection, characterization, and separation,* Lab on a Chip **12**, 1753 (2012).

[111] T. J. Kim and C. Hidrovo, *Pressure and partial wetting effects on superhydrophobic friction reduction in microchannel flow,* Physics of Fluids **24**, 112003 (2012).

[112] L. Nan, Z. Jiang, and X. Wei, *Emerging microfluidic devices for cell lysis: a review,* Lab on a Chip **14**, 1060 (2014).

[113] S.-S. Chang, H.-L. Hsu, J.-C. Cheng, and C.-P. Tseng, *An Efficient Strategy for Broad-Range Detection of Low Abundance Bacteria without DNA Decontamination of PCR Reagents,* PLoS ONE **6**, e20303 (2011).

[114] D. I. Walsh, D. S. Kong, S. K. Murthy, and P. A. Carr, *Enabling Microfluidics: from Clean Rooms to Makerspaces,* Trends in Biotechnology **35**, 383 (2017).

[115] Y. Temiz, R. D. Lovchik, G. V. Kaigala, and E. Delamarche, *Lab-on-a-chip devices: How to close and plug the lab?* Microelectronic Engineering **132**, 156 (2015).

[116] J. Li, Y. Wang, E. Dong, and H. Chen, *USB-driven microfluidic chips on printed circuit boards,* Lab on a Chip **14**, 860 (2014).

[117] D. Webb, D. Hutt, N. Hopkinson, P. Conway, and P. Palmer, *Packaging of Microfluidic Devices for Fluid Interconnection Using Thermoplastics,* Journal of Microelectromechanical Systems **18**, 354 (2009).

[118] S. van den Driesche, F. Lucklum, F. Bunge, and M. Vellekoop, *3D Printing Solutions for Microfluidic Chip-To-World Connections,* Micromachines **9**, 71 (2018).

[119] M. B. Dentry, J. R. Friend, and L. Y. Yeo, *Continuous flow actuation between external reservoirs in small-scale devices driven by surface acoustic waves,* Lab Chip **14**, 750 (2014).

[120] S. Waheed, J. M. Cabot, N. P. Macdonald, T. Lewis, R. M. Guijt, B. Paull, and M. C. Breadmore, *3D printed microfluidic devices: enablers and barriers,* Lab on a Chip **16**, 1993 (2016).

[121] M. Jamal, A. M. Zarafshar, and D. H. Gracias, *Differentially photo-crosslinked polymers enable self-assembling microfluidics,* Nature Communications **2**, 527 (2011).

2

BIFUNCTIONAL MICELLAR

NANOWIRES

All models are wrong

but some are useful.

George Edward Pelham Box [1]

The construction of self-assembled nanowires based on a simple formulation, bio-compatibility, and their accessibility for bio-chemical decoration with relevant bio-molecules is a challenge. A mix of native, methacrylate (MA)- and azide (Az)-modified PS-b-PEO was created to produce click chemistry-compatible micellar nanowires for bioconjugation. The two functional groups can be used independently to link to a surface and a biocomponent. A simple dewetting approach on micro-patterned surfaces allows to arrange wires in structured arrays. The azide end-group was added to the PEO part, using a two-step reaction involving methanesulfonyl chloride as an intermediate. The azide group was chosen, as its small size should not interfere significantly with the micelle self-assembly behaviour of the much larger polymer chains. Nanowires of up to $100\,\mu m$ length and more could be obtained after addition of the azide end-group.

Our simple approach offers a modular platform in programming the micellar nanowires by decorating them with several functional-molecules for bio-sensing and bio-separation applications.

2.1. INTRODUCTION

Functionalization of nanowires with biomolecular targets provides biofunctionality and allows interaction with relevant molecules, that enables to detect specific biomarkers as a bio-sensing platform. Being one-dimensional (1D) nanostructures, nanowires show distinct features not available in the respective bulk material [2, 3]. Polymeric nanowires, in particular, have become essential in several biomedical applications such as drug delivery and bio-sensing, making use of the manifold materials and well-established (bio)chemical modifications available [4, 5].

When several chemical modifications and precise placement of the nanowires are needed, however, synthesis is often complicated and costly. [6]

And depending on the process and the materials used, the number and length of the polymeric nanowires that can be created differ. How do we currently synthesize polymeric nanowires, and which properties are desired for bio-sensing applications?

(1) Electrospinning [7] yields large quantities of very long wires (mm and cm regime [7, 8]); *(2)* Electrosynthesis [9, 10], allows precise positioning and electrical contacting of the nanowire by the placement of the electrodes, however, has limitations in the number and length of nanowires; *(3)* Worm like micelles yield high numbers of long wires with a simple setup but are susceptible to changes in monomer composition [11].

How do we place the wires in a specific orientation? Controlled positioning can be required to achieve well-defined structures, optical signal patterns, or electrical contact. Known methods include the use of magnetic or electric fields, requiring external application of the fields. The application of magnetic fields is limited in polymeric materials, as ferromagnetic properties would be required. Addition of Fe_3O_4 nanoparticles has been utilized to achieve this, although it was shown in a case of electrospinning, Lorentz force on the wires can be sufficient for alignment without magnetic additives. [12, 13]

Electric fields are a possibility, as was shown with electrosynthesis, but microelectrodes and external appliances are needed, limiting number and dimension of nanowires

and complicating the setup. To tackle this problem, flow-guided patterned surfaces were developed. A variety of dewetting techniques on different microstructures have been demonstrated [14–16]. This way, many nanowires can be positioned in one batch, if required. In combination with contact printing and functionalized surfaces, this offers a simple way of precise localization of many nanowires, including their attached functions, such as binding sites for analytes or attached biomolecules and other compounds. [2, 17]

For sensing applications, especially biological, a specific modification is often required to functionalize the nanowire. Polymers are accessible to a vast number of known chemical modifications. These modifications can occur in pre- and post-processing, before and after creation of the actual nanowire. While especially in the case of micelles, post-processing is rather limited by the thermal and physical stability of the wire, pre-processing can disable the self-assembly behaviour.

This chapter presents a synthesis method for polymeric self-assembling micellar nanowires to overcome these limitations. Our approach allows separate modification of the native polymer before wire-growth and subsequent decoration. The technique offers a modular system by mixing polymers with different, self-assembly compatible end groups before micelle creation. Using click-chemistry, the stable nanowires can be modified with end groups that would have otherwise interfered with the assembly. High numbers and lengths of 100 µm and more can be achieved using this simple immiscible solvent process. Our method makes it possible, to manufacture a multi-functional large nanowire array outside a cleanroom environment using microgrid dewetting and contact printing.

Our micellar nanowires can be modified with two functional groups without hindering self-assembly. In this way, both a fixation on a substrate and the addition of a bio-orthogonal binding site for biomolecules can be performed. These micellar nanowires can capture large biomolecules such as streptavidin and allow fixation through methacrylate end groups. The amount of available binding sites was sufficient to immobilize

microbeads. Concerning the click-chemistry, both copper(I)-catalyzed alkyne-azide cycloaddition (CuAAC [18–20]) and (copper-free) strain promoted alkyne azide cycloaddition (spAAC) [21] can be used. This is of importance, as copper ions can inhibit biochemical reactions and thus limit compatibility with future applications. For this reason all tests except initial fluorophor linking were carried out using spAAC with dibenzocyclooctyne (DBCO) as the azide reactive group. Adding different binding sites and other biomolecules, such as antibodies, is a feasible next step. There are possible applications in delivery of drugs, capture of pathogens or organized placement of biomolecules such as proteins. Using polymeric nanowires allows access to the versatile toolbox of organic chemistry and eases the adaptability to other linker systems, if necessary.

2.2. MATERIALS AND METHODS

2.2.1. POLYMER MODIFICATION AND SYNTHESIS OF MICELLAR NANOWIRES

METHACRYLATE PS-b-PEO

PS-b-PEO (0.5 g, 0.02 mmol) was dissolved in 20 mL tetrahydrofuran (THF) and Et_3N (triethylamine, 1.95 mL, 14 mmol). Next, methacryloyl chloride (1.27 mL, 13 mmol) was added drop wise, and the mixture was stirred for 24 hours at room temperature. Afterwards, the product was centrifuged three times (12 500 rcf, 15 min) and decanted to remove the salt. The polymer solution was precipitated into heptane, filtered on paper, and thoroughly washed with ethanol, then dried in a vacuum oven at 40 °C (adapted from [16]).

AZIDE PS-b-PEO

The modification is performed in two steps:

(1) PS-b-PEO (0.5 g, 0.02 mmol) was dissolved in THF (20 mL), kept under argon atmosphere and Et_3N (1.25 mL, 9 mmol) was added. While stirring on ice, methanesulfonyl

chloride (700 μL, 9 mmol was added drop wise. The ice bath was removed and the reaction was stirred for 4 hours at room temperature. The product was centrifuged, decanted, precipitated in heptane, filtered and washed with ethanol and dried in vacuum oven (40 °C), obtaining the mesylated PS-b-PEO as a white powder.

(2) Obtained Me-PS-b-PEO was dissolved in 20 mL dimethylformamide (DMF). Kept under argon atmosphere, NaN_3 (0.1 g, 1.5 mmol) was added and stirred at 80 °C for 5 hours. The product was centrifuged three times (12 500 rcf, 15 min) and decanted to remove salt slurry. The DMF was removed under vacuum, product dissolved in THF and precipitated in heptane, followed by filtration, washing with ethanol and drying in vacuum oven (40 °C).

PS-b-PEO self assembly

Respective proportions of native, methacrylated and azide-modified PS-b-PEO were dissolved in chloroform (total 10 mg/mL) and mixed with DiI dye (0.2 wt%). For methacrylate micelles, 10 wt% MA polymer was used, for mixed MA/Az micelles proportions were 9 wt% methacrylated and 1 wt% azide-modified polymer.

100 μL of the solution were pipetted onto the bottom of a sealed glass vessel containing 2.3 mL DI water and stirred overnight with a glass stirring rod (300 rpm). Lid was then removed to allow evaporation of chloroform and watery nanowire solution was obtained (adapted from [11, 22]).

Fixation of nanowires on a glass substrate

Nanowires were fixed to a glass surface as previously demonstrated (see Figure 2.1) [15, 23]: lithium phenyl-2,5,6 trimethyl benzoyl phosphite (LAP), 5 mg/mL) was added to watery nanowire solution and either pipetted directly onto methacrylate covered glass or stretched on a PDMS microstructure and then contact printed to the glas. The nanowires were crosslinked to the surface using UV light (10 min, 365 nm, 40 W, 10 cm below source). Methacrylated glass was obtained through plasma activation and reaction with fumes of 3-(Trichlorosilyl)propyl methacrylate.
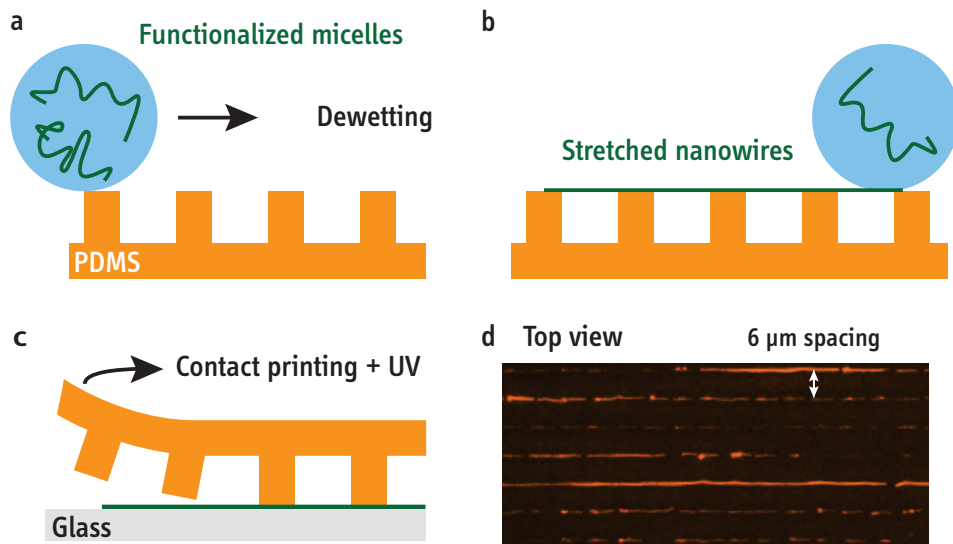
Figure 2.1: Schematic of stretching and printing process with micellar nanowires: a) Solution of assembled micellar nanowires was deposited on microstructured PDMS stamp. b) Dragging the solution across the microstructure stretches the nanowires into direction of droplet movement, adhering to the PDMS during dewetting. c) Contact printing transfers the stretched nanowires to methacrylated glass surface d) Creating a linear array of single nanowires, which are bonded through the methacrylate end groups activated using UV irradiation and added LAP photoinitiator.

2.2.2. Characterisation of binding sites

Click chemistry

Using CuAAC, $400\,\mu$L phosphate-buffered saline (PBS) (pH 7.4) containing $60\,\mu$M Alkyne-Alexafluor488, 0.1 mM copper(II) sulfate and 5 mM sodium ascorbate were pipetted onto glass slides with previously crosslinked nanowires. Incubation at room temperature for 4 hours followed, then rinsing with water from wash bottle.

Binding of Large Biomolecules: Streptavidin-Fluorescin

To investigate the linking to large biomolecules, streptavidin-fluorescein isothiocyanate (FITC) conjugates were linked to the nanowires: Mixed native/methacrylate/azide-PS-b-PEO nanowires were cross linked to the methacrylated glass substrate using LAP (1 mg/mL) and subsequently reacted with DBCO-sulfo-biotin ($30\,\mu$M in PBS (1x, pH 7.4), 4 hours,

room temperature). Streptavidin-FITC (8 μg/mL in PBS) was added and washed with buffer after 1 hour of incubation.

CAPTURE OF BIO-CONJUGATED MICROBEADS

Nanowires were stretched, fixed on glass in cell chambers (μ-slide 4-well, Ibidi) and biotinylated as in previous section. 500 μL 1x PBS 0.1 % Tween 20 containing 1 μL of 2 μm – 2.9 μm streptavidin coated polystyrene microbeads (SVP-20-5, 5 % w/v, Spherotec) was added to each chamber and after settling overnight washed with same buffer through gentle pipetting. Five different wire prints each were examined in different areas for microbeads using an inverted fluorescence microscope (total of 25 subsets scanned azide-modified, 80 non-modified).

2.3. RESULTS AND DISCUSSION

2.3.1. BIFUNCTIONAL MICELLAR PS-B-PEO NANOWIRES

The azide group was selected for this modification, with the intent to add a rather small molecule of low polarity to not disrupt the self-assembly process, while enabling further modification after formation of the micelles.

To confirm the ability of the mixed modified polymer to self-assemble into nanowires, TEM images were taken (Figure 2.2). The results confirm, that nanowire self-assembly of polymer modified with both methacrylate and azide end groups is possible and both modifications are available as linking groups on the grown nanowire. The used proportions of native and modified polymer (9 wt% methacrylated, 1 wt% azide-modified polymer) yield wires of similar length compared to native PS-b-PEO wires.

The azide group as such has already been used as a bioorthogonal linker to bind biocomponents outfitted with azide specific linkers such as alkyne and DBCO [20, 24, 25]. The use of DBCO can be advantageous if subsequent steps are incompatible with copper. Access to other linker systems are possible using bifunctional linkers after micelle

self-assembly, as demonstrated in following results. This approach allows subsequent modifications of the nanowire that otherwise would inhibit the micelle formation.
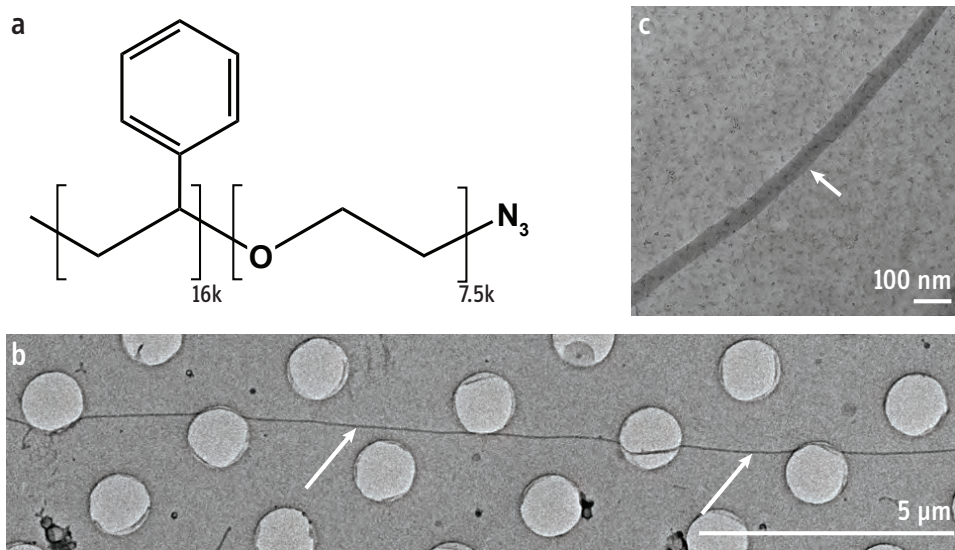
Figure 2.2: a) Chemical structure of azide modified PS-b-PEO polymer with respective number average molecular weight M_n; b) TEM image of azide-PS-b-PEO micellar nanowire; c) TEM image of nanowire in very high magnification shows diameter of ~50 nm.

2.3.2. Analysis of azide binding sites

fourier-transform infrared spectroscopy (FT-IR) analysis indicated a successful modification (see sup. Figure 2.9). Additionally, a variety of linkers were used to directly show the abundance of available azide modified binding sites, as shown in the following.

However, nuclear magnetic resonance (NMR) testing of the azide-modified polymer was more difficult. As discussed by Semple et al. [26], the PEG signals in standard proton scans overlap azide peaks too much to be distinct and used as proof of successful modification (see Figure 2.12). However, using ^{15}N-^{1}H heteronuclear multiple bond correlation (HMBC) (heteronuclear multiple bond correlation) scans we were able to show two long range H-N couplings (Figure 2.13). They correlate well with the relative shift of Me$-$N$_3$ δ^{15}N(1) and δ^{15}N(2) values presented by Wrackmeyer [27]. The 61 MHz ^{15}N NMR

HMBC spectrum of PS-b-PEO, was obtained from a THF-d_8 solution (0.6 mL) at 24 °C, using a Bruker Avance 600 spectrometer, after 93 h. The 2D spectrum was acquired using 128 scans and 700 increments (FIDs). An additional ^{13}C scan shows a signal correlating well with a CH_2-N_3 detectable in benzyl azide (see Figure 2.14). This again indicates the presence of an azide group on the polymer.

^{1}H NMR (600 MHz, THF-d_8)

δ(ppm) = 7.25 - 6.82 (m, 154H, ortho-, para-C**H**-styrol-ring),

6.80 – 6.32 (m, 100H, meta-C**H**-styrol-ring),

3.56 (d, **J** = 1.3 Hz, 236H, PEG-C**H**$_2$),

2.21 - 1.76 (m, 52H, C**H**CH$_2$-styrol-backbone),

1.68 - 1.18 (m, 111H, CHC**H**$_2$-styrol-backbone).

H-N HMBC (^{15}N) NMR (600/61 MHz, THF-d$_8$, unreferenced)

δ(ppm) = 248.8 (CH$_2$**N**NN), 68.3 (CH$_2$N**N**N)

^{13}C NMR (151 MHz, THF-d_8)

δ(ppm) = 51.7 (**C**H$_2$NNN)

Signals of ^{15}N would be enhanced using ^{15}N enriched azide in the modification of the polymer. However, NMR testing of this modification using ^{13}C and especially ^{15}N is very time-consuming and FT-IR in combination with fluorophor attachment both sufficiently proofs the successful modification and additionally its availability for linking reactions.

CuAAC click chemistry

Two fluorophores (DiI, Alexafluor488-Alkyne) were used to investigate the micelles' basic functionality. DiI, due to its hydrophobic character, is incorporated into the micelle core during wire growth, while Alexafluor488 is crosslinked via the alkyne to the azide moieties on the wire's corona after wire growth. In this way, both nanowire core and active binding sites can be observed. Figure 2.3 and Figure 2.4 show composite images for
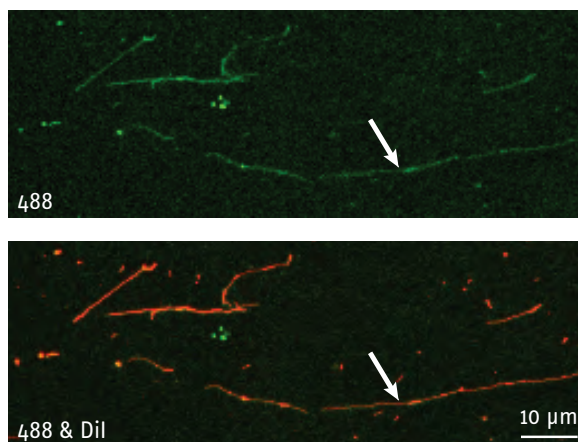
Figure 2.3: Confocal image of unstretched methacrylate/azide-modified PS-b-PEO nanowires linked to alkyne-Alexafluor488 through CuAAC click reaction. Compound picture with red fluorescence from hydrophobic DiI incorporated in micelle cores shows good overlap of both signals.

randomly deposited and stretched and printed nanowires of their red DiI (exc. 550 nm, emi. 564 nm) and green Alexafluor488 fluorescence (exc. 490 nm, emi. 525 nm). There is mostly coinciding fluorescence (orange) to be seen along the nanowire structures, indicating the wires have gained ability to bind the azide reactive component, as opposed to non azide-modified wires seen in Figure 2.5.

The ability to bond the nanowires to a methacrylated glass surface, allows for washing steps after addition of both additional linking agents and the sample itself. This is a critical step, as it removes signal molecules that have not specifically bound and enables the use of the spatially well defined wire arrays as analytical binding assays.

SPAAC CLICK CHEMISTRY AND BIOTIN-STREPTAVIDIN SYSTEM

To further investigate the compatibility to well-established biochemical linker systems, the nanowires were stretched and bonded on a glass substrate and outfitted with Biotin using the same DBCO click chemistry (see Figure 2.6 b). Streptavidin-FITC was then allowed to bond to available azide binding sites. With a size of 52.8 kDa, the streptavidin protein is much larger than the previously shown Alexafluor488 (0.6 kDa). Figure 2.6 a shows the green fluorescent signals of FITC covering the nanowires.

2
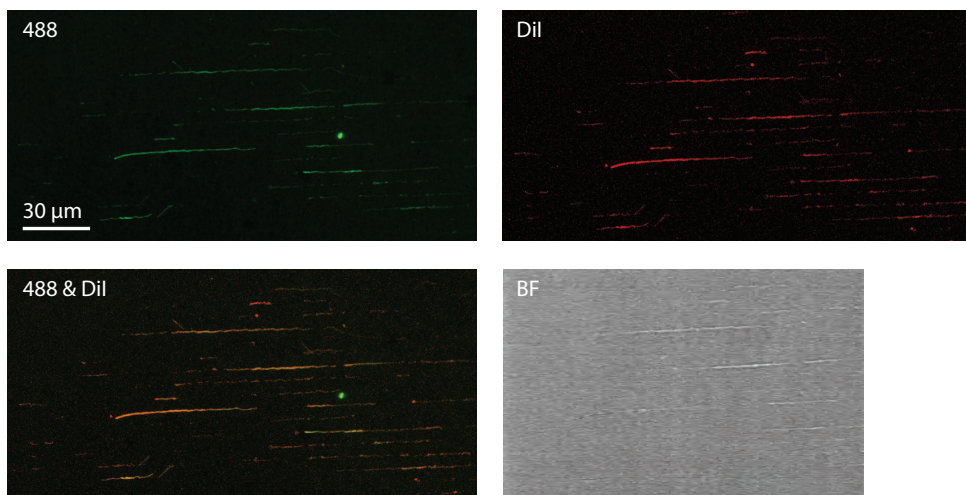
Figure 2.4: Confocal images of stretched methacrylate/azide-modified PS-b-PEO nanowires exposed to alkyne-Alexafluor488 for CuAAC click reaction. Wires were grown using 1 wt% azide- and 9 wt% methacrylate-modified PS-b-PEO per native polymer. They show green fluorescence after incubating and washing. Compare Figure 2.5 for negative test.
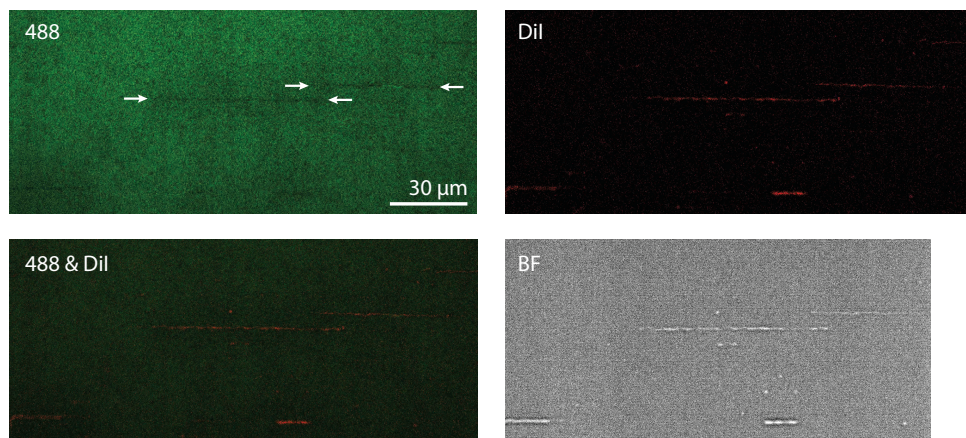
Figure 2.5: Confocal images of stretched methacrylate-modified PS-b-PEO nanowires exposed to alkyne-Alexafluor488 for CuAAC click reaction. No azide-modified polymer was added and wires exhibit no green fluorescence signal.
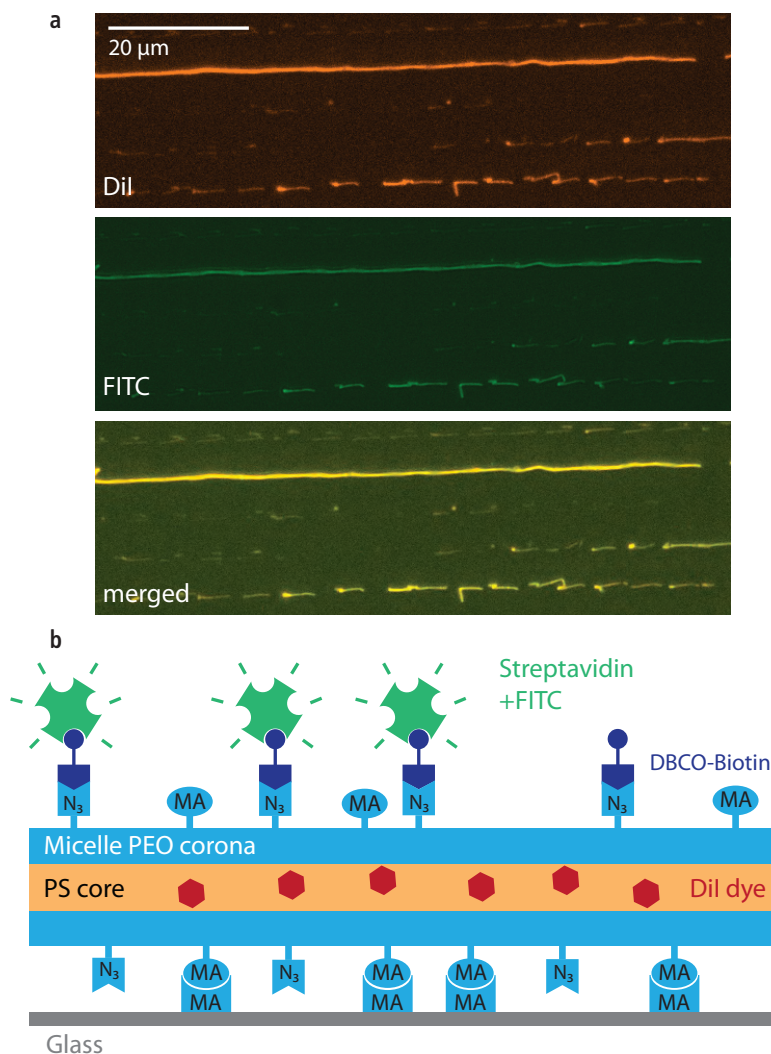
Figure 2.6: a) Nanowires outfitted with DiI dye and biotin, after incubation with streptavidin-FITC exhibit green fluorescence; b) Schematic of a nanowire with binding sites and functional compounds (methacrylate end groups MA, azide end groups N_3). Methacrylate groups were used to crosslink the nanowire to the methacrylated glass surface using UV light and LAP photoinitiator.

BINDING OF STREPTAVIDIN MICROBEADS ON FUNCTIONALIZED NANOWIRES

With the general ability to provide active binding sites on the nanowires, we tested the capture of larger particles on the wires. Using the azide end groups, DBCO-biotin was

2

added to the wires to allow capture of streptavidin coated microbeads. Microbeads provide interesting applications and their large size allows easy observation with standard optical microscopes [28, 29].

Fluorescence microscope pictures were taken pre- and post-wash and beads were counted on both samples containing azide-modified and azide-free nanowires (Figure 2.7). The results are depicted in Figure 2.8 and show a higher percentage of beads on the surface after washing (33%) when using azide compared to azide-free nanowires (9%). Visual inspection indicates a majority of bound microbeads to be situated on a nanowire in the case of present azide-modification (compare sup. Figure 2.10).

2.4. CONCLUSION

Mixtures of native PS-b-PEO with proportions of 9% methacrylate- and 1% azide-modified PS-b-PEO form worm like micelles comparable to the native-only polymer. The methacrylate is available for fixing the nanowires on methacrylated substrates as demonstrated before. In addition, the azide end groups provide active binding sites for biochemical compounds to be added using click chemistry. Modification with Alkyne-Alexafluor488 or DBCO-biotin after micelle formation is possible through this two-step approach and shows no disturbance of the micelle structure. Also washing of stretched nanowires that have been crosslinked to the substrate is possible, thus allowing removal of unbound compounds for use in a biomolecular assay. The available binding sites were sufficient to bind streptavidin-FITC conjugates and streptavidin coated 2.1 µm microbeads. The use of other large biomolecules and functional particles appear feasible, enabling easy contact printing creation of patterned bioassays and point-of-care developments.

2
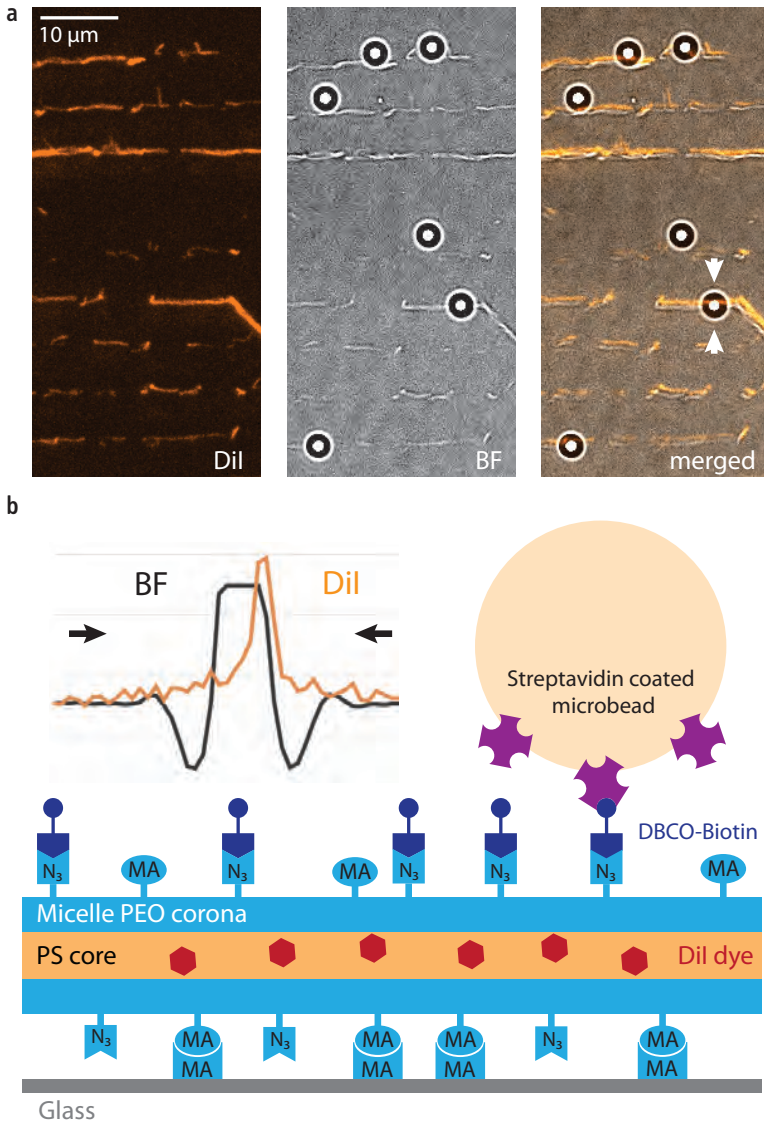
Figure 2.7: a) Fluorescence microscopy picture of beads on fixed DiI stained azide-modified nanowires after wash; b) Overlay of linescans for both channels illustrates co-localization of bead and wire; Schematic of the nanowire-microbead conjugation.
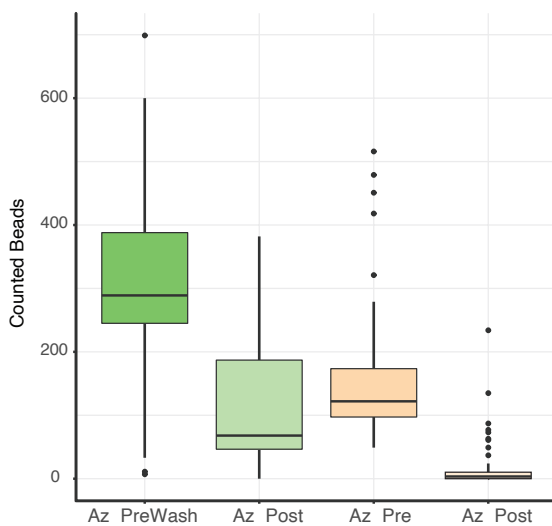
Figure 2.8: Boxplot showing the count of streptavidin beads pre/post wash on nanowires with (Az+) and without (Az-) azide modification. Nanowires with azide modification were able to bind 33% of the beads on average, while without azide groups present only 9% of beads remain on the surface after washing. The boxes indicate the 25-, 50- and 75-percentile, the whiskers the minima and maxima, outliers are dotted, $n \geq 25$. Plotted using R in RStudio and packages [30–34].

2.5. APPENDIX
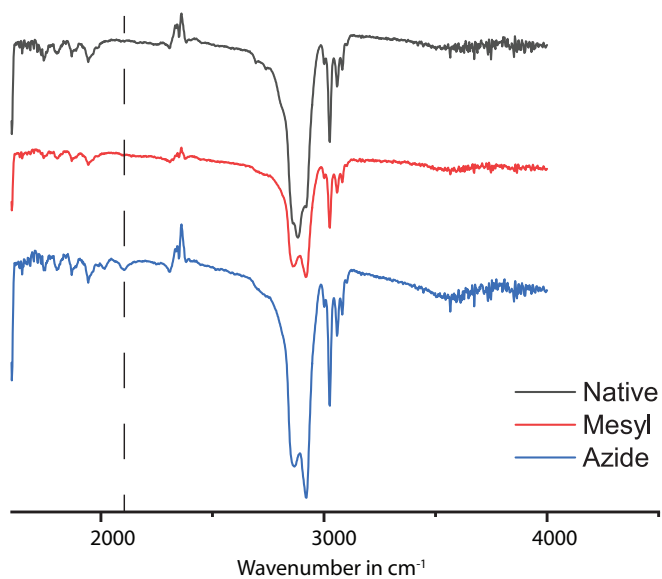
Figure 2.9: FT-IR analysis of native polymer, mesylated intermediate and azide-modified end product. Distinctive peak at around 2100 cm^{-1} is observed after azide modification.

2

DiI & BF

30 µm
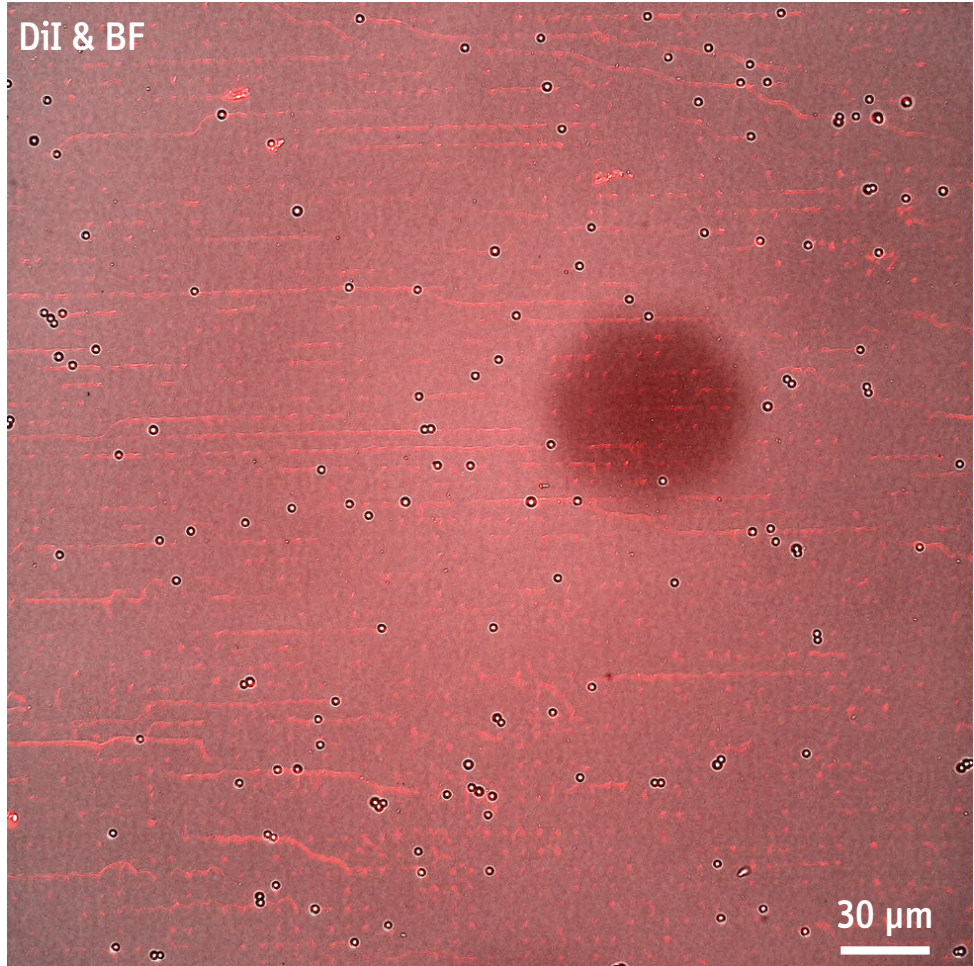
Figure 2.10: Composite image of brightfield and DiI channels of azide-DBCO-biotin modified nanowire print with attached streptavidin microbeads after washing steps. Visual inspection shows good overlap of bound microbeads and underlying nanowires.
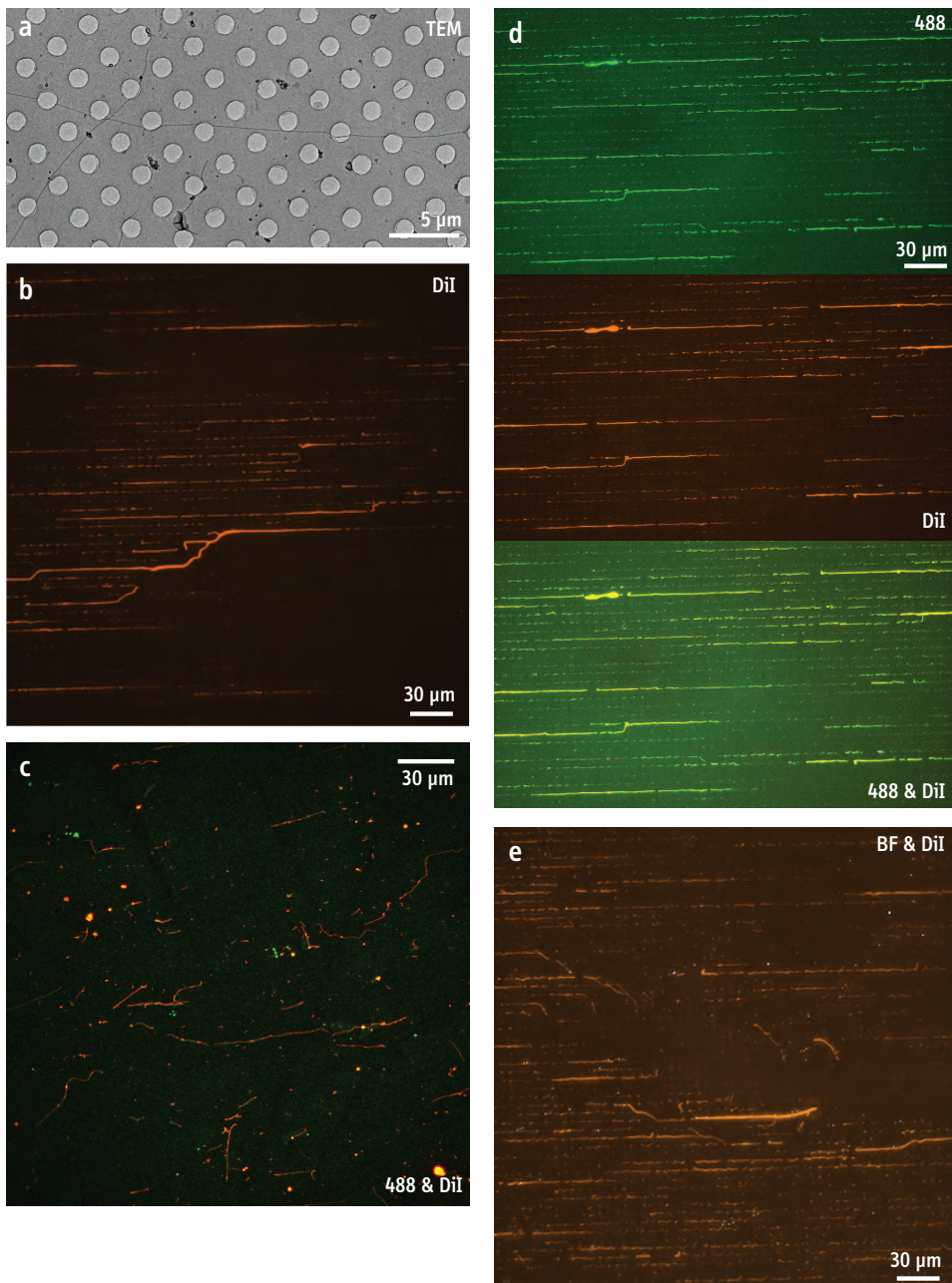
Figure 2.11: Full images of the previously shown regions of interest for a) Figure 2.2, b) Figure 2.1, c) Figure 2.3, d) Figure 2.6, e) Figure 2.7

2
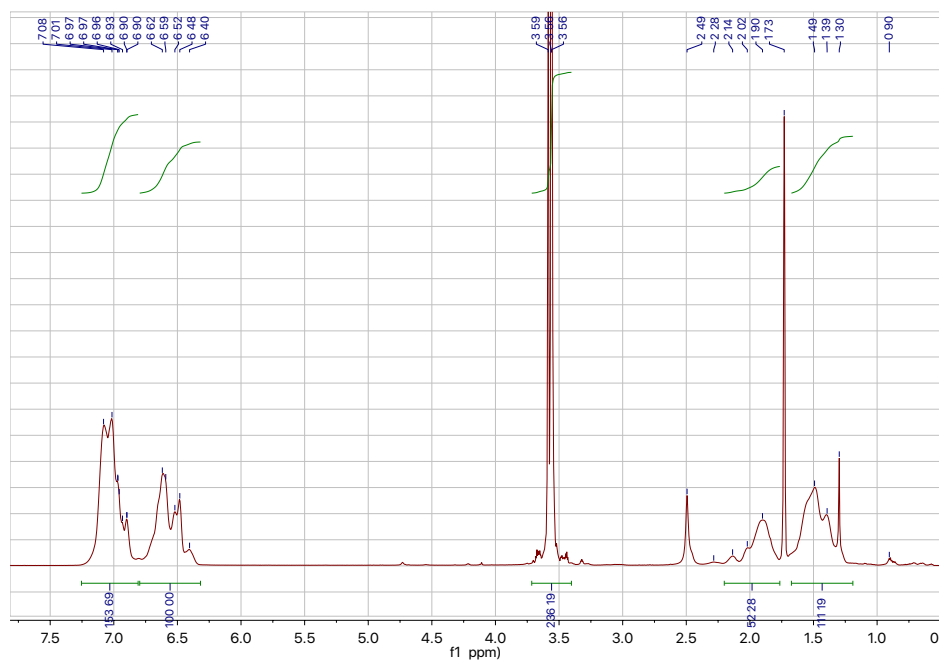
Figure 2.12: PS-b-PEO-azide ^{1}H NMR (600 MHz, THF-d$_8$) δ(ppm) = 7.25 - 6.82 (m, 154H, ortho-, para-C**H**-styrol-ring), 6.80 – 6.32 (m, 100H, meta-C**H**-styrol-ring), 3.56 (d, **J** = 1.3 Hz, 236H, PEG-CH$_2$), 2.21 - 1.76 (m, 52H, C**H**CH$_2$-styrol-backbone), 1.68 - 1.18 (m, 111H, CHC**H**$_2$-styrol-backbone).

2
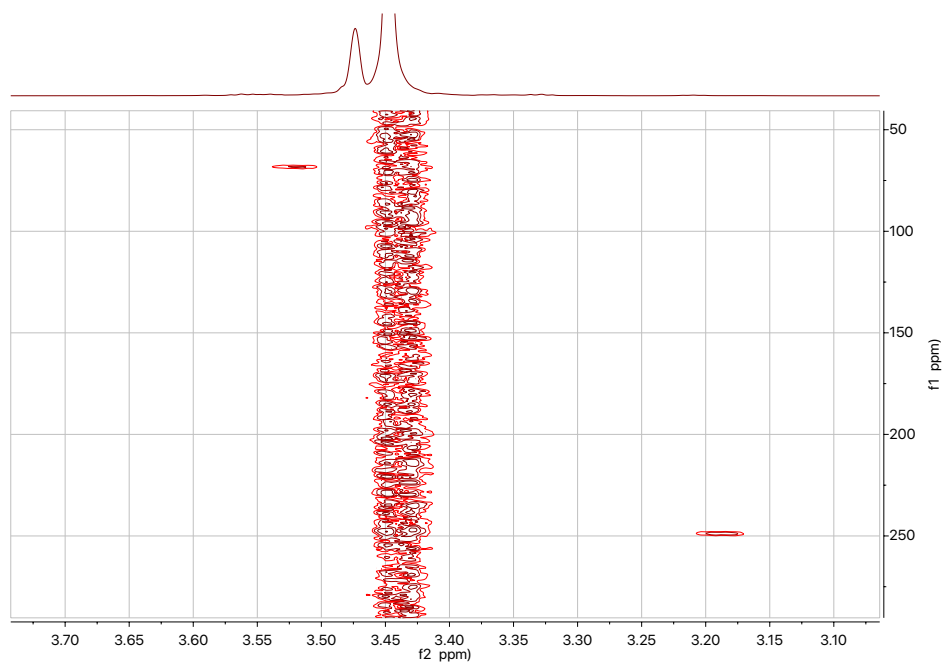
Figure 2.13: PS-b-PEO-azide H-N HMBC (^{15}N) NMR (600/61 MHz, THF-d$_8$, unreferenced) δ(ppm) = 248.8 (CH$_2$**N**NN), 68.3 (CH$_2$N**N**N)
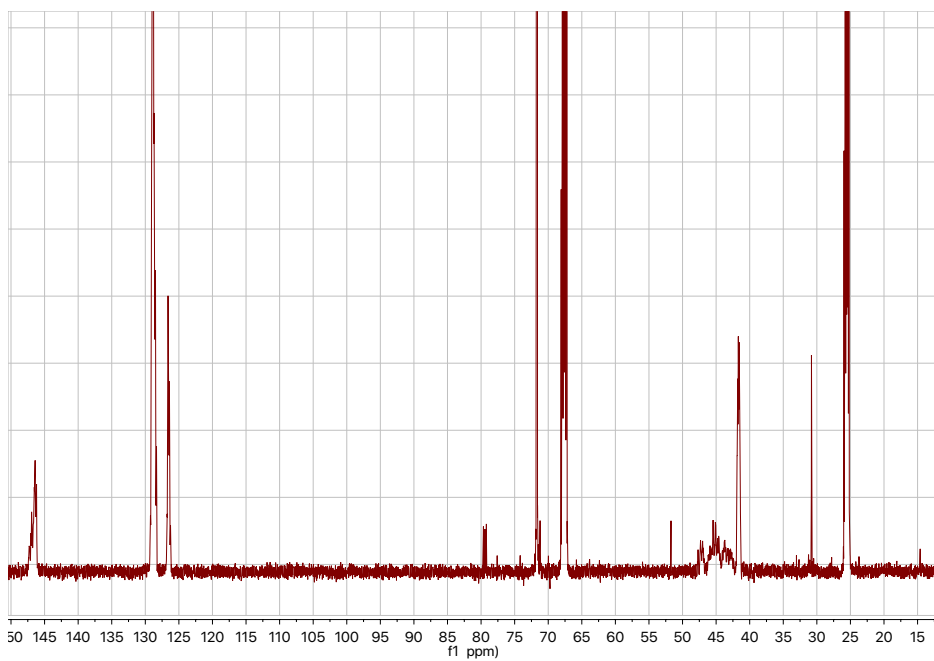
Figure 2.14: PS-b-PEO-azide ^{13}C NMR (151 MHz, THF-d$_8$) δ(ppm) = 51.7 (**C**H$_2$NNN).

2

REFERENCES

[1] G. E. P. Box, *Robustness in the strategy of scientific model building,* in *Robustness in Statistics* (Elsevier, 1979) pp. 201–236.

[2] H. Hubbe, E. Mendes, and P. E. Boukany, *Polymeric nanowires for diagnostic applications,* Micromachines **10** (2019).

[3] L. Jennings, O. Ivashchenko, I. J. C. Marsman, A. C. Laan, A. G. Denkova, G. Waton, F. J. Beekman, F. Schosseler, and E. Mendes, *In vivo biodistribution of stable spherical and filamentous micelles probed by high-sensitivity SPECT,* Biomaterials Science **4,** 1202 (2016).

[4] Z. Wang, S. Lee, K. Koo, and K. Kim, *Nanowire-Based Sensors for Biological and Medical Applications,* IEEE Transactions on NanoBioscience **15,** 186 (2016).

[5] B. D. Malhotra and M. A. Ali, *Chapter 8 - nanostructured materials for dna biochip,* in *Nanomaterials for Biosensors,* Micro and Nano Technologies, edited by B. D. Malhotra and M. A. Ali (William Andrew Publishing, 2018) pp. 221–262.

[6] L. Rems, D. Kawale, L. J. Lee, and P. E. Boukany, *Flow of DNA in micro/nanofluidics: From fundamentals to applications,* Biomicrofluidics **10,** 043403 (2016).

[7] G. Yang, X. Li, Y. He, J. Ma, G. Ni, and S. Zhou, *From nano to micro to macro: Electrospun hierarchically structured polymeric fibers for biomedical applications,* Progress in Polymer Science **81,** 80 (2018).

[8] V. Beachley and X. Wen, *Effect of electrospinning parameters on the nanofiber diameter and length,* Materials Science and Engineering: C **29,** 663 (2009).

[9] B. Kannan, D. E. Williams, K. Khoshmanesh, G. A. Bowmaker, and J. Travas-Sejdic, *The electrochemical growth of conducting polymer "nanowires",* Journal of Electroanalytical Chemistry **669,** 82 (2012).

[10] Y. Hu, H. Lee, S. Kim, and M. Yun, *A highly selective chemical sensor array based on nanowire/nanostructure for gas identification,* Sensors and Actuators, B: Chemical **181**, 424 (2013).

[11] P. J. Glazer, L. Bergen, L. Jennings, A. J. Houtepen, E. Mendes, and P. E. Boukany, *Generating Aligned Micellar Nanowire Arrays by Dewetting of Micropatterned Surfaces,* Small **10**, 1729 (2014).

[12] Y. Liu, X. Zhang, Y. Xia, and H. Yang, *Magnetic-Field-Assisted Electrospinning of Aligned Straight and Wavy Polymeric Nanofibers,* Advanced Materials **22**, 2454 (2010).

[13] D. Yang, B. Lu, Y. Zhao, and X. Jiang, *Fabrication of aligned fibrous arrays by magnetic electrospinning,* Advanced Materials **19**, 3702 (2007).

[14] J. Guan, B. Yu, and L. J. Lee, *Forming highly ordered arrays of functionalized polymer nanowires by dewetting on micropillars,* Advanced Materials **19**, 1212 (2007).

[15] K. Zhang, P. J. Glazer, L. Jennings, S. Vedaraman, S. Oldenhof, Y. Wang, F. Schosseler, J. H. van Esch, and E. Mendes, *A facile approach for the fabrication of 2D supermicelle networks,* Chem. Commun. **52**, 12360 (2016).

[16] K. Zhang, A. Arranja, H. Chen, S. Mytnyk, Y. Wang, S. Oldenhof, J. H. van Esch, and E. Mendes, *A nano-fibrous platform of copolymer patterned surfaces for controlled cell alignment,* RSC Advances **8**, 21777 (2018).

[17] B. Su, Y. Wu, and L. Jiang, *The art of aligning one-dimensional (1D) nanostructures,* Chemical Society Reviews **41**, 7832 (2012).

[18] V. V. Rostovtsev, L. G. Green, V. V. Fokin, and K. B. Sharpless, *A Stepwise Huisgen Cycloaddition Process: Copper(I)-Catalyzed Regioselective "Ligation" of Azides and Terminal Alkynes,* Angewandte Chemie International Edition **41**, 2596 (2002).

[19] C. W. Tornøe, C. Christensen, and M. Meldal, *Peptidotriazoles on Solid Phase: [1,2,3]-Triazoles by Regiospecific Copper(I)-Catalyzed 1,3-Dipolar Cycloadditions of Terminal Alkynes to Azides,* The Journal of Organic Chemistry **67**, 3057 (2002).

[20] L. Liang and D. Astruc, *The copper(I)-catalyzed alkyne-azide cycloaddition (CuAAC) "click" reaction and its applications. An overview,* Coordination Chemistry Reviews **255**, 2933 (2011).

[21] N. J. Agard, J. A. Prescher, and C. R. Bertozzi, *A Strain-Promoted [3 + 2] Azide-Alkyne Cycloaddition for Covalent Modification of Biomolecules in Living Systems,* Journal of the American Chemical Society **126**, 15046 (2004).

[22] J. Zhu and R. C. Hayward, *Spontaneous Generation of Amphiphilic Block Copolymer Micelles with Multiple Morphologies through Interfacial Instabilities,* Journal of the American Chemical Society **130**, 7496 (2008).

[23] C. Zhang, J. Chen, and L. Xu, *Dual-templating approach to ordered mesoporous Pt nanowires with various morphologies,* Materials Letters **223**, 97 (2018).

[24] C. Ornelas, J. Broichhagen, and M. Weck, *Strain-promoted alkyne azide cycloaddition for the functionalization of poly(amide)-based dendrons and dendrimers,* Journal of the American Chemical Society **132**, 3923 (2010).

[25] S. S. Nguyen and J. A. Prescher, *Developing bioorthogonal probes to span a spectrum of reactivities,* Nature Reviews Chemistry **4**, 476 (2020).

[26] J. E. Semple, B. Sullivan, T. Vojkovsky, and K. N. Sill, *Synthesis and facile end-group quantification of functionalized PEG azides,* Journal of Polymer Science Part A: Polymer Chemistry **54**, 2888 (2016).

[27] B. Wrackmeyer, *Calculation of ^{15}N NMR parameters of azides and some related compounds. revisiting the methylation of nitrous oxide N_2O,* Zeitschrift für Naturforschung B **66b**, 1079 (2011).

2

[28] J. Zhang, S. Shikha, Q. Mei, J. Liu, and Y. Zhang, *Fluorescent microbeads for point-of-care testing: a review,* Microchimica Acta **186** (2019).

[29] S. Rödiger, C. Liebsch, C. Schmidt, W. Lehmann, U. Resch-Genger, U. Schedler, and P. Schierack, *Nucleic acid detection based on the use of microbeads: a review,* Microchimica Acta **181**, 1151 (2014).

[30] R Core Team, *R: A Language and Environment for Statistical Computing*, R Foundation for Statistical Computing, Vienna, Austria (2022).

[31] RStudio Team, *RStudio: Integrated Development Environment for R*, RStudio, PBC., Boston, MA (2020).

[32] H. Wickham, *ggplot2: Elegant Graphics for Data Analysis* (Springer-Verlag New York, 2016).

[33] H. Wickham, R. François, L. Henry, and K. Müller, *dplyr: A Grammar of Data Manipulation* (2022), r package version 1.0.10.

[34] M. Dowle and A. Srinivasan, *data.table: Extension of 'data.frame'* (2022), r package version 1.14.4.

3

TESTING BIORELEVANT

PERFORMANCE

*Es ergiebt sich aus diesen Untersuchungen endlich, dass die Erfahrung eine
Unergründlichkeit der organischen Schöpfungen dem kleinsten Raume zugewendet zeigt,
wie die Sternenwelt dem grössten, deren nicht naturgemässe Grenzen die optischen
Hülfsmittel ziehen.*

Christian Gottfried Ehrenberg [1]

*From these investigations it finally emerges, that experience shows an unfathomability of
organic creations turned towards the smallest space, like the starry world towards the
largest, whose non-natural limits are drawn by the optical aids.*

Performance of self-assembled, bifunctional micellar nanowires was further investigated using a virus and a cell model: Giant unilamellar vesicles show similarities to cells and were used to test limits of binding large and complex particles. To investigate the ability to bind viral particles, fluorescent bacteriophages were employed as a virus model and captured on the nanowires.

3

3.1. INTRODUCTION

In this chapter, the performance of the bifunctional nanowires was further validated using bio-relevant objects. In previous chapter we demonstrated that this bifunctional nanowire can be attached to a glass substrate and capture streptavidin protein (~5 nm) and solid polystyrene microbeads (2.3 µm). It remains a challenge to demonstrate the ability of these wires for other biologically relevant species. To investigate the limits of large and complex particle binding such as cells, GUVs were utilized. Furthermore, for testing the ability to bind viral particles, a bacteriophage was used as a model virus system: it is similar in size to the viruses of interest and nonhazardous to human health. Also, bacteriophages in general are of great interest in current research. For an overview of the range of particle sizes tested for binding including this chapter see Figure 3.1.
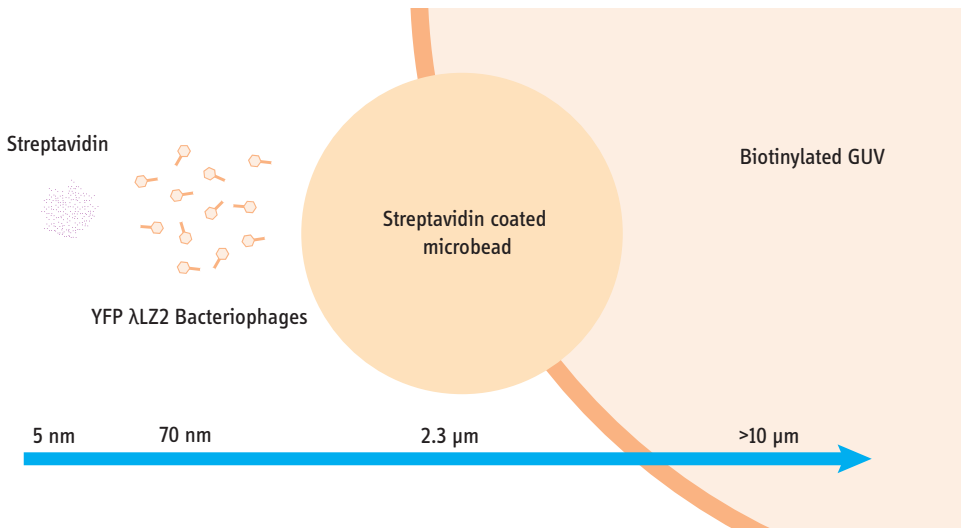
Figure 3.1: Scaled size comparison of the different biologically relevant species tested on the nanowire binding arrays.

3.2. BINDING OF BIOMIMETIC CELLULAR MEMBRANES:

CAPTURE OF GUVS

The research on artificial vesicles has provided many interesting varieties in production, method and composition by mimicking specific function of cells to investigate biological processes and cellular functions in living cells [2, 3]. The GUV, as a subtype of lipid vesicles, is of special interest regarding its simplistic model character of mimicking a cell. It consists of one non-covalent molecular lipid bilayer (membrane) creating a hollow sphere usually filled with a watery solution; structurally a core-shell particle with a liquid core[1] [5, 6]. It is noted that concerning the creation of artificial cells, vesicle-in-vesicle constructs (vesicles incorporating smaller vesicles) are the state-of-the-art in creating artificial cells [7].

Similar to the natural counterpart it is often used to model, the GUVs lipid membrane is water-permeable, while ions and macromolecules are not able to pass the lipid bilayer. These constructs are of interest in (bio-)chemical reactions: Closed "microreactor" compartments of picoliter volumes allow synthetic reactions not possible in bulk media [8]. Also, many biochemical reactions are nowadays known to be exposed to very different intracellular constraints as compared to in vitro conditions, thus mimicking these conditions in a bottom-up approach is a simplification towards artificial cells, that helps the understanding of cellular systems [9]. There is much to be learned from cells and their perfected organization and build. Lipid vesicles for example are one basic building block in the compartmentalisation of cells into organelles, to separate catalytic cycles and both allowing rate control and avoid interference of different compounds. In general GUVs present an ideal model for a cell due to their size and structure. However, lacking a cytoskeleton, they are more deformable and fragile than a cell and more prone to rupture from mechanical or osmotic stress. However, they allow for exactly defined composition

---

[1]A useful perspective to model light-scattering phenomena in vesicle solutions [4]

of the membrane, avoiding interferences of the numerous functionalities a natural cell would carry. [10]
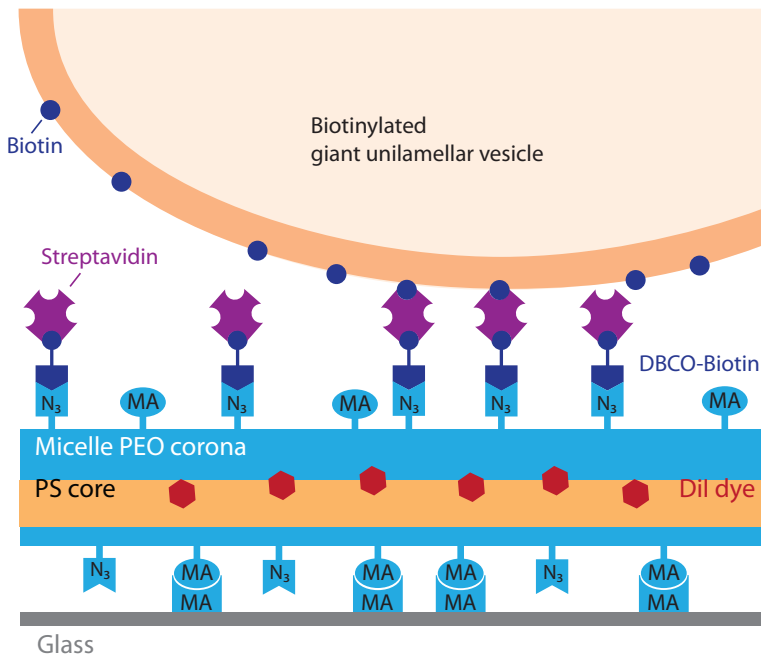
Figure 3.2: Schematic representation of the GUV experiment: bifunctional nanowire bonded to a glass substrate outfitted with streptavidin to capture the GUVs containing biotin end groups on the surface of their membrane.

The binding of GUVs on the presented nanowire arrays was tested. The GUVs were assembled using electroswelling with outside-facing biotin endgroups to facilitate linking to streptavidin. Rhodamine B was incorporated into the membrane for easy observation in fluorescence microscopy (see Figure 3.2).

3.2.1. MATERIALS AND METHODS GUVS

The method of GUV production was adapted from [11–13].

Two ITO (indium tin oxide) coated microscopy glass slides were thoroughly cleaned with Ethanol, DI water and lens tissues, then preconditioned on a hotplate (153 °C 20 min).

To prepare the lipid membrane of the GUVs 98.5 mol% 1,2-dioleoyl-sn-glycero-3-

phospholine (DOPC), 0.5 mol% 1,2-dioleoyl-sn-glycero-3-phosphoethanolamine-N-(lissamine rhodamine B sulfonyl) (ammonium salt) (DOPE-RhoB, exc. 560 nm, em. 583 nm) to provide good visibility in fluorescence microscope and 1 mol% 1,2-dioleoyl-sn-glycero-3-phosphoethanolamine-N-(biotinyl) (sodium salt) (BiotinylPE) to facilitate binding to streptavidin on the nanowires (see Figure 3.3).
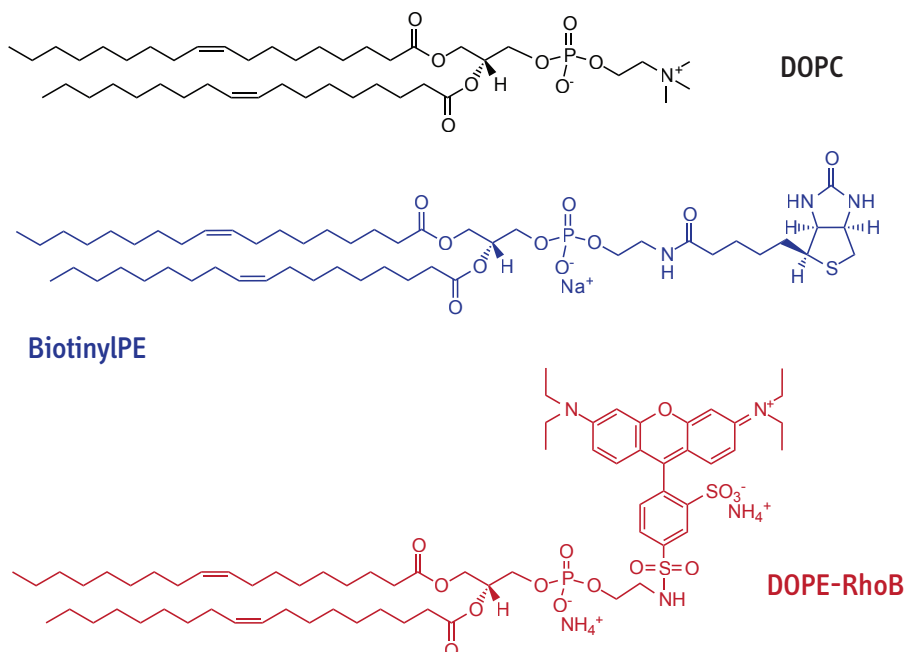
Figure 3.3: Membrane components of the GUVs: DOPC, 98.5 mol%; BiotinylPE, 1,2-dioleoyl-sn-glycero-3-phosphoethanolamine-N-(biotinyl) (sodium salt), 1 mol%; DOPE-RhoB, 1,2-dioleoyl-sn-glycero-3-phosphoethanolamine-N-(lissamine rhodamine B sulfonyl) (ammonium salt), ex/em 560 nm/583 nm, 0.5 mol%

Stock solutions of each component were prepared in chloroform (1 mg/mL) and separately stored under argon atmosphere at $-20\,°C$. $10\,\mu L$ of freshly prepared mixture was pipetted onto the conductive surface of two Indium Tin Oxide (ITO) covered slides (purchased from Sigma Aldrich) and left to dry under vacuum for more than 2 hours. The ITO slides were then inserted into a polytetrafluoroethylene (PTFE) swelling chamber, conductive sides facing each other with 1.5 mm distance. 1 mL of a 236 mM watery sucrose

solution were added in between the facing slides. With the swelling chamber kept at room temperature, a sinusoidal current of 70 Hz, 2.4 V_{pp} was applied for 3 hours using an Agilent 33220A waveform generator. Afterwards each slide was washed with 0.5 mL glucose solution (200 mM) into the PTFE chamber.

Using the streptavidin's ability to bind to several biotin molecules, streptavidin carrying nanowire samples were then covered with GUV solution. After allowing the GUVs to settle 4 h, the substrate was carefully washed to remove unbound vesicles.

3.2.2. RESULTS AND DISCUSSION GUVS

The synthesized GUVs were clearly visible in fluorescence microscopy through incorporation of Rhodamine B (Figure 3.4). Electroswelling did produce very large but polydisperse

20 µm
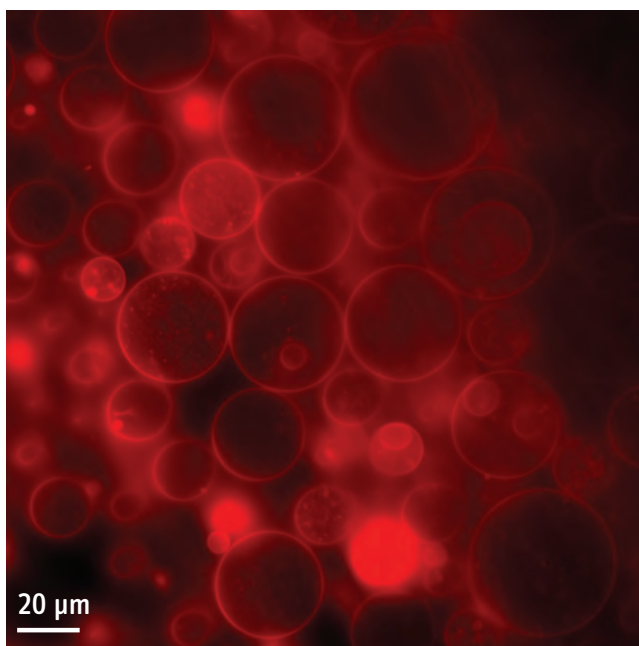
Figure 3.4: Giant unilamellar vesicles containing biotin and Rhodamine B moieties, viewed through fluorescence microscope.

vesicle sizes ranging from ~4 µm – 54 µm. If a more uniform distribution of vesicle sizes is desired, different methods such as a droplet-based microfluidic approach [14, 15]

or a combination of microcontact printing for creating well-defined dimensions with electroformation [6] can be of interest (also good overview in [10]).
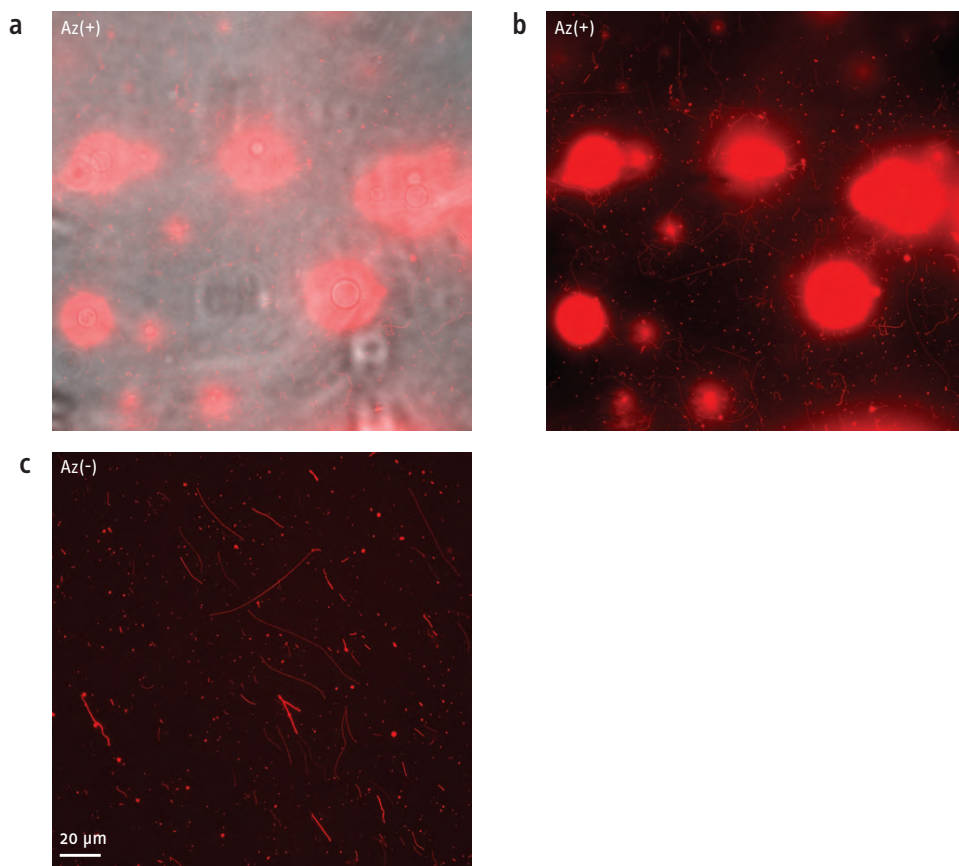
Figure 3.5: a) Few GUVs on nanowire substrate after careful washing, fluorescence and brightfield composite image; b) Red channel only for view of underlying nanowires. Fixation was observed to be very fragile: GUVs were randomly detaching and floating after initial apparent fixture to substrate c) A negative control substrate with randomly deposited wires, without streptavidin addition; no fixation of GUVs could be observed

Results of the GUV capture are depicted in Figure 3.5. After addition of the GUVs to the nanowire array, the settling time and careful wash, the negative substrate showed no residual lipid vesicles (Figure 3.5 b)). In the positive substrate, however, few GUVs remained (Figure 3.5 a)). The high fluorescence intensity required the overlay of a brightfield image to visualize both GUVs and nanowires. Some of the residual GUVs were

around 10 μm in size, larger GUVs were not observed. Two components could contribute to a disadvantage of larger GUVs when applying a flow for washing: Stoke's law describes the drag force on a spherical particle moving through a viscous fluid as $F_d = 6\pi\eta R v$, with η the dynamic viscosity of the medium, R the particle's radius and its velocity v relative to the medium. Larger GUVs will suffer a bigger force from the moving liquid through their increased radius. But additionally, the larger vesicle radius might lead to exposure to higher flow velocities than in case of small vesicles: the flow further away from the bulk increases with the parabolic profile of a laminar Hagen-Poiseuille flow. These two effects might predominate the fact, that a larger vesicle with its larger surface area offers a higher number of binding sites. [16]
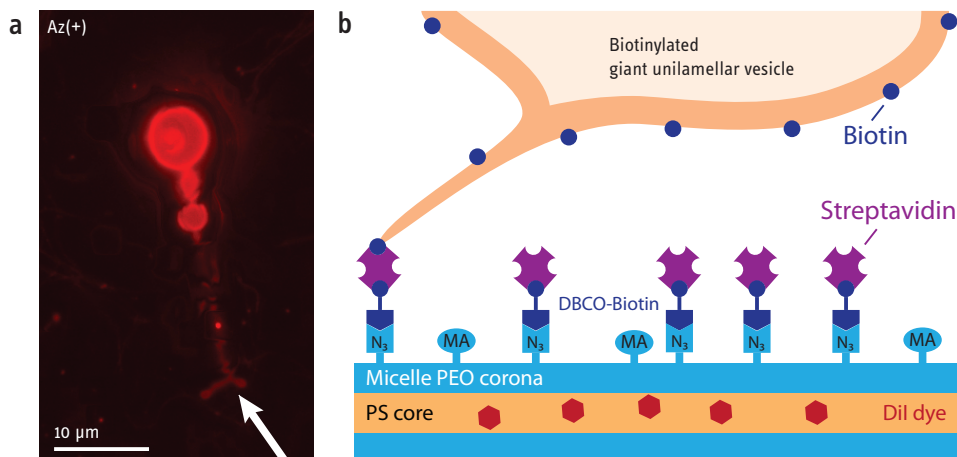
Figure 3.6: a) Multifocus fluorescence image of GUV attached by a string: arrow points to connection with substrate, speculating this might be a tether, as depicted in sketch b) A known effect in GUVs, when the flexibility of the membrane leads to a thin extension.

The membranes of the GUVs appear very deformable, which might lead to rupture or detachment during washing steps. Some vesicles are out of focus and are suspected to be tethered or to have detached from the surface after wash. Tethering is a known effect often observed with lipid vesicles, where the lipid membrane stretches into a thin extension under force, with the vesicle staying intact and generally keeping its shape [17].

A tether-like string attachment could be observed in one example (Figure 3.6) where we speculate the GUV bonded again to the nanowire substrate in some distance due to the tether formation.

3.3. BINDING OF VIRAL PARTICLES: CAPTURE OF BACTERIOPHAGES

A major prospect of the research on this biofunctional nanowire system is the application of virus sensing. However, so far these polymeric nanowires have not been employed to capture viruses. In this section, we will provide proof-of-concept that these nanowires are suitable to capture and isolate viral particles. Problems could arise from unspecific binding to the micelles and on the other hand it needed to be shown that binding of marked viral particles is possible on corona-mounted micellar binding sites. In order to investigate compatibility of viral particles with this polymeric nanowire platform, fluorescence labelled bacteriophages were outfitted with a DBCO-linking moiety and exposed to the stretched, multifunctional nanowires.

Bacteriophages provide a good model virus for testing applicability of the developed system to viral pathogens without big safety concerns. The first characterisation of bacteriophages (Greek βακτήριον "small rod"[2] and φαγάς "devourer") dates back to the beginning of the 19th century, when William Twort (in 1915 [18]) and Felix d'Herelle (in 1917 [19], translated from french [20]) independently of each other described observations indicating the existence of a bacteria antagonistic ultra-microscopic virus. A decades long dispute of priority followed and retrospectively allows some interesting thought about scientific discoveries and priority [21]; earlier description of phage activity are also discussed [22]. However, a mixture of fundamental shortcomings in the production of phage solutions and application of the treatment in the 1930s [23, 24], political discord

---

[2]A term established by Christian Gottfried Ehrenberg 1828 [1], owing to the shape of the described organism
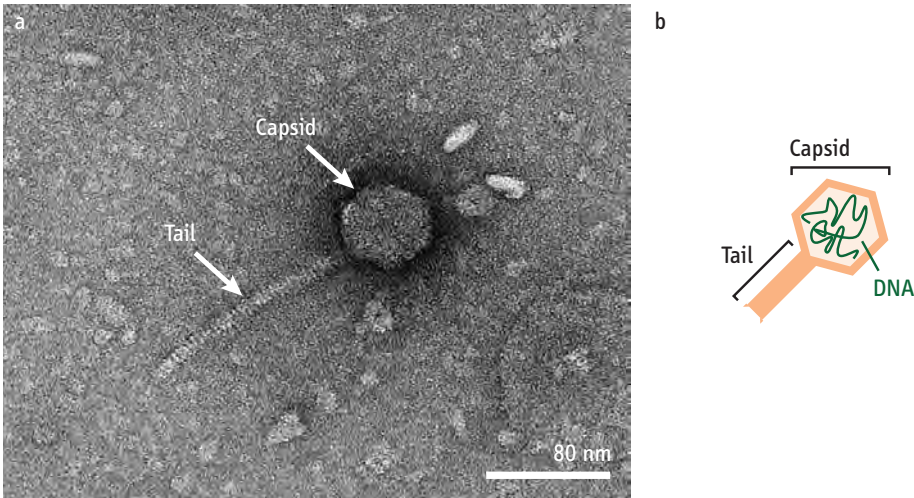
Figure 3.7: a) Transmission electron microscope picture of a lambda phage, specifically the fluorescent λLZ2 co-expressing wild type and YFP-fusion versions of the capsid gpD protein as used in the experiments (picture Chris van Toor, Rebecca McKenzie and Boris Estrada-Bonilla, courtesy of Brouns Group, TU Delft); b) Schematic depiction of the lambda phage consisting of the capsid containing double-strand linear DNA genome and the tail.

and the successful establishment of chemical antibiotics in the 1940s suppressed research in this field shortly after its discovery. Until recently, only some, mostly Eastern European/ Soviet institutes had continued working on the thematic [25–28].[3]

Most natural phages will not post a danger to human health and can thus be handled in a biosafety level 1 (BSL-1) setting [31]. Additionally, they are of high interest themselves and gained increasing attention in recent research, especially therapeutic research. Being extremely host-specific towards the respective bacteria, they pose alternatives to antibiotics and thus phage therapy is seen as a promising path to overcome the increasing number of pathogens with antibiotic resistance [26, 32–40].

The strain used in these experiments is a fluorescent Lambda phage λLZ2 co-expressing wild type and yellow fluorescent protein (YFP)-fusion versions of the capsid gpD protein,

---

[3]The curious reader may add the story of Salvarsan to this picture, showing that similar shortcomings can be found in the history of the then upcoming antibiotic treatments, before Penicillin brought the breakthrough [29, 30].

developed by Zeng and Golding [41] (see Figure 3.7). While the capsid is only 70 nm in size and thus comparable to the relevant tropical fever viruses concerning this project, the YFP (exc. 513 nm, em. 527 nm) allowed for easy detection using a fluorescent microscope setup. This avoided electron microscopy techniques and allowed for much more freedom in the design of the experiments.

3.3.1. MATERIALS AND METHODS BACTERIOPHAGES

10 mM NHS-DBCO stock solution was prepared under argon atmosphere and stored in aliquots of argon-filled falcons at −20 °C (StockA). For each experiment, 610 μL 1x PBS 0.05 % Tween20, 10 μL λLZ2 phage stock (1.0×10^{10} PFU/mL), were mixed with 70 μL StockA. Incubation at room temperature followed for 30 min. Ready solution was added to Ibidi chamber containing azide/methacrylate nanowires bonded to the bottom glass surface as described in section 2.2. Incubated for 2 h at room temperature, chambers were carefully washed 5x with same PBS using a pipette. Negatives were prepared accordingly, omitting addition of azide-modified polymer to the nanowires.

3.3.2. RESULTS AND DISCUSSION BACTERIOPHAGES

Distinct signals of YFP fluorescence could be detected coinciding with the nanowires after washing of the assay (see Figure 3.8).

Contrary to that, in case of azide-free nanowire negatives, no significant signal could be detected. Despite the size of the viral particles, no unspecific binding to the micellar nanowires was observed. Binding sites on the nanowires are functional and sufficient to provide a significant signal. The methacrylated glass surface does contribute with some noise probably due to unspecific binding, which was reduced by using 0.05 % Tween20 surfactant. Using a blocking agent (e.g. bovine serum albumin (BSA)) might further enhance the background noise. The wire pattern has the advantage allowing disregarding most of the background noise.
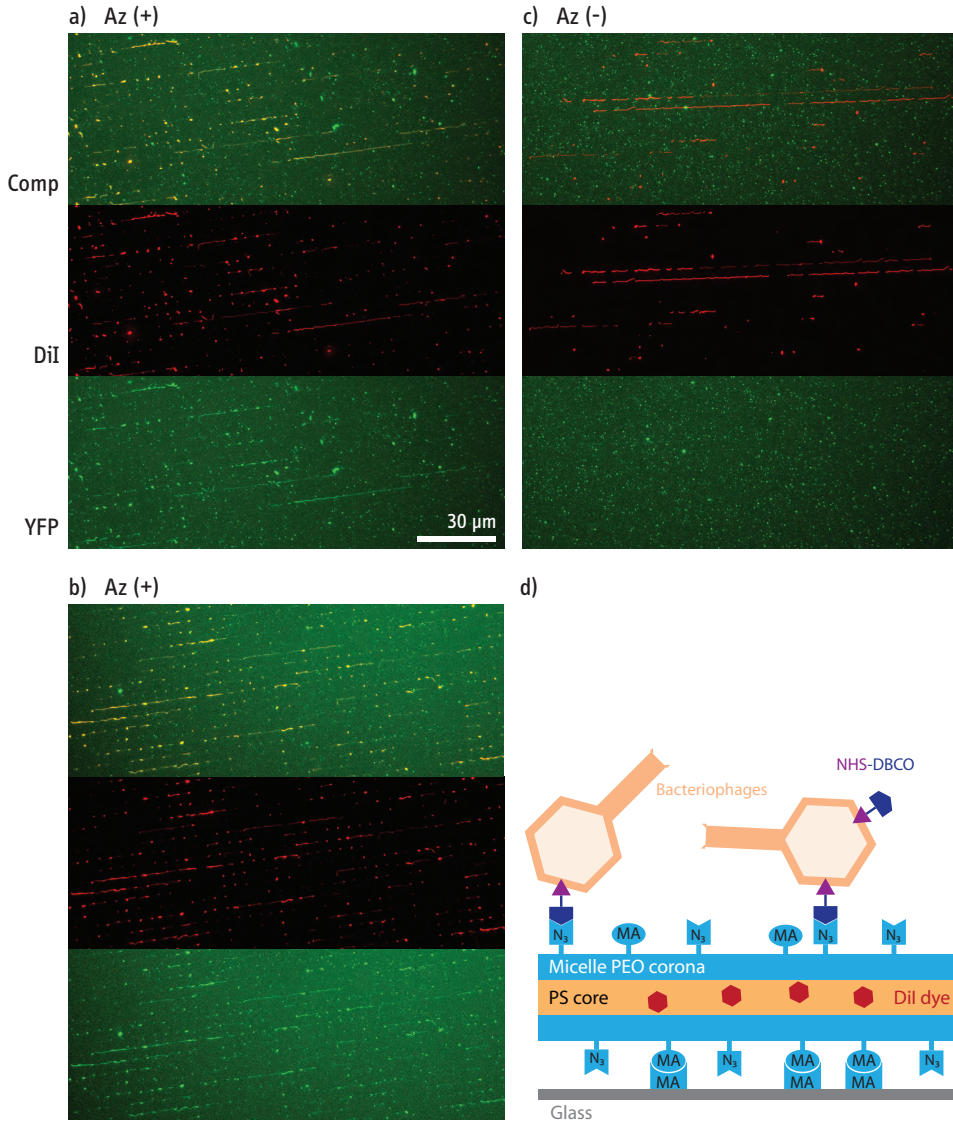
Figure 3.8: Results of bacteriophage capture on stretched multifunctional nanowires. While DiI stained nanowires (red channel) are well visible for both azide-modified Az(+) (see a) and b)) and the azide-free Az(-) control nanowires (c), the fluorescent signal of captured YFP-modified bacteriophages shows only on azide-modified nanowires (YFP channel and composite image). Schematic of the bacteriophage capture is illustrated in d).

3.4. CONCLUSION

Biotinylated GUVs exhibited limited binding to the streptavidin coated wires, but proved

very unstable and weak in such interaction. As the concept of streptavidin binding to

these nanowires has shown to function in previous chapter, it is most likely that GUVs are too large in combination with too few bonding sites and too weak a membrane. This is a known problem of GUVs and could be overcome using reinforced membrane structures such as an actin cortex. [42]

In case of viral particles, the experiments with fluorescent bacteriophages showed distinctive signals on the nanowire patterns and no unspecific binding to the nanowires was observed, leading to the fact, that printed micellar nanowires are capable of targeted capture of viral particles.

3.5. OUTLOOK

The viral particle model showed good results and a next step would be to change the chemical dual linker moiety for a specific antibody or aptamer creating an assay for virus detection. Capturing viruses on suspended nanowires, without full-length contact to bulk substrate would omit background noises and should be investigated. A polydimethylsiloxane (PDMS) micropillar stamp as used in this work for the dewetting and microprinting, functionalized with methacrylate through silanisation can also be a good starting point for a carrier of suspended nanowires. The wires would be deposited as before, but then crosslinked to the PDMS stamp with parts of them spanning the spaces in-between pillars. The high surface tension of water should be kept in mind as a potential threat to the integrity of suspended nanowire constructs.

Besides the results presented above, concerning large biological entities, our methodology can prove useful in other research topics such as in cell migration experiments, where there is no flow and the cells migrate naturally. The nanowire pattern is a useful way to produce specific molecules in a well defined patterned area to cells and observe their migration behaviour.

3.6. APPENDIX

Further results and full images of the previously depicted excerpts of bacteriophage experiments on nanowire assays are shown in the following figures.
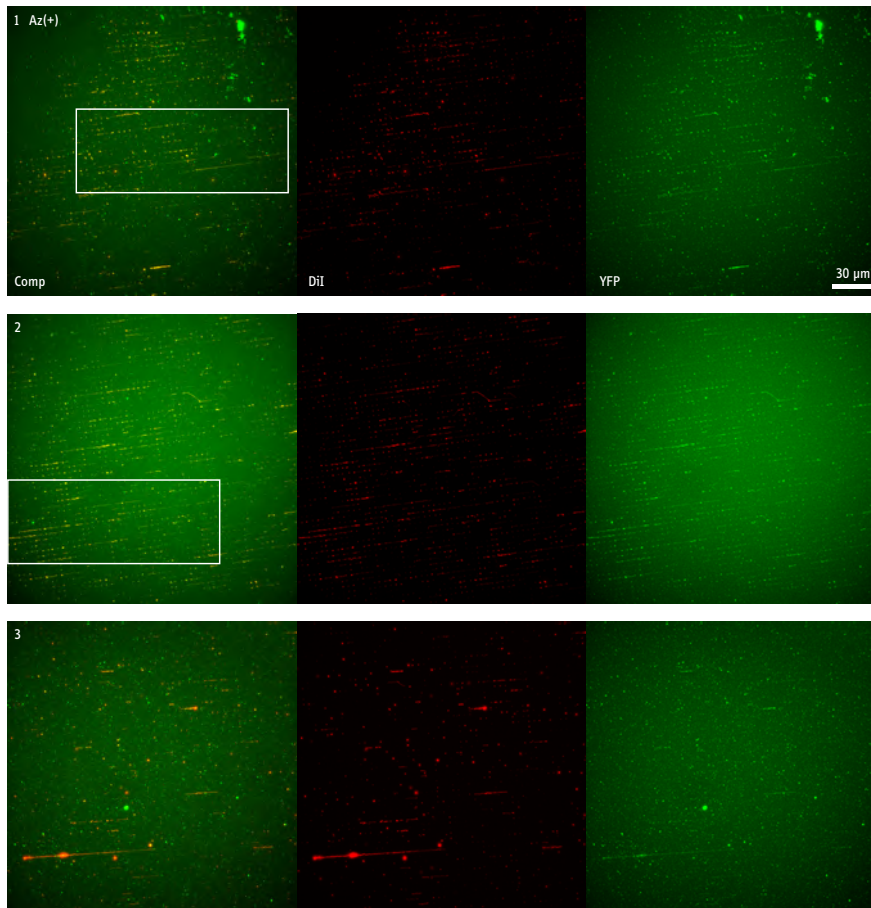
Figure 3.9: Results of bacteriophage capture on stretched Az(+) multifunctional nanowires. DiI, YFP and a composite of both are depicted. White boxes represent excerpt shown in discussion.

3
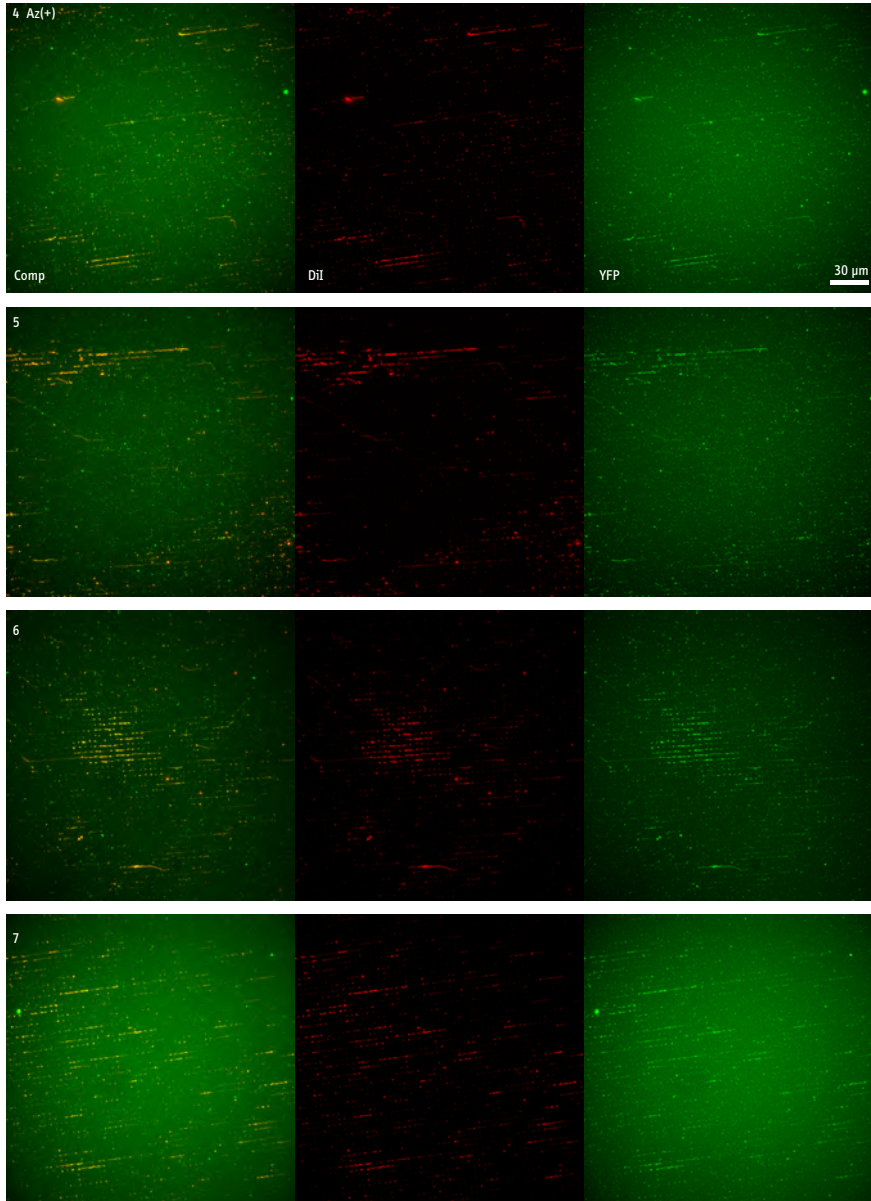
Figure 3.10: Results of bacteriophage capture on stretched Az(+) multifunctional nanowires. DiI, YFP and a composite of both are depicted.
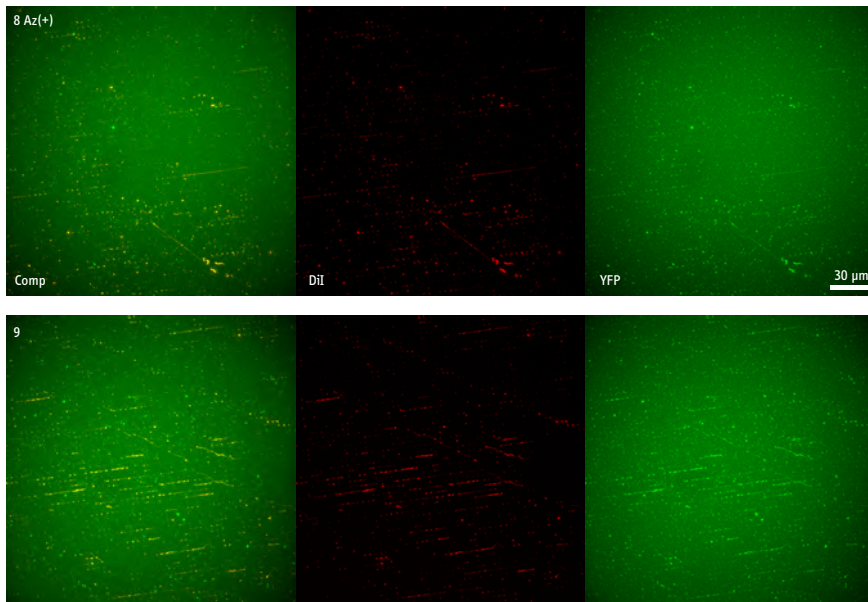
Figure 3.11: Results of bacteriophage capture on stretched Az(+) multifunctional nanowires. DiI, YFP and a composite of both are depicted.
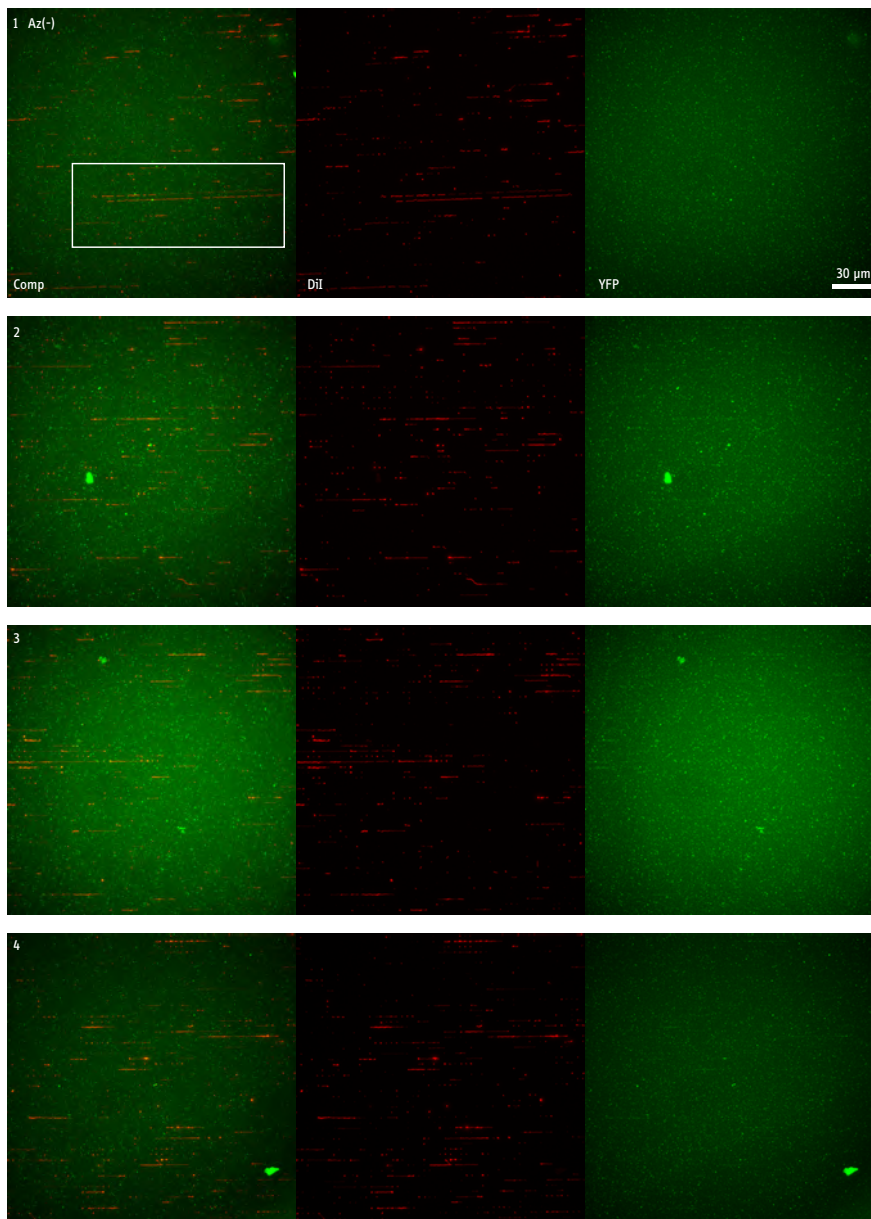
Figure 3.12: Control experiment of bacteriophage capture on stretched Az(-) functional nanowires. No significant signal of bacteriophage YFP fluorescence on the nanowires. White box represents excerpt shown in discussion.
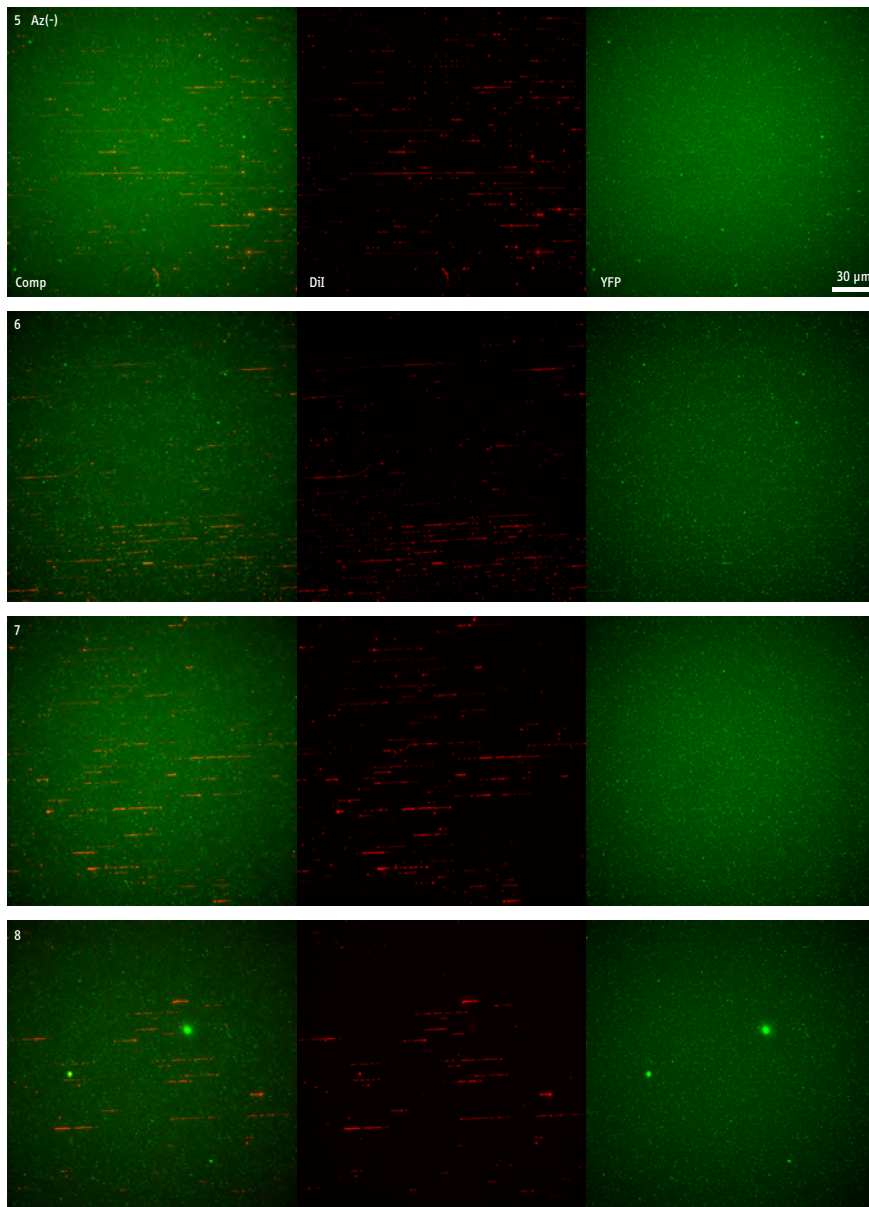
Figure 3.13: Control experiment of bacteriophage capture on stretched Az(-) functional nanowires. No significant signal of bacteriophage YFP fluorescence on the nanowires.

3
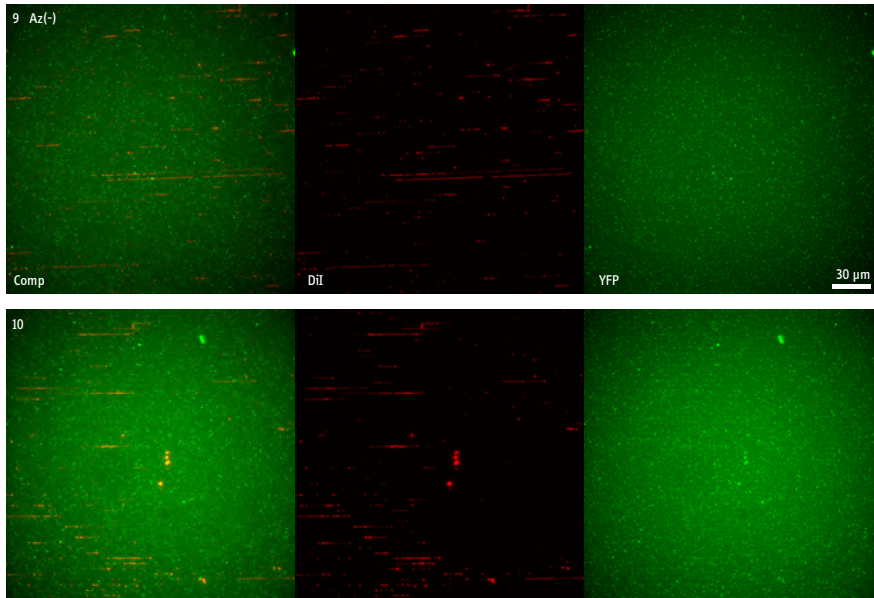
Figure 3.14: Control experiment of bacteriophage capture on stretched Az(-) functional nanowires. No significant signal of bacteriophage YFP fluorescence on the nanowires.

REFERENCES

[1] C. G. Ehrenberg, *Die Infusionsthierchen als vollkommene Organismen. Ein Blick in das tiefere organische Leben der Natur* (L. Voss, 1838).

[2] J. M. Rabanel, P. L. Latreille, A. Lalloz, P. Hildgen, and X. Banquy, *Chapter 4 - nanostructured nanoparticles for improved drug delivery,* in *Nanostructures for Drug Delivery*, Micro and Nano Technologies, edited by E. Andronescu and A. M. Grumezescu (Elsevier, 2017) pp. 149–182.

[3] D. L. Perrier, L. Rems, and P. E. Boukany, *Lipid vesicles in pulsed electric fields: Fundamental principles of the membrane response and its biomedical applications,* Advances in Colloid and Interface Science **249**, 248 (2017).

[4] A. Wang, C. C. Miller, and J. W. Szostak, *Core-shell modeling of light scattering by vesicles: Effect of size, contents, and lamellarity,* Biophysical Journal **116**, 659 (2019).

[5] K. Nishimura, T. Matsuura, K. Nishimura, T. Sunami, H. Suzuki, and T. Yomo, *Cell-free protein synthesis inside giant unilamellar vesicles analyzed by flow cytometry,* Langmuir **28**, 8426 (2012).

[6] C. Zhu, Q. Li, M. Dong, and X. Han, *Giant unilamellar vesicle microarrays for cell function study,* Analytical Chemistry **90**, 14363 (2018).

[7] W. Zong, S. Ma, X. Zhang, X. Wang, Q. Li, and X. Han, *A fissionable artificial eukaryote-like cell model,* Journal of the American Chemical Society **139**, 9955 (2017).

[8] P. Yang, R. Lipowsky, and R. Dimova, *Nanoparticle formation in giant vesicles: Synthesis in biomimetic compartments,* Small **5**, 2033 (2009).

[9] K. Nishimura, S. Tsuru, H. Suzuki, and T. Yomo, *Stochasticity in gene expression in a cell-sized compartment,* ACS Synthetic Biology **4**, 566 (2014).

3

[10] S. Aden, T. Snoj, and G. Anderluh, *Chapter eight - the use of giant unilamellar vesicles to study functional properties of pore-forming toxins,* in *Pore-Forming Toxins,* Methods in Enzymology, Vol. 649, edited by A. P. Heuck (Academic Press, 2021) pp. 219–251.

[11] D. L. Perrier, A. Vahid, V. Kathavi, L. Stam, L. Rems, Y. Mulla, A. Muralidharan, G. H. Koenderink, M. T. Kreutzer, and P. E. Boukany, *Response of an actin network in vesicles under electric pulses,* Scientific Reports **9**, 8151 (2019).

[12] S. Sachdev, A. Muralidharan, D. K. Choudhary, D. L. Perrier, L. Rems, M. T. Kreutzer, and P. E. Boukany, *DNA translocation to giant unilamellar vesicles during electroporation is independent of DNA size,* Soft Matter **15**, 9187 (2019).

[13] E. Schäfer, M. Vache, T.-T. Kliesch, and A. Janshoff, *Mechanical response of adherent giant liposomes to indentation with a conical AFM-tip,* Soft Matter **11**, 4487 (2015).

[14] N.-N. Deng, M. Yelleswarapu, and W. T. S. Huck, *Monodisperse uni- and multicompartment liposomes,* Journal of the American Chemical Society **138**, 7584 (2016).

[15] B. G. Carvalho, B. T. Ceccato, M. Michelon, S. W. Han, and L. G. de la Torre, *Advanced microfluidic technologies for lipid nano-microsystems from synthesis to biological application,* Pharmaceutics **14**, 141 (2022).

[16] F. M. White, *Fluid mechanics,* 7th ed., McGraw-Hill series in mechanical engineering (McGraw Hill, New York, N.Y., 2011).

[17] C. Steinem and M. Meinecke, *ENTH domain-dependent membrane remodelling,* Soft Matter **17**, 233 (2021).

[18] F. Twort, *An investigation on the nature of ultra-microscopic viruses,* The Lancet **186**, 1241 (1915).

[19] F. d'Herelle, *On an invisible microbe antagonistic to dysentery bacilli,* CR Acad Sci Paris **165**, 373 (1917).

[20] F. d'Herelle, *On an invisible microbe antagonistic to dysentery bacilli (translation from french),* Bacteriophage **1**, 3 (2011).

[21] W. C. Summers, *The discovery of bacteriophages and the historical context,* in *Bacteriophages: Biology, Technology, Therapy,* edited by D. R. Harper, S. T. Abedon, B. H. Burrowes, and M. L. McConville (Springer International Publishing, Cham, 2021) pp. 387–400.

[22] S. T. Abedon, C. Thomas-Abedon, A. Thomas, and H. Mazure, *Bacteriophage prehistory,* Bacteriophage **1**, 174 (2011).

[23] D. E. Fruciano and S. Bourne, *Phage as an antimicrobial agent: D'herelle's heretical theories and their role in the decline of phage prophylaxis in the west,* Canadian Journal of Infectious Diseases and Medical Microbiology **18**, 19 (2007).

[24] W. C. Summers, *Bacteriophage therapy,* Annual Review of Microbiology **55**, 437 (2001).

[25] R. Międzybrodzki, N. Hoyle, F. Zhvaniya, M. Łusiak-Szelachowska, B. Weber-Dąbrowska, M. Łobocka, J. Borysowski, Z. Alavidze, E. Kutter, A. Górski, and L. Gogokhia, *Current updates from the long-standing phage research centers in georgia, poland, and russia,* in *Bacteriophages: Biology, Technology, Therapy,* edited by D. R. Harper, S. T. Abedon, B. H. Burrowes, and M. L. McConville (Springer International Publishing, Cham, 2021) pp. 921–951.

[26] D. R. Harper, *Introduction to bacteriophages,* in *Bacteriophages: Biology, Technology, Therapy,* edited by D. R. Harper, S. T. Abedon, B. H. Burrowes, and M. L. McConville (Springer International Publishing, Cham, 2021) pp. 3–16.

[27] V. H. Aswani and S. K. Shukla, *An early history of phage therapy in the united states: Is it time to reconsider?* Clinical Medicine Research **19**, 82 (2021).

3

[28] N. Chanishvili, *Chapter 1 - phage therapy—history from twort and d'herelle through soviet experience to current approaches,* in *Bacteriophages, Part B*, Advances in Virus Research, Vol. 83, edited by M. Łobocka and W. Szybalski (Academic Press, 2012) pp. 3–40.

[29] L. Zaffiri, J. Gardner, and L. H. Toledo-Pereyra, *History of antibiotics. from salvarsan to cephalosporins,* Journal of Investigative Surgery **25**, 67 (2012), pMID: 22439833.

[30] F. G. Mildenberger, *Unbeugsam und unbelehrbar,* Der Urologe **59**, 713 (2019).

[31] J.-P. Pirnay, M. Merabishvili, H. Van Raemdonck, D. De Vos, and G. Verbeken, *Bacteriophage production in compliance with regulatory requirements,* in *Bacteriophage Therapy: From Lab to Clinical Practice*, edited by J. Azeredo and S. Sillankorva (Springer New York, New York, NY, 2018) pp. 233–252.

[32] J. Lin, F. Du, M. Long, and P. Li, *Limitations of phage therapy and corresponding optimization strategies: A review,* Molecules **27**, 1857 (2022).

[33] I. M. Abd-Allah, G. S. El-Housseiny, I. S. Yahia, K. M. Aboshanab, and N. A. Hassouna, *Rekindling of a masterful precedent; bacteriophage: Reappraisal and future pursuits,* Frontiers in Cellular and Infection Microbiology **11** (2021).

[34] A. León-Buitimea, F. de Jesús Balderas-Cisneros, C. R. Garza-Cárdenas, J. A. Garza-Cervantes, and J. R. Morones-Ramírez, *Synthetic biology tools for engineering microbial cells to fight superbugs,* Frontiers in Bioengineering and Biotechnology **10** (2022).

[35] S. S. Issabekov, N. S. Syrym, A. A. Sambetbayev, K. D. Alikhanov, and B. A. Yespembetov, *Prospects of bacteriophage collections in disinfectant applications,* Veterinary World , 220 (2022).

[36] E. Stone, K. Campbell, I. Grant, and O. McAuliffe, *Understanding and exploiting phage–host interactions,* Viruses **11**, 567 (2019).

[37] P. Domingo-Calap, P. Georgel, and S. Bahram, *Back to the future: bacteriophages as promising therapeutic tools,* HLA **87,** 133 (2016).

[38] M. Jamal, S. M. A. U. S. Bukhari, S. Andleeb, M. Ali, S. Raza, M. A. Nawaz, T. Hussain, S. u. Rahman, and S. S. A. Shah, *Bacteriophages: an overview of the control strategies against multiple bacterial infections in different fields,* Journal of Basic Microbiology **59,** 123 (2018).

[39] S. Sharma, S. Chatterjee, S. Datta, R. Prasad, D. Dubey, R. K. Prasad, and M. G. Vairale, *Bacteriophages and its applications: an overview,* Folia Microbiologica **62,** 17 (2016).

[40] A. A. Cisek, I. Dąbrowska, K. P. Gregorczyk, and Z. Wyżewski, *Phage therapy in bacterial infections treatment: One hundred years after the discovery of bacteriophages,* Current Microbiology **74,** 277 (2016).

[41] L. Zeng and I. Golding, *Following cell-fate in e. coli after infection by phage lambda,* Journal of Visualized Experiments (2011).

[42] D. Brüggemann, J. P. Frohnmayer, and J. P. Spatz, *Model systems for studying cell adhesion and biomimetic actin networks,* Beilstein Journal of Nanotechnology **5,** 1193 (2014).

3

4

MICROSTRUCTURE PLATFORMS FOR

BIOLOGICAL APPLICATIONS

This chapter contains collaborative work as declared in the text.

Various fabrication techniques to produce micro-structured platforms were reviewed. Both biomolecules as well as living cells can be manipulated for a wide variety of biomedical applications. The techniques comprise direct laser writing, two photon polymerisation, and ebeam lithography in combination with reactive ion etching and Bosch process deep reactive ion etching. With some exceptions of direct writing, the goal was production of molds for PDMS soft lithography. Micro topographies were created to sort nanowires using dewetting as demonstrated in the previous chapters. Other topographies were created with partner projects to research cell migration and glial cell behaviour towards synthetic model axons. Furthermore, microfluidic systems were fabricated for insulator-based dielectrophoretic sorting of mitochondria, a single-cell trap array for localized electroporation and a two-phase system for microbucket production.

4

4.1. INTRODUCTION

Microstructuring is the basic tool for manufacturing of many analytical devices, also microfluidic platforms. It can be used as a tool to mimic the micro environment of living systems to further understanding of their function and biology. The scope of this chapter focuses on surface topologies and microfluidic structures for manipulating biomolecules and cells, excluding the broad range of microelectronics, micro optics and microelectromechanical systems (MEMS). Most important for the project, was the fabrication of micropillar topographies for stretching of the nanowires. In preparation for a future complete system design, development and fabrication of microfluidic flowcells was investigated in collaborations with other projects.

Many processes are known for use in microstructuring. The basic considerations to make when deciding for a process are resolution, turn-around time and materials. Operational differences such as machine availability or cost should also be considered. The chapter provides details on direct laserwriting, two-photon polymerization, electronic beam writing and silicon dry etching. A good overview of the various other techniques available especially in microfluidics was given by Scott and Ali [1].

Being able to handle microliters of analytes in a reproducible manner is a prerequisite to allow small sample sizes and low amounts of functional (bio-)chemicals [2]. While the latter mainly aims at reducing manufacturing costs, there are situations, where the sample size is very limited (e.g. forensic samples) or at least desired to be minimal (e.g. blood samples, blood sugar test with capillary blood). In addition, the micro domain offers physical properties not, or not easily available in traditional (macro)fluidic handling, such as a reliable laminar flow. The conditions to this are best estimated by the Reynolds number $Re = \frac{\rho v L}{\mu}$, with the fluid's density ρ, velocity v, characteristic linear dimension L and dynamic viscosity μ [3]. For values $Re < 2000$ laminar flow tends to occur in enclosed systems, and most microfluidic chips exhibit a Reynolds number way beyond 100. Thus

microfluidic processes are almost exclusively laminar flow dominated.[1]

Another, related effect is the ratio of advective and diffusive molecular transport, expressed by the Péclet number $Pe = \frac{vL}{D}$, with diffusion coefficient D. It can also be understood as the ratio of diffusion time per convection time. Owing to the small dimensions, diffusion time is usually much reduced, speeding up reactions, especially regarding macromolecules such as DNA and proteins.

With small volumes and corresponding small liquid masses, gravity becomes less of a factor and the surface and interfacial tension have a much higher influence at the microscale. Also capillary forces can be utilized and have led to many successful application in the field of paper based diagnostics, where self-pumping of the papers soft matrix capillaries is used. [7]

Demonstrative examples of applications of these microfluidic effects related to the presented work lie in the versatile modes of utilizing laminar flow, e.g. for particle focusing flow cytometry, a high throughput analysis of cells [8]; the lack of turbulence can also be a challenge for mixing of liquids and has been addressed by much research [9, 10]. Also flow sheathing is possible, offering interesting applications such as sheathed droplet creation to produce microbuckets [11], single particle separation and capture (especially interesting for cells and subcellular components, e.g. localized electroporation and gene transfection [12]).

However, it should not go unnoticed, that asides from the continued advances in functionality, microfluidics is still deficient in the actual transfer to applications and usable devices [13–16]. In most cases the compact microfluidic chips require many auxiliary devices, such as precision pumps, spectrometers, microscopes, power supplies and the like. A main difficulty also lies in interfacing the system to its context, especially adding or retrieving a sample. Also sample preparation is often required and not integrated into the system. [17, 18] Or to quote Mohammed et al. [14]: "Lab-on-a-chip or Chip-in-a-lab",

---

[1]Although literature on turbulence (not just chaotic advection [4, 5]) at very low Reynolds number does exist [6].

while usually the latter is the truth.

Microstructuring also gained rising importance in the mimicking of biological surfaces, be it for research on the behaviour of organisms or cells to certain topologies (e.g. cell migration[19], nerve regeneration [20], adhesion of insect feet [21]) or the biomimetic reproduction of such surface for understanding the function or the technological use (e.g. lotus effect [22] and rose petal effect, as two examples of the huge variety of wetting scenarios on hierarchical structures [23, p. 2268][24], shark-skin surfaces reducing fluid drag and bio-fouling [25–28], gecko-inspired adhesive [29] or continuous directional water transport on the surface of the carnivorous plant *Nepenthes alata* [30]).[2]

In this work, several micro manufacturing techniques (Figure 4.2) were applied to manufacture designs for applications and different techniques were compared to find the optimal process for an efficient production: Suitable micropillar molds were created for stretching the polymeric nanowires shown in the previous chapters. Additionally, microfluidic chips and micropillar topographies were manufactured and developed in cooperation with different partners: Micropillar arrays researching the migration behaviour of cancer cells and the sheathing by glial cells; and microfluidic flow cells for electroporation of single cells, microbucket manufacturing, micropipette aspiration of cells and a label free cell sorter based on a dielectrophoretic approach.

4.1.1. EVALUATION OF HIGH ASPECT RATIO CAVITIES

To assess the quality of molds produced using different lithography techniques and parameters, it was desirable to visualize the surface of the molding cavities. However, it proved very difficult to achieve this, at least for micrometer sized, high-aspect ratio cavities. The first constraint is the high resolution required. With diameter sizes of the cavities ranging down to $1\,\mu m$, we are close to the wavelength of visible light, thus classical optical methods are limited in detail to begin with. A conventional limit to

---

[2]On the history of Biotechnik/Bionik/bionics/biomimetics, more overview and the aspect of sustainability consult [31–33]

4
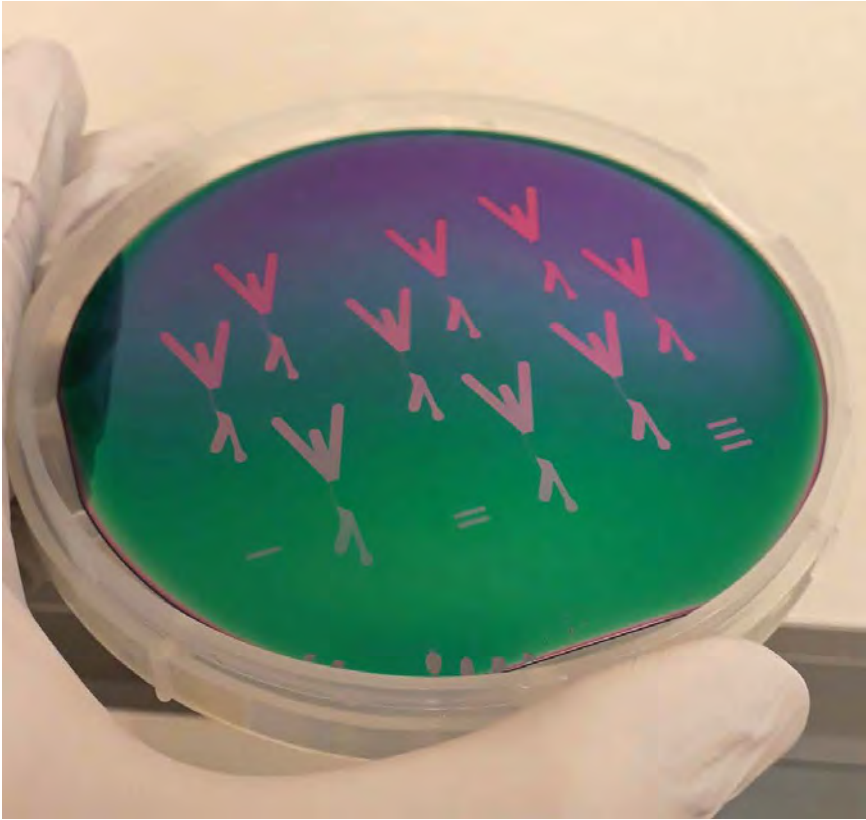
Figure 4.1: Example of a 100 mm silicon wafer with macro and micro structures during processing. The wafer was covered with a thin SiO$_2$ hardmask creating the color effect. The structure was created using negative resist and ebeam writing and was transferred into the hardmask in the following etching step, which in turn served to etch the pattern deeper into the silicon substrate using Bosch process deep reactive ion etching. The wafer would then be the mold for an insulator-based dielectrophoretic device for continuous sorting of cells and bioparticles such as mitochondria (see Figure 4.6).

resolution in light microscopy was described by Rayleigh [34, 35] [3] as the minimum distance $d = \frac{0.61\lambda}{NA} = \frac{0.5\lambda}{n\sin(\theta)}$ where two objects are still discernible, using the wavelength λ and the numerical aperture NA as product of refractive index of the medium n and maximal half-angle θ of the cone of light that can enter or exit the lens. This basic approach results in a theoretical resolution of ~200 nm for $\lambda = 400$ nm.

---

[3] and Abbe, who allows a smaller distance $d = \frac{0.5\lambda}{NA}$ where the overlap of two Airy profiles just shows a dip in between the two maxima: $d = \frac{0.5\lambda}{NA}$ [36]; the Sparrow limit used in astronomy goes even further and is satisfied with a flat intensity profile $d = \frac{0.47\lambda}{NA}$ [37]; these criteria are not the only factors governing resolution and there are techniques overcoming the limits of the classical Abbe/Rayleigh criteria using super-resolution techniques [38–40]
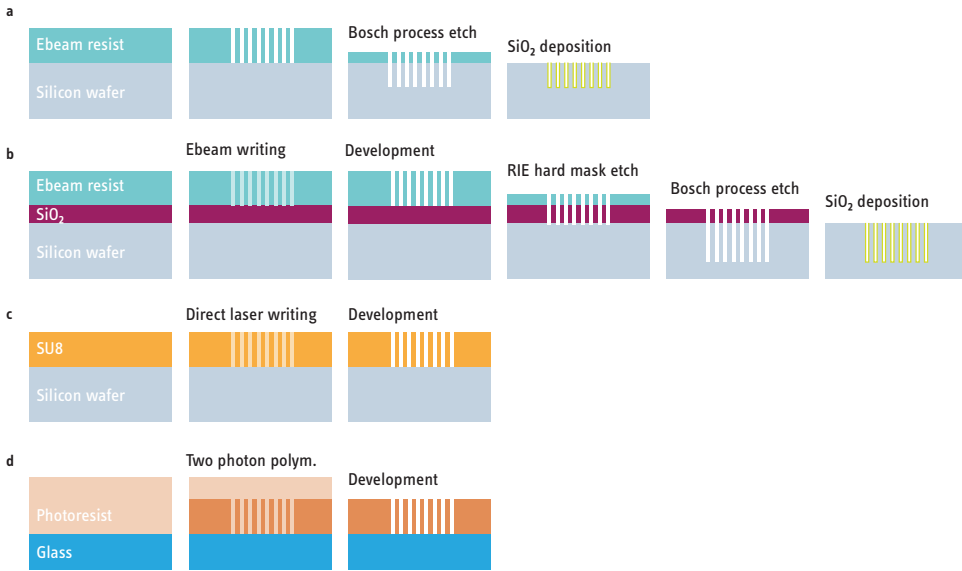
Figure 4.2: Schematic overview of evaluated processing techniques: a) Ebeam lithography & deep reactive ion etching (DRIE) Bosch process followed by deposition of a SiO$_2$ thin layer to enhance immediate silane reactivity, used for medium depth structures <20 µm; b) Same process including more durable plasma-enhanced chemical vapor deposition (PECVD) SiO$_2$ hard mask structured with fluorine chemistry reactive ion etching (RIE) to allow for deeper etching ≫20 µm; c) Direct laser writing in SU-8 negative resist, precise spin coating is necessary to define structure heights; d) Two photon polymerization (2PP) of photo resist on glass, precise 3D voxel writing inside drop of photo resist with subsequent development

Much higher resolution is achieved with electron microscopy, utilizing the de Broglie wavelength of high impulse electrons $\lambda_D = \frac{h}{p} = \frac{h}{\sqrt{2meV}}$, with Planck constant h, impulse p, mass m, elementary charge e and accelerating voltage V [41]. With conventional scanning electron microscopy, energies of 5 keV–40 keV are usual. This equals a λ_d of 17 pm–6 pm and can be regarded as a hint towards the achievable resolution. It is noted however, that other than in case of TEM, the Rayleigh criterion can not be used to derive resolution for scanning electron microscope (SEM), where the actual resolution is defined by a much more complicated interplay of different factors, including electron energy, electron-specimen interaction, detection and the selected signal. This is also owed to the fact, that the signal is not derived directly from an optical path but indirectly, e.g. through secondary electrons or back scattered electrons. [42]

The second constraint is that vertical wall high-aspect ratio holes are basically tubes. And optically examining the inner sidewalls of a thin tube from its opening using non-penetrating rays is difficult by design. The reflection angle is bad, and the tube acts as a trap, leading to weak signals. Also the sidewall blocks part of the field-of-view, disturbing the aperture of the detector. So even using higher wavelength such as the electron beam of a SEM does not solve the fact that we try to visualize the vertical walls of a deep tunnel from a relatively far away viewpoint at a steep angle. SEM does have plenty of resolution
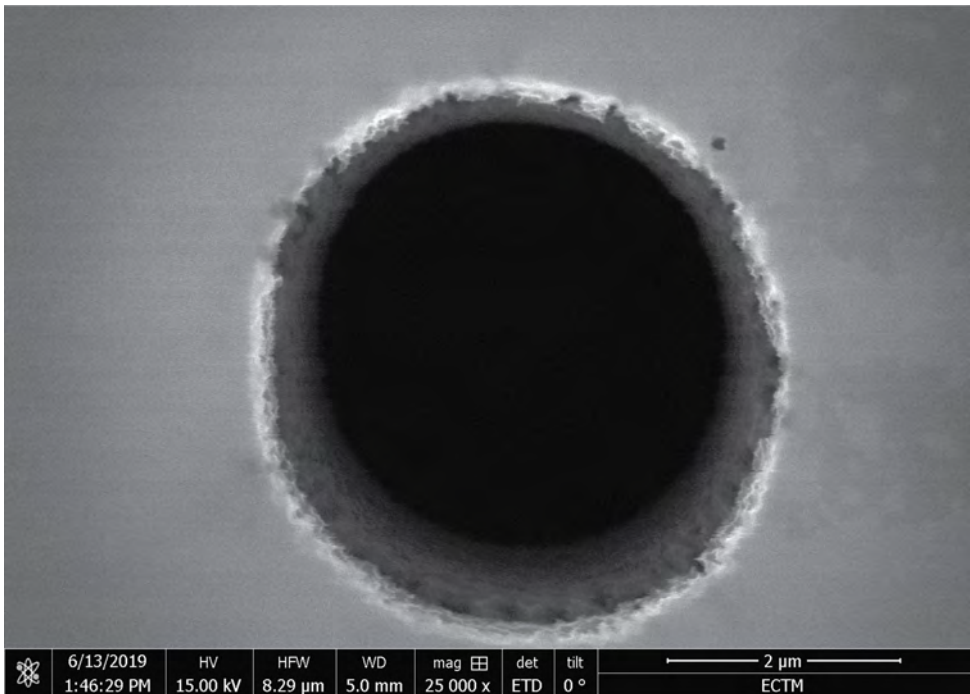
Figure 4.3: SEM picture of 4.5 µm cavity etched into Si wafer using Bosch process dry etching. Other than near-surface, the signal is too weak and out of focus. The angle is also too steep to allow for much detail.

for the task, but the scanning angle of the sidewalls will not yield much backscatter or secondary signal. Plus the depth requires big focal length or multifocal stacking, just as the optical light pendant would. Trials were made using SEM (Figure 4.3), but it resulted in the admission, that it is easier to cast the mold and analyze the released structures. In the few cases where a detailed view of the mold's interior side wall was needed, e.g.

when optimizing the dry etching process and understanding the exact shape of the (non-vertical) cavities, the mold had to be sacrificed and sawed open to view the profile (Figure 4.4).
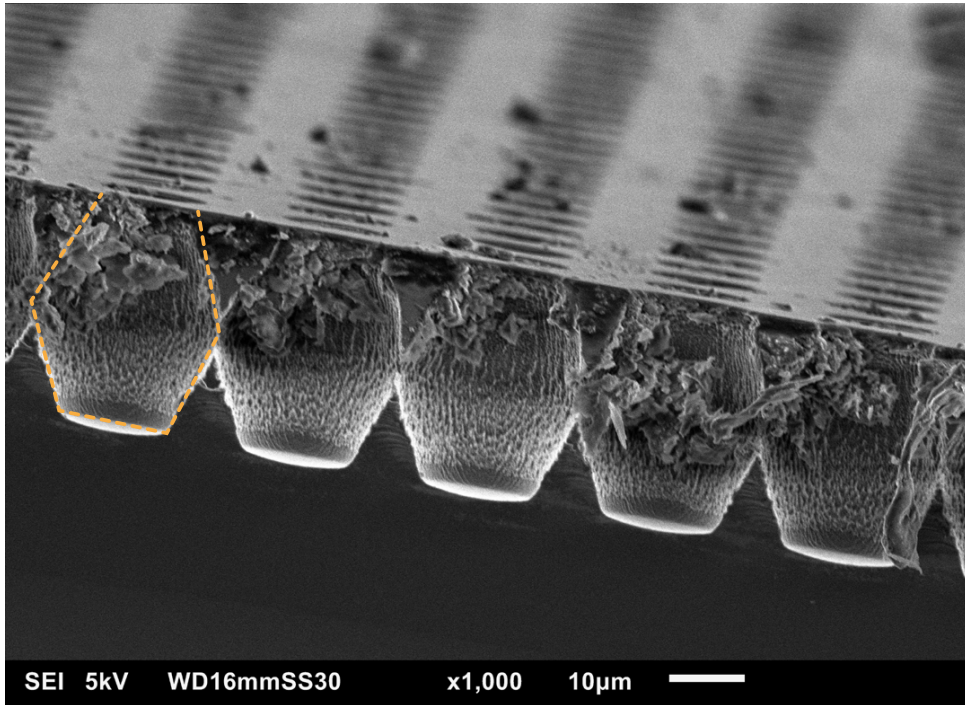
Figure 4.4: Cross section of a wafer mold surface cut with a dicing saw, that did not produce any pillars on the cast PDMS substrate. A common problem when adapting Bosch process etching: a wrong ratio of etch time and passivation time created cavities (orange dotted line) instead of vertical sidewalls. Cast with PDMS, the resulting pear-shaped structures are usually unable to be released from mold and were severed when the cured PDMS was peeled off. The PDMS is still stuck inside the cavities. An increase of the passivation step time yielded the intended vertical sidewalls. However, with careful adaption of the undercut and good sidewall treatment, convex shapes are possible to be cast and released if desired, compare Figure 4.16.

A technique with surprising resolution and very short scanning and preparation times was white light interferometry. Although it also comes with limitations concerning steep/vertical sidewalls, it allows for quick estimation of the quality of a sample area in the µm regime (depending on the topography, resolution of this technique can be much higher) [43]. Both molds and casts could be characterized using this technique (Figure 4.5).
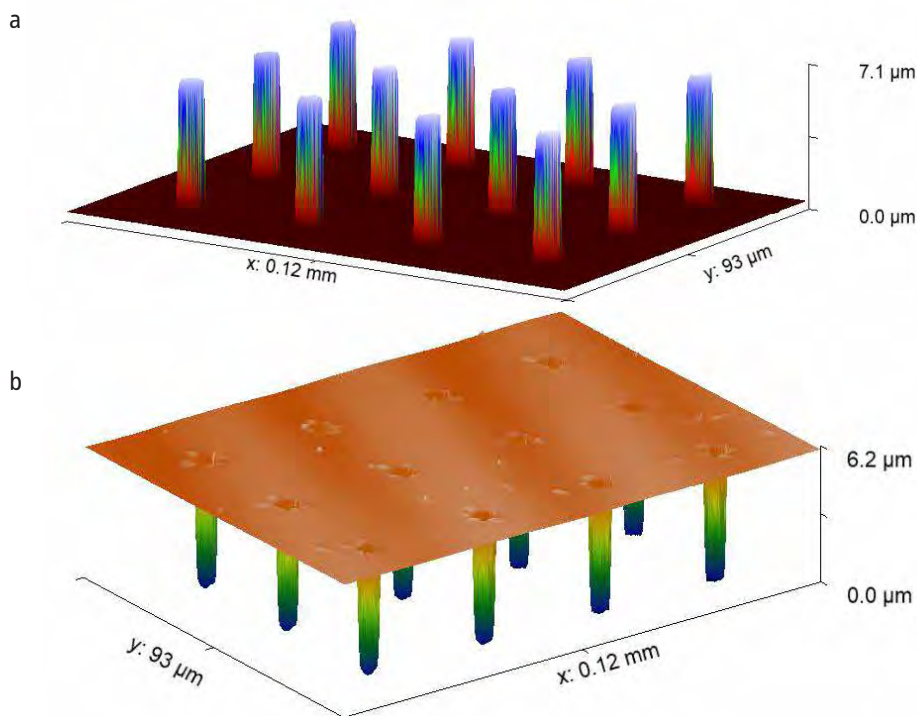
Figure 4.5: White light interferometry scans using Bruker ContourGT-K, (Billerica MA, USA) of a two-photon polymerization printed mold (b) and its cast PDMS structure (a). The method offers good resolution and a quick overview without the need for sample preparation. The problem of visualizing steep sidewalls persists however, also sharp edges can produce artifacts. (Measurement done in collaboration with Ahmed Sharaf)

4.1.2. BASIC MICROFABRICATION APPROACHES

The microstructures can be created either using direct machining or replication by molding a negative. If possible for the choice of materials and the structure, molding usually allows for easier and quicker reproduction and is preferred, when a multitude of the same structure will be produced. Problems can arise from the material choice: How is the physical and chemical interaction of substrate and mold? PDMS for example easily bonds to silicon and requires surface modification for reliable demolding [44, 45]. The same applies for casting of PDMS in PDMS molds [46]. Very small features in high aspect ratio might require very low friction forces or a high robustness of mold and substrate. Also cavities are usually not able to be demolded, so profiles with undercut can require

methods other than molding or a sacrificial mold (that e.g. can be dissolved for release of the substrate).

Direct machining is very time consuming, although it can be required in cases of non-moldable structures. This will mainly be the case in early prototyping, for 3D structures or very soft materials not surviving a demold.

Concerning materials used in microfluidics, a predominance of PDMS was observed and it is also the main final substrate used in this work. The reason for this lies in its numerous advantages: Although industry related persons might disagree and point to cheaper polymers, for research lab standards it is reasonably inexpensive, especially compared to silicon wafers [47]. Polymerisation can be controlled using temperature and is quick but not too fast. Using bubble-free centrifugal mixing, the turnover time can be minimized. The resolution is excellent, with up to molecular-scale reported [48], while being sufficiently water impermeable (but gas permeable, good for cell cultures), optically transparent (240 nm – 1100 nm) with low autofluorescence [49], basically biocompatible, electrically insulating and sealable/stackable with glass or additional PDMS structures through plasma activated bonding [50].

If silicon wafers are used as master mold for PDMS casting, a surface treatment is needed to avoid bonding of PDMS to the silicon. In this work all structured wafer's surfaces were functionalized through silanization of the activated silicon with fumes of a fluorinated compound: After plasma surface treatment (40 mbar, 100 W, 3 min), the wafer molds were exposed to fumes of 200 μL Trichloro(1H,1H,2H,2H-perfluorooctyl)silane (CAS 78560-45-9, Sigma Aldrich) in a desiccator under vacuum for 4 h.

4.2. DIRECT LASERWRITING

Direct laserwriting poses a maskless alternative to standard photolithography, which uses a photomask. It might be compared to what digital printing is opposed to offset printing. A laser is used to scan the photoresist and transfer an image to the photoresist pixelwise.

As such, it allows for rapid prototyping and fast realisation of multitudes of single designs, but also enables the exposure of material not compatible with a photomask, such as liquids. For the application with microfluidic designs, direct laserwriting is especially interesting in combination with a high thickness, high aspect ratio photoresist, such as SU-8. It combines high thickness >200 μm and aspect ratios with the flexibility of a scanner, resulting in the ability to fast prototype micrometer resolution structures in deep channels with vertical sidewalls, without the need for a mask. [51]

It should be noted, this is a 2.5D technique, as the beam of standard laser writers will polymerize the whole cross section of a photoresist layer, thus producing 3D structures, but constrained to extruded projections on the surface. Stepwise building up separately exposed layers is possible and allows for a little more freedom in design. This idea is utilized in stereolithography, nowadays a quite common 3D printing method [52].

The machine used (MLA 150 Heidelberg Instruments) consists of wafer holder and a laser writing head, mounted to be movable against each other in X, Y and Z direction to allow scanning of the wafer and focusing of the laser. Two laser wavelengths are available (375 nm and 405 nm). Resolution is ca. 1 μm and the writing time of a full 100 mm wafer 35 min[4].

It was used to fabricate several microfluidic structures in partner projects, and allowed to reduce waiting time for ordering printed photomasks while allowing a sub 10 μm resolution and fast processing time of full wafers (<1 h incl. setup). Main factor for choosing this technique, apart from the very fast turnover time, was the large structure height and aspect ratio of the microfluidic structures: heights of up to 200 μm were required. SU-8 is well suited for these large thicknesses and also high aspect ratios. Figure 4.6 shows the mold of a microfluidic channel created for cell nuclei extraction (SU-8 on silicon wafer).[5] Structure height is 100 μm, while the thinnest connects in

---

[4]According to Heidelberg Instruments
[5]A cooperation with Georg Pesch, Univ. College Dublin and Yara Ehlert, Univ. of Bremen [53], who designed the structures and tested the functionality, while I adapted the required processes and fabricated the structures.

between teeth are 25 µm in width. With structures of this size, temperature change related stress is a huge challenge. It can be avoided by careful temperature ramping.

Another example is shown in Figure 4.7: here a structure for production of microbuckets was fabricated for a partner project, that combines sheaths of several fluids followed by crosslinking. The microbuckets were then used as a 3D cell culture platform. [11, 54]
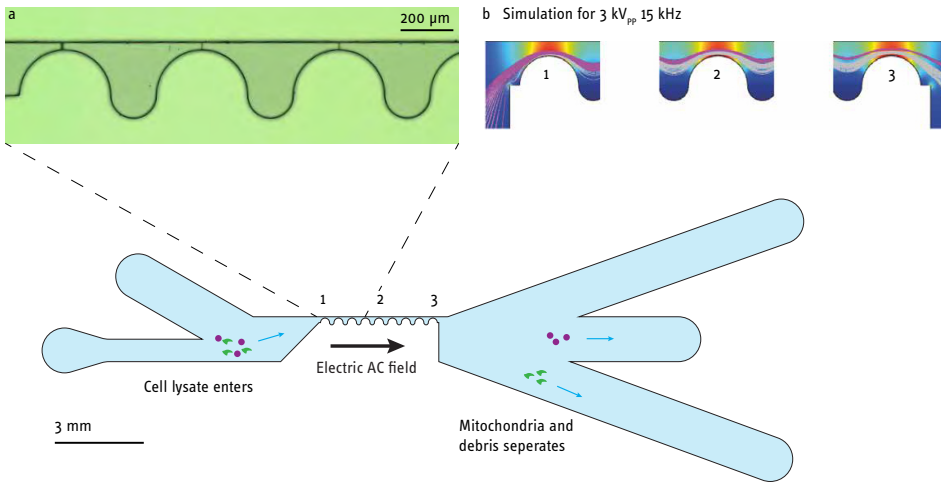
Figure 4.6: Direct laser writing in SU-8 of microfluidic channels for mitochondria/cell lysate separation. The device allows for insulator-based dielectrophoretic sorting in a flow: two electrodes create an alternating electrical field parallel to the flow. At the insulator channel constrictions, the field distortion creates a dielectrophoretic force on polarizable particles $F_{DEP} = 2\pi r^3 \varepsilon_m \frac{(\varepsilon_p^* - \varepsilon_m^*)}{(\varepsilon_p^* + 2\varepsilon_m^*)} \nabla |E|^2$, depending on the particle radius r, electric field gradient $\nabla |E|$ the permittivity of free space ε_0, the complex relative dielectric constants of medium ε_m^* and particle ε_p^*. [55–57] a) Full structure schematic with enlarged microscope picture of separation channel (top view, channel height 100 µm); cell lysate is pumped through thin channel with wavy sidewall. The AC electric field induces forces perpendicular to the flow on particles, depending on particle properties. b) simulation of electric field (3 kV$_P$P, 15 kHz) and exemplary trajectories for 2 µm (purple) and 0.5 µm (grey) particles. A cooperation with G. Pesch, Univ. College Dublin, simulation provided by Y. Ehlert, Univ. of Bremen [53], I adapted the required processes and fabricated the structure

4.3. Two Photon Polymerization

Two photon polymerization (2PP) shows interesting properties compared to conventional optical lithography: it enhances the resolution limits of photolithography by using two-photon absorption of a larger wavelength.[6] This seems contradictory at first, as usually

[6]Work on 2PP was done in collaboration with Ahmed Sharaf during his Master Thesis in this project [58].
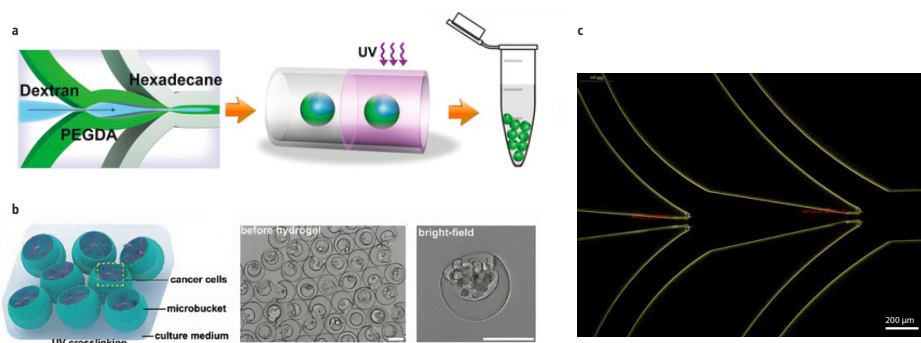
Figure 4.7: a) Device schematic for production of soft core-shell particles using a multiflow sheathing approach followed by UV crosslink. Removal of the dextrane part results in crescent shaped microbuckets; b) The hollow buckets can be seeded with cells and fixed in a microgel to observe (cancer) cell migration behaviour; c) Dark field optical image of results of direct laser writing in SU-8: microfluidic channels for microbucket creation through flow laminating. Channel height is 100 μm. (Figure a) reprinted from Liu et al. [54] licensed under CC BY 4.0; figure b) reprinted from Liu et al. [11] licensed under CC BY-NC 4.0; figure c) own work, I fabricated the structures for parts of the experiments)

the wavelength limits the resolution through the Rayleigh criterion and diffraction-limit of focal spot size, where a shorter wavelength (with photons of higher energy) allows for higher resolution, like discussed in 4.1.1. However, two-photon absorption is a non-linear optical process, and resolution here is also governed by the voxel size of excited photoresin. A single photon of this longer wavelength is not energetic enough to excite a valence electron transition and trigger a reaction. A two photon absorption event is sufficient in its combined energy, but simultaneous absorption is proportional to the square of the optical intensity [59, 60]. Only in the focal volume the intensity is high enough for a two photon absorption to occur. Outside of the focal volume, intensities are too low for a two-photon absorption event to take place (see Figure 4.8 for an illustrative example using two-photon fluorescence) [61]. This constricts the effective volume of the beam and enables a very high resolution.

Additionally – resulting from this approach – it is a scanning voxel method, that opposed to direct laser writing as presented in the previous section, has a three dimensional spatial restriction of its polymerization. This results in the ability of actual 3D printing,

as opposed to the sometimes called 2.5D of lithographic approaches. Resolutions of up to 100 nm have been reported using hydro gels [62]. The previously mentioned SU-8 can also be used in this process [63]. Another important advantage over e.g. ebeam lithography is that no vacuum system is needed. Disadvantage of the method is the duration of exposure: scaling with the volume of exposed material, exposure time and stage moving can amount to several hours of writing time, especially for high resolution and big objects. [64–66]
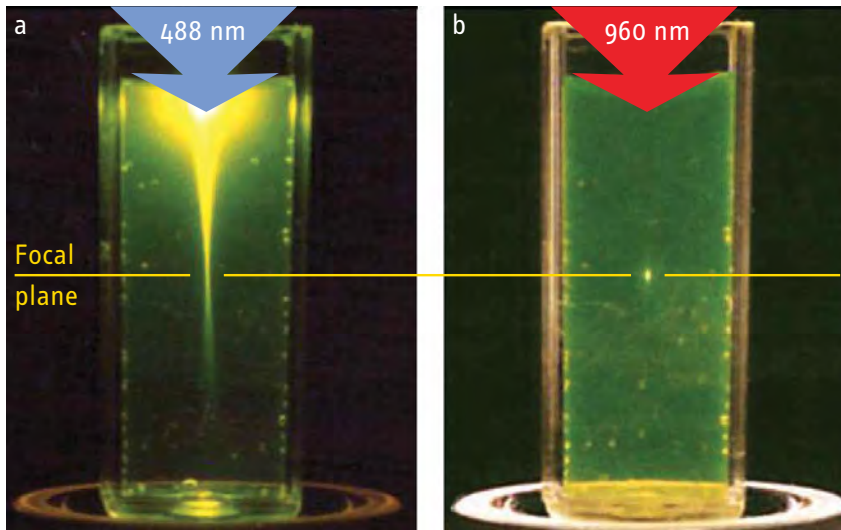
Figure 4.8: Excitation volumes of linear absorption and 2PP absorption in a fluorophor. While usually the minimum feature size in lithography is reduced using shorter wavelength (Rayleigh criteria), 2PP achieves higher resolution by constricting the space of photo activation to the small voxel in which the high intensity allows two photons to be absorbed simultaneously, combining their energy to a level sufficient for activation of the chemical reaction. A shorter wavelength can in theory be focused to a smaller area, but will – through linear absorption – activate photoresist in its beam path outside of the focus point, as the photons hold sufficient energy already. Figure reprinted from Zipfel et al. [64], copyright 2003, reproduced with permission from SNCSC

4.3.1. MATERIALS AND METHODS 2PP

2PP was performed on a Nanoscribe Photonic Professional GT (Nanoscribe GmbH & Co. KG, Eggenstein-Leopoldshafen DE) to create arrays of micropillars in dimensions down to 1 μm diameter and aspect ratios of up to 18 (see Figure 4.11). Also printing of a negative

mold of the same micropillars was prepared (see Figure 4.10).

Two different approaches were used with negative photoresist IP-Dip (Nanoscribe GmbH): Direct printing of the pillar structures on glass in conventional mode, and printing of a mold on a silicon substrate using dip-in laser lithography (DiLL) mode. The direct print was also used to cast a PDMS master mold from it. In addition, molds were created utilizing the positive resist AZ4562 (Microchemicals GmbH, Ulm DE) applied to a glass substrate via spincoating. Recipes are summarized in Table 4.1.

Table 4.1: Methods used with two photon polymerisation

	Fabrication Process		
Steps	Positive Resist	Negative Resist	Neg. R. on Silicon
Resist	AZ4562	IP-Dip	
Chemistry	Novolak/DNQ[7]	Acrylic resin	
Substrate	Glass $\varnothing$ 3 cm, 170 µm thick		Silicon chip 24 mm^2
Preconditioning	ICP rinse, blow-dry		+ Oxygen plasma 100 W, 25 kPa, 5 min
Spincoat	500 rpm, 5 s $\Rightarrow$ thickness 10 µm	Simple drop deposition	
Softbake	110 °C, 5 min	–	
Rehydrate	5 min	–	
Printing mode	Conventional		DiLL
Development bath	AZ400K/dH$_2$O 1:4 v/v 8 min	PGMEA,[8] 25 min	
Cleaning	dH$_2$O	ICP, 5 min	

A 63x objective lens (Numerical Aperture 1.4) and the standard laser wavelength of 780 nm were used for polymerizing the structures. 3D computer-aided design (CAD) models were imported to the Describe software (Nanoscribe GmbH) to segment the model into the actual laser scanning path and setting parameters such as scanning speed and laser power. The standard method defines horizontal z-stack layers (slicing), which

---

[7] Diazonaphtho-quinone
[8] Propylene glycol monomethyl ether acetate

are then each divided into arrays of lines at specific angles for the laser to scan (hatching). In this manner the whole CAD designed 3D body is transferred into the resin.
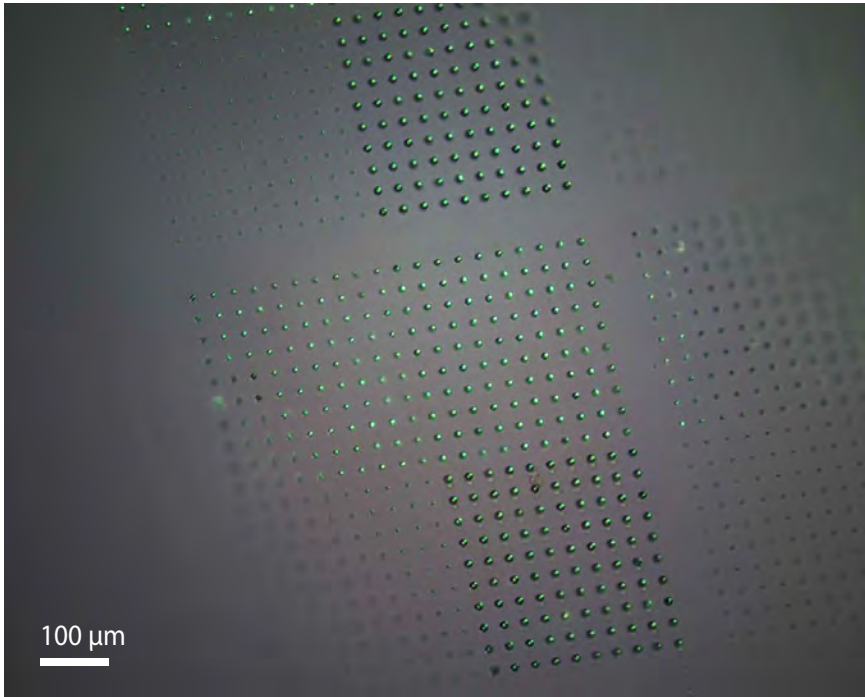
Figure 4.9: Multi focal image composite overview using a set of 2PP printed low aspect ratio pillar structures of different diameter.

Mainly, pillars of $1\,\mu m - 5\,\mu m$ diameter were printed (see Figure 4.9). The heights of the pillars ranged from $5\,\mu m$ to $18\,\mu m$. The laser power and scan speed used were $10\,\%$ and $4000\,\mu m\,s^{-1}$.

On the Nanoscribe printer used for these studies, two configurations are possible: conventional and DiLL. The conventional configuration is basically the setup of an inverted microscopy with oil-immersion. A drop of photoresist on top of a thin glass slide, and the objective below the glass, are connected through a drop of optical immersion oil enhancing the numerical aperture.

Using DiLL mode, the photoresist is cast onto the substrate and the lens itself is immersed in the hanging droplet of resist. In this mode, the substrates thickness and

optical quality are not relevant and opaque substrates such as silicon wafers can be used. This setup also allows for much taller structures, as the beam is not obstructed by previously exposed resin.
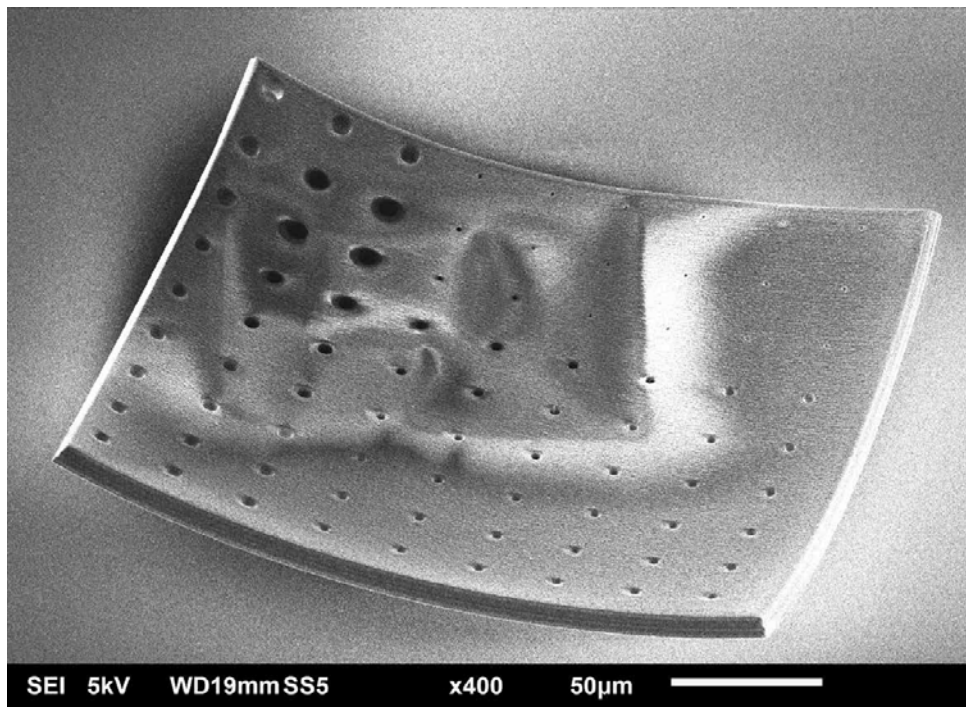
Figure 4.10: 2PP printed micromold made of negative resist on glass showed surface adhesion issues. This is probably due to tensions in the larger bodies of crosslinked resist.

4.3.2. RESULTS AND DISCUSSION

The production of micropillars was investigated using two-photon polymerization 3D printing on a Nanoscribe machine. With available standard recipes, desired results could not be obtained and much optimization was required for each new design (Figure 4.11). With adapted writing parameters, results have been of surprising quality. Hatching traces of the laser scan path[9] as still visible in Figure 4.12 could be reduced beyond visibility (see Figure 4.13 and Figure 4.14).

---

[9] Reminding one of the scalloping seen in Bosch process deep reactive ion etching (DRIE), see Figure 4.15
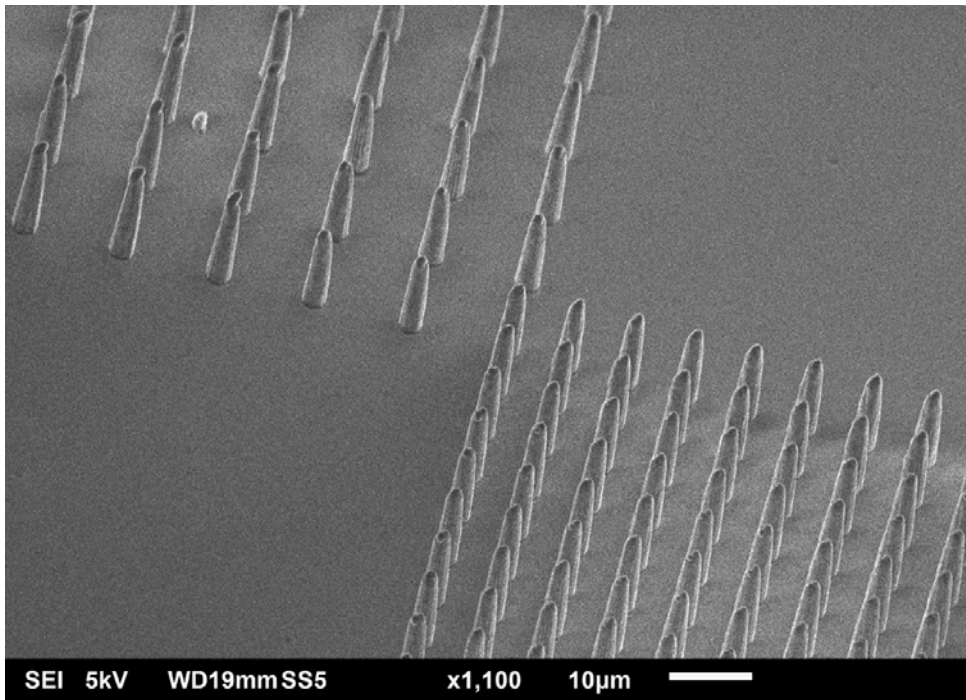
Figure 4.11: Nanoscribe direct printing of high aspect ratio pillars showed high degree of deformity. Further optimization would be necessary to achieve high quality print.
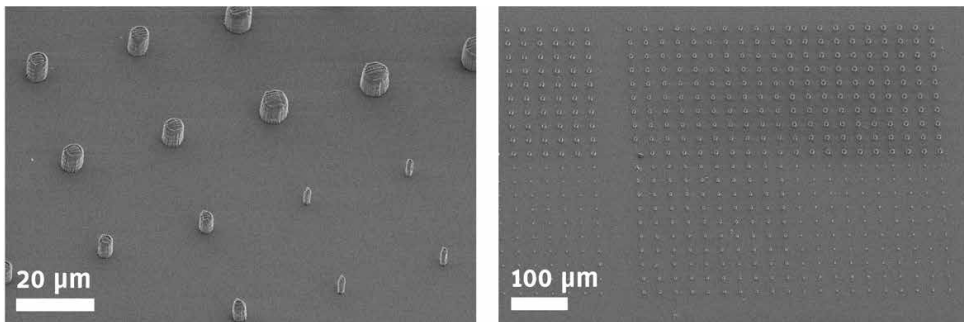
Figure 4.12: SEM picture of micropillars with low aspect ratio. The surface roughness is high with the tested writing parameters.

Using negative resist IP-Dip, pillar structures of $1\,\mu m - 15\,\mu m$ diameter were written. For $1\,\mu m$ diameter, heights of $5\,\mu m$ showed stable results. Higher aspect ratios up to 18 were possible, but lead to some pillars collapsing, probably during the development bath or drying (see Figure 4.14).

The creation of a PDMS mold negative was attempted after functionalizing the surface using the fluorosilane compound described earlier in this chapter, but reproducability was very poor for pillars of 5 μm and smaller. Most of these were peeled of with the cast PDMS and then stuck inside the PDMS mold. A better adhesion of the IP-Dip to glass might be obtained by printing a thin pedestal covering the glas surface, but this would largely increase writing time and trials were discontinued in favor of the positive resist.

Writing times even for small areas ($< 10x10$ mm^2) were in the 10+ hours, and thus too long to present an alternative to the faster ebeam/DRIE process. However, if large aspect ratios and very soft materials such as hydrogels are required, the technique of direct printing can proof very useful. It is easier to carefully develop weak printed structures, than to demold very soft substrate without destroying it.

Generally molding is faster than direct writing. And molding is more flexible regarding the cast materials, as the cast material does not have to be 2PP curable. However, writing of a master mold structure proved difficult with the standard negative resists, as shrinking of the large, flat body of polymerized resin produces much tension and often delaminated the structure (Figure 4.10), an effect known for negative resists [67]. Also with the structure at hand – a large body with only small details – writing time with negative resist rises extremely with the volume to be exposed.

Thus the positive AZ4562 resist appeared as the better solution, where only the small features have to be scanned. In combination with a precisely spincoated thickness it has shorter writing times and showed good adhesion to the surface with no delamination observed. Results of this approach are shown in Figure 4.10 and Figure 4.5. The surfaces appear smooth and release of the cast PDMS was unproblematic.

4.4. Ebeam writing

Ebeam lithography is a widely used technique in nanotechnology and microelectronics. It is a direct writing process: a stage holds and moves the sample and the electron beam
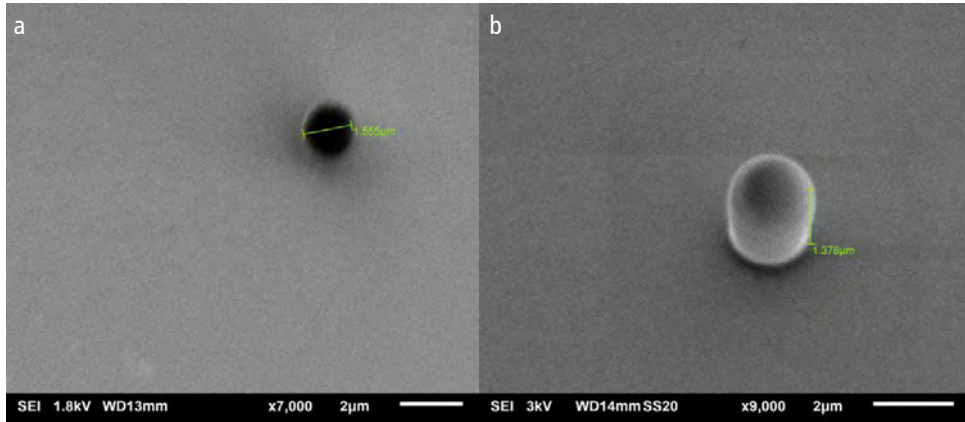
Figure 4.13: SEM picture of a) 2PP written AZ4562 mold and b) cast PDMS. Image taken at a 20° angle. (Experimental work and image by Ahmed Sharaf [58])
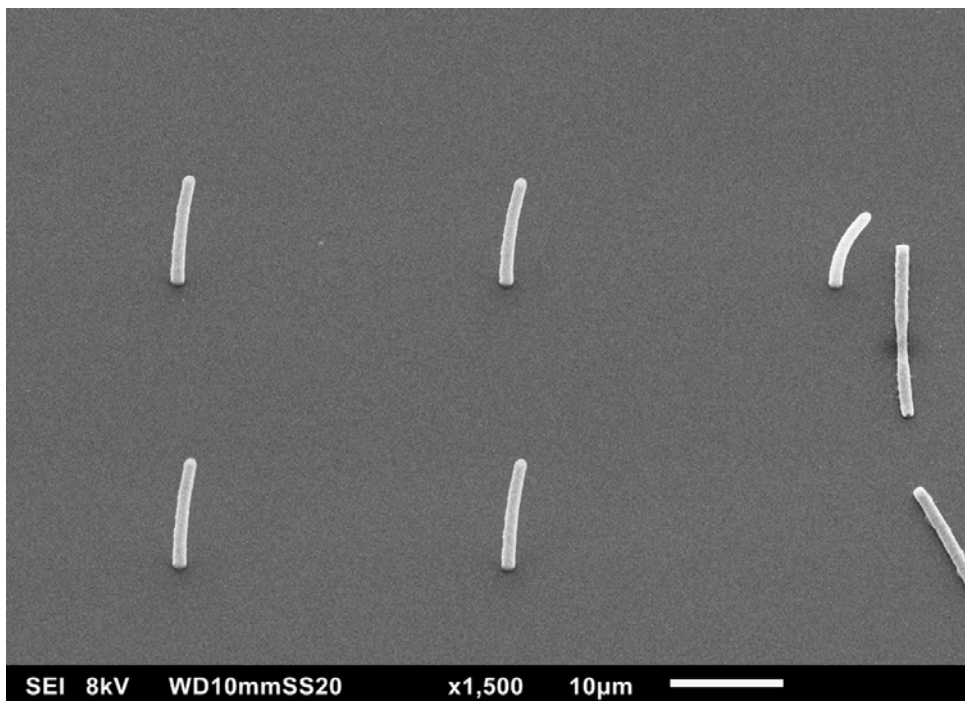
Figure 4.14: Nanoscribe direct printing of very high aspect ratio pillars: 1 µm diameter ~18 µm height were possible, however adhesion is critical. (Experimental work and image by Ahmed Sharaf)

scans the sample to produce the image in the resist. Sophisticated beam optics and alignment procedures together with high acceleration voltages assure high precision and resolution. The main advantage of ebeam lithography is resolution, which can – using conventional resist – go down to ~4 nm [68]. Thus in cases of structure details well below 10 µm, when laser diffraction begins to limit possibilities of direct laser writing, ebeam lithography starts to become of interest. Apart from the high cost of machinery and maintenance, resist thickness is much more limited, thus it will usually be combined with subsequent (dry) etching steps to produce higher structures. These etching techniques will be described in the following section 4.5.

Two basic designs with high resolution requirements were produced using ebeam lithography: a microfluidic chip for cell capture and electroporation and a micropillar structure that was used for dewetting of micellar nanowires and to observe the wrapping behaviour of oligodendrocytes towards axon-like structures. All structures underwent a dry etching to structure the substrate after ebeam patterning of the resist. The respective decision to use negative or positive resist was made layout-dependent to reduce the writing time: for microfluidic layouts, negative resist offered minimal writing areas, while the micropillar details were much faster written using the positive resist. An overview of both prrocesses is given in Table 4.2.

4.4.1. MICROFLUIDIC CHIP: NEGATIVE RESIST + OPTIONAL HARDMASK

The microfluidic patterns were fabricated on 100 mm silicon wafers, using ebeam lithography of negative resist and dry etching. If structures higher than 18 µm were required, the durability of the resist was not sufficient and a SiO_2 hard mask with higher selectivity towards the following etch step was required. For this the blank silicon wafer was covered with ~500 nm SiO_2 using plasma-enhanced chemical vapor deposition (PECVD) as a first step (see subsection 4.5.1).

With or without hardmask, the surface of the wafer was then primed to enhance resist adhesion by spin-coating with the diphenylsilanediol based AR 300-80 (Allresist GmbH Germany) at 4000 rpm for 1 min and was baked subsequently at 180 °C for 2 min. Spincoating with negative resist AR-N7700.18 (Allresist GmbH Germany) at 4000 rpm for 1 min followed and a soft bake at 85 °C for 60 s. A Leica EBPG 5000+ at 100 kV was used to write the desired pattern on the spin-coated wafer with a dose of $117\,\mu C\,cm^{-1}$. After post-exposure bake at 105 °C for 2 min, the patterns were developed in a bath of MF321 (The Dow Chemical Company) for 2 min, followed by diluted 1:10 v/v MF321/H_2O solution for 30 s and deionized water for 60 s.

Table 4.2: Process details of the ebeam lithography performed for this section

Steps	Fabrication Process	
	Negative Resist	Positive Resist
Preclean	3 min each: isopropanol (IPA), aceton, dH_2O; N_2 blow dry	
Adhesion promoter	AR 300-80, spincoated 4000 rpm, hotplate 2 min 180 °C	
Spincoat resist	AR-N7700.18[10]	AR-P6200.18[11]
	4000 rpm, 60 sec	
Softbake hotplate	85 °C, 2 min	180 °C, 3 min, slow cooldown
E-beam exposure	$117\,\mu C\,cm^{-1}$, 100 kV	$300\,\mu C\,cm^{-1}$, 100 kV
Post exposure bake	105 °C, 2 min	–
Development bath	MF321[12] 2 min, 2x fresh MF321/dH_2O (1:10) 15 sec, H_2O dip & rinse	Pentyl acetate 5 min, MIBK/IPA[13] (1:1) 3 min, IPA 3 min
Hardbake	120 °C 5 min	130 °C 1 min

---

[10] Novolak-based
[11] Poly(α-methyl styrene-co-α-chloroacrylate methylester)
[12] TMAH-based (tetramethylammonium hydroxide)
[13] Methyl isobutyl ketone/isopropanol

4.4.2. MICROPILLAR MOLDS: POSITIVE RESIST

For creation of micropillar molds in silicon, a positive resist was used to minimize writing time of the ebeam. The surface of the wafer was primed to enhance resist adhesion by spin-coating with AR 300-80 (Allresist GmbH Germany) at 4000 rpm for 1 min and was baked subsequently at 180 °C for 2 min. Next, the wafer was spin-coated with positive resist AR-P6200.18 (Allresist GmbH Germany) at 4000 rpm for 1 min and was soft baked at 125 °C for 60 s. The standard processing was modified, as cracks were commonly encountered after development: baking temperature was increased and the cooling down after softbake was done gradually on the hotplate to reduce stress (ca. 10 min to 90 °C).

4.5. SILICON DRY ETCHING

To produce high structures even with limited resist thicknesses, dry etching is a useful tool. Etching processes have come a long way, mainly developing to the needs of microelectronics and MEMS. Where first miniature devices could rely on traditional (chemical) wet etching as a tool for subtractive manufacturing, the fast miniaturization soon required to further abilities, especially concerning directional etching. Wet etching (apart from effects such as crystal plane preference in potassium hydroxide etching of monocrystalline silicon) usually occurs isotropically[14], which might be negligible in certain designs and at larger feature sizes. However, with structures getting smaller, there was a need for etching processes with high anisotropy[15], which certain dry etching processes can offer, together with more process control. [69]

In general, chemical and physical etch processes are used for dry etching separately or in a combination: chemical dry etching, meaning the substrate chemically reacts with the applied plasma activated compound[16], forming volatile reaction products. And physical interaction, where the substrate is evaporated by high momentum collisions of

---

[14]equally into all directions
[15]from Greek ἀν- ἴσος τρόπος literally "un-equally directed", meaning it has a preferred direction
[16]or even without the need for a plasma, e.g. in case of XeF_2 or using the $F_2 + NO \longrightarrow F + FNO$ reaction [70, 71]

the accelerated particles with the substrate. [5, 72]

A relevant example of a pure chemical dry etching (CDE) is plasma activated CF_4 on silicon. Different species are formed, including highly reactive $CF_3 \cdot$ and $F \cdot$ radicals, which react with the silicone forming volatile SiF_4, being pumped out of the reaction chamber and thus etching the sample. This technique is isotropic, which limits its applicability. The selectivity however is very high and many more etchant gases can be used, depending on the process requirements and materials [5, p.124]. Also mixtures of different gases showed good control of selectivity. [69]

Purely physical dry etching usually utilises accelerated ions (e.g. Ar^+) and their momentum when impacting the substrate and ejecting particles of it (also known as sputtering). Etch rates are rather slow and limit the use of this technique and redeposition of the sputtered material can be a problem, but it did gain importance in focused ion beam milling, that allows nanometer-precise removal of material similar to a traditional computer numerical control (CNC) milling machine. Selectivity with physical etching is very low, which can be of advantage depending on the application. [73]

Combining both effects gave rise to reactive ion etching (RIE), where plasma and an electrical field together create both chemically reactive species and particle bombardment, strongly enhancing the etch rate and at the same time offering some anisotropy. The acceleration voltage is usually created through negative self bias charging of the high frequency electrode facing the grounded substrate: the high frequency electrode is coupled through a capacitor, conducting the high frequency but blocking any direct current. Through the large discrepancy in mobility between the heavy positive ions and the light and mobile free electrons, the electrode builds up a high negative bias voltage, which in turn accelerates the heavy ions towards the substrate. The isotropy of the etch process can be varied to some extent by changing the pressure, which influences the mean free path of the particles: With a higher pressure, more collisions occur and more particles deviate from the perpendicular path towards the substrate. [74, 75]

4
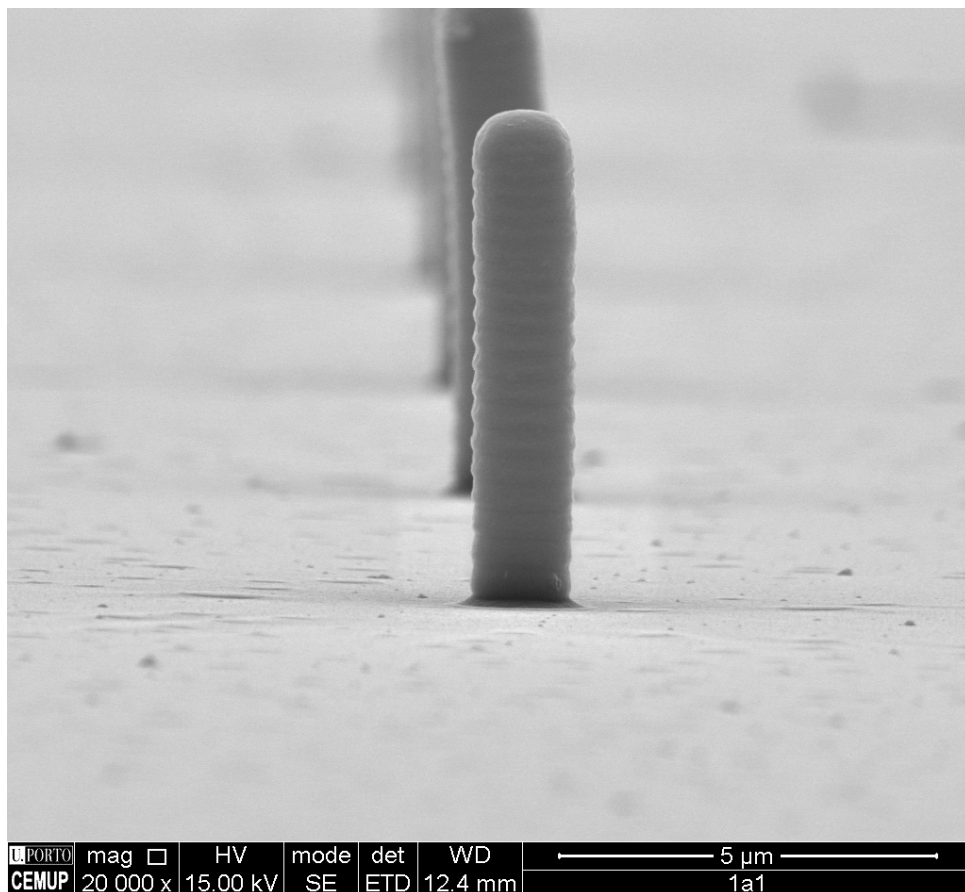
Figure 4.15: High aspect ratio pillar casted with PDMS. The silicon mold was created with ebeam lithography and Bosch process dry etching. Surface roughness of the etch cycles is visible. This effect can be reduced using shorter cycles, if required. (Own work, picture provided by Eva Carvalho, i3S - Institute for Research and Innovation in Health, Porto, Portugal)

Yet again, with higher requirements on the anisotropy also RIE became insufficient at a point. High aspect ratio structures, e.g. deep trenches with vertical sidewalls can not be achieved with anisotropy relying purely on vertically directed ion bombardment, the side walls are still degraded. The solution is a sidewall passivation. This can achieved through cooling of the substrate to extreme temperatures <100 °C. It already enhances selectivity regarding the organic photoresist. Addition of ~10 % O_2 however, creates a deposition of SiO_xF_y, protecting the sidewall from chemical erosion (sputtering is negligible on sidewalls because of the inclination and direction of the ion flux). On the bottom of the trench however, this compound is removed through ion bombardment and the chemical etching continues. The process has excellent anisotropy, and was shown to be capable of creating sub 20 nm structures, however its limit is reached at an aspect ratio of >30. While successfully employed in many research settings, the requirement of cooling with liquid nitrogen has hindered application in industrial processes. [76, 77]

Of industrial importance with very high etch rates and excellent anisotropy is the Bosch process: a time-multiplexed alternating process, where short periods of etching take turns with short periods of creating a passivation layer (Figure 4.15). While the reactive radicals resulting from plasma activated SF_6 again creates volatile SiF_4 molecules etching the substrate, C_4F_8 added during passivation steps decomposes to CF_2 monomers, which deposit and polymerize on the substrate surface. Again, this protective layer is more stable on the sidewalls, while it is immediately removed by the ion bombardment on surfaces perpendicular to the ions trajectory. If carefully balanced, the alternating etching and refreshing of the passivation will yield a vertical sidewall during very deep etch depths. [5, 76]

4.5.1. HARDMASKS

A major limiting factor for etching depth is the mask used: although mask selectivity (etch rate substrate per etch rate mask) can be very high depending on the materials and choice

of etching parameters, some etching of the mask will occur and mask thickness has to be chosen accordingly. With the ebeam resist used in the previous section, etching down to 18 µm was feasible using Bosch process before the mask was destroyed. Using tougher and/or thicker resist, higher values are well possible, but hard masks are the preferred option for deep etching. Common materials are metals (Cr [78], Al [79]), nitrides (Si_3N_4, ScAlN [80]), metal oxides (Al_2O_3 [81–83], Cr_2O_3 [84]) and SiO_2 [85]. In this work a SiO_2 mask was chosen, showing sufficient selectivity against the Si substrate during etching and being easily and quickly available: for hardmask deployment a PECVD process was used on a Plasmalab80Plus machine (Oxford Instruments). With the wafer heated to 300 °C, a combination of SiH_4, N_2O and N_2 (8.5/710/165 SCCM) were showered into the plasma above the wafer for 8 min to yield an expected thickness of 500 nm SiO_2 (Table 4.3). [86]

To pattern the hardmask, a simple fluorine RIE recipe was utilized. Reactive ion etching has a depth limitation through side wall etching (lower anisotropy). Depth of 30 µm have been reported, but for high aspect ratios and perpendicular side walls the

Table 4.3: Dry etching process including optional hardmask deposition and etching. If a hardmask is used, resist can be removed after hardmask etching and before DRIE, to obtain a smoother surface. Printing of the structure is described in previous sections. Compare illustrative overview in Figure 4.2

Steps	Details
Preclean	3 min each: ICP, aceton, dH_2O; N_2 blow dry
PECVD SiO_2 hardmask	SiH_4, N_2O and N_2 (8.5/710/165 SCCM), 300 °C, 8 min
Structure printing	E.g. ebeam lithography, direct laser writing
RIE hardmask etching	CHF_3 and O_2 (50/2.5 SCCM), 350 V bias, 50 W RF power, 0.8 Pa pressure 12 min
Resist removal	O_2 (200 SCCM), 3 min, 1000 W ICP power
Bosch process DRIE Steps repeated for desired depth	Etching 1: SF_6 (200 SCCM), 2.2 s ICP power 1800 W, 6 W LF power
	Etching 2: SF_6 (300 SCCM), 2.6 s, ICP power 1800 W
	Passivation: C_4F_8 (300 SCCM), 2.8 s, 1500 W ICP power
Plasma ashing	Optional for resist residues: O_2 (200 SCCM), 3 min, 1000 W ICP power

mag □	HV	det	mode	WD	———— 50 µm ————
2 000 x	15.00 kV	ETD	SE	15.0 mm	Ma2
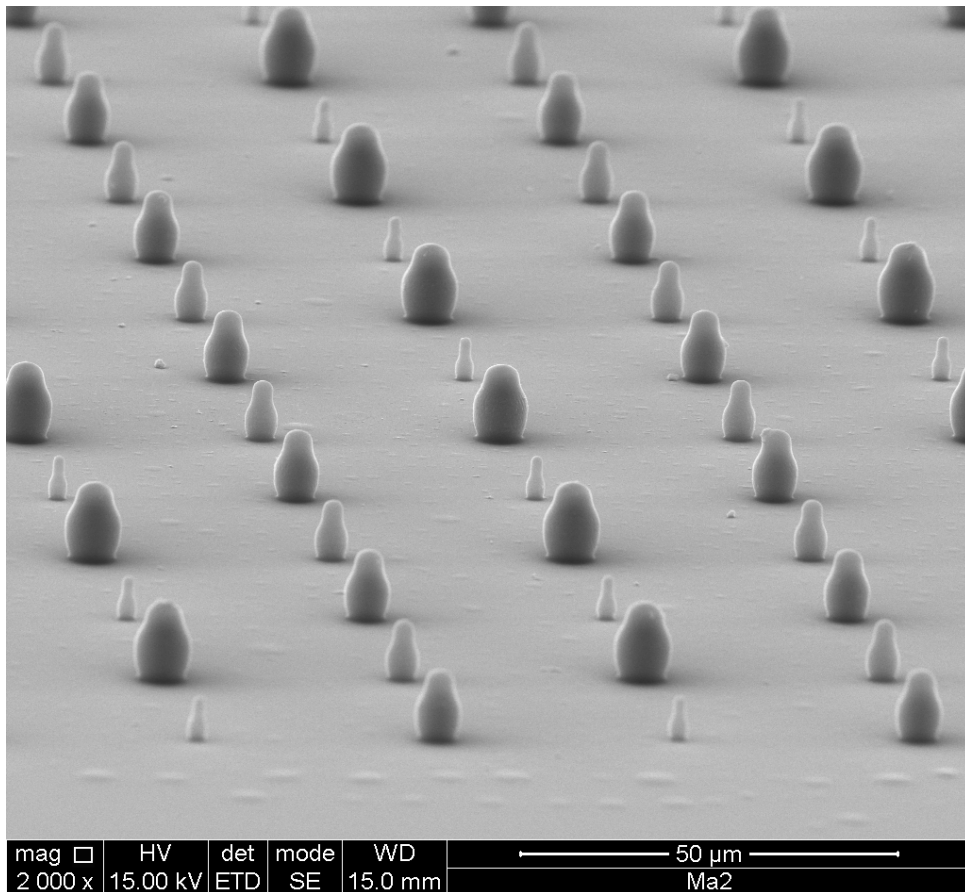
Figure 4.16: Using DRIE, it is possible to create cavities in the etching mold, and thus produce pear shaped pillars. If the undercut is moderate and the cast material sufficiently elastic, concave bodies can be released from the mold. This has applications in the research of wetting behaviours as introduced at the beginning of this chapter. (Own work, picture provided by Eva Carvalho, i3S - Institute for Research and Innovation in Health, Porto, Portugal)

process has to be altered (see DRIE in following section) [87]. However, the anisotropy of the process and the chemical selectivity towards resist and underlying silicon layer are sufficient to transfer the structure to the hardmask and open the patterns in the 500 nm SiO_2 for subsequent etch of the Si substrate. To structure the hardmask with RIE, CHF_3 and O_2 (50/2.5 SCCM) were used with a 350 V bias and 50 W RF power at ca. 0.8 Pa pressure to achieve laser controlled opening of the 500 nm SiO_2 hardmask in ca. 12 min.
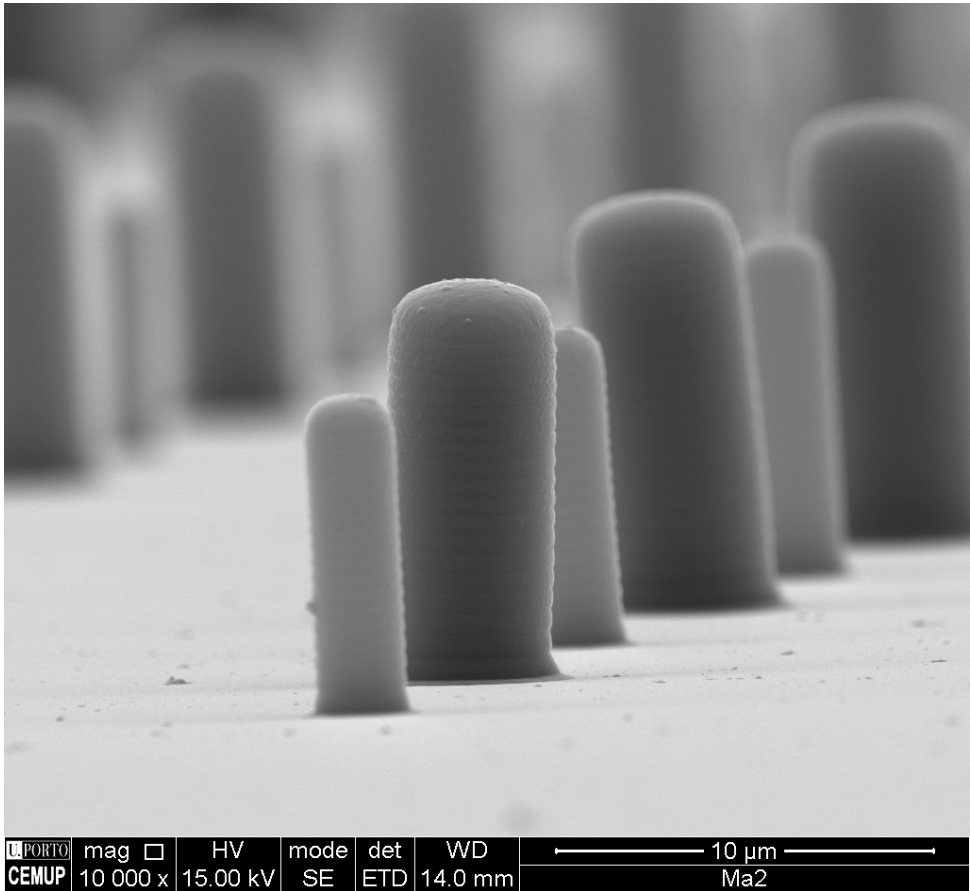
Figure 4.17: PDMS pillars of mixed diameter in detail: the mold was ebeam structured and DRIE etched. Well visible effect of aspect ratio dependent etching resulting in different etch depths/different pillar heights for each diameter. (Own work, picture provided by Eva Carvalho, i3S - Institute for Research and Innovation in Health, Porto, Portugal)

4.5.2. DEEP ETCH/BOSCH PROCESS DRIE

When etching depths of tens of micrometers were required, in combination with perpendicular sidewalls, the Bosch process showed very good results (Figure 4.1). Under certain conditions it would be able to etch through the complete thickness of a 500 µm wafer. There are many parameters influencing the etch result. The main parameters to be varied are step time of etch and passivation, chamber pressure, RF power/bias power and gas flow (SF_6 and C_4F_8). Depending on the aspect ratio, total depth and requirements

concerning side wall roughness, parameters have to be adjusted. Most relevant factor is the balancing of passivation and etch cycle duration, to obtain the desired side wall angle (in most cases vertical, compare Figure 4.15). A higher pressure can increase etch rate and mask selectivity at the expense of etch uniformity. Increase in bias power can reduce mask selectivity and increase sidewall angle (underetch).[88]

Etch rates of this process are very high ($3\,\mu m/min - 5\,\mu m/min$), with only few minutes overhead for loading a sample and reaching vacuum/temperature. The sidewall quality depends on the chosen step size of the etching process. Smaller step sizes will reduce the roughness and extend the process time, which only becomes a factor for very deep etch depths. Figure 4.17 allows to see the side wall roughness resulting from the chosen switching intervals of etch and passivation steps. If smoother sidewalls are required, a higher switching frequency can be set, but lowest sidewall roughness is reached using the cryo-process instead. [89]

Another aspect of this technique is the dependence of etch rate on the aspect ratio, an effect that can be reduced. Figure 4.17 shows this effect, called aspect ratio dependent etching: The smaller diameter pillars are clearly lower in height, showing how the etch rate inside the smaller mold structures is reduced. There are ways to reduce this effect through optimization of the process parameters or a buried etch stop layer, but it remains a common problem of this process [89, 90].

Etching in the presented work was done in cycles using a stepped Bosch process DRIE recipe. Passivation occurred for 2.8 s using C_4F_8 (300 SCCM) at 1500 W ICP power. Etching continued using SF_6 for 2.2 s (200 SCCM) with higher ICP power 1800 W and additional 6 W LF power, followed by the main isotropic etching with SF_6 for 2.6 s (300 SCCM) at ICP power 1800 W. Each cycle etches ~450 nm, although the exact value varies with the aspect ratio and the amount of exposed substrate.

Figure 4.19 shows the results of a high aspect ratio single cell electroporation design, produced using negative resist ebeam lithography and subsequent dry etching and PDMS

| U. PORTO CEMUP | mag □ 2 000 x | HV 5.00 kV | mode SE | det ETD | WD 10.0 mm | ———— 50 µm ———— M |
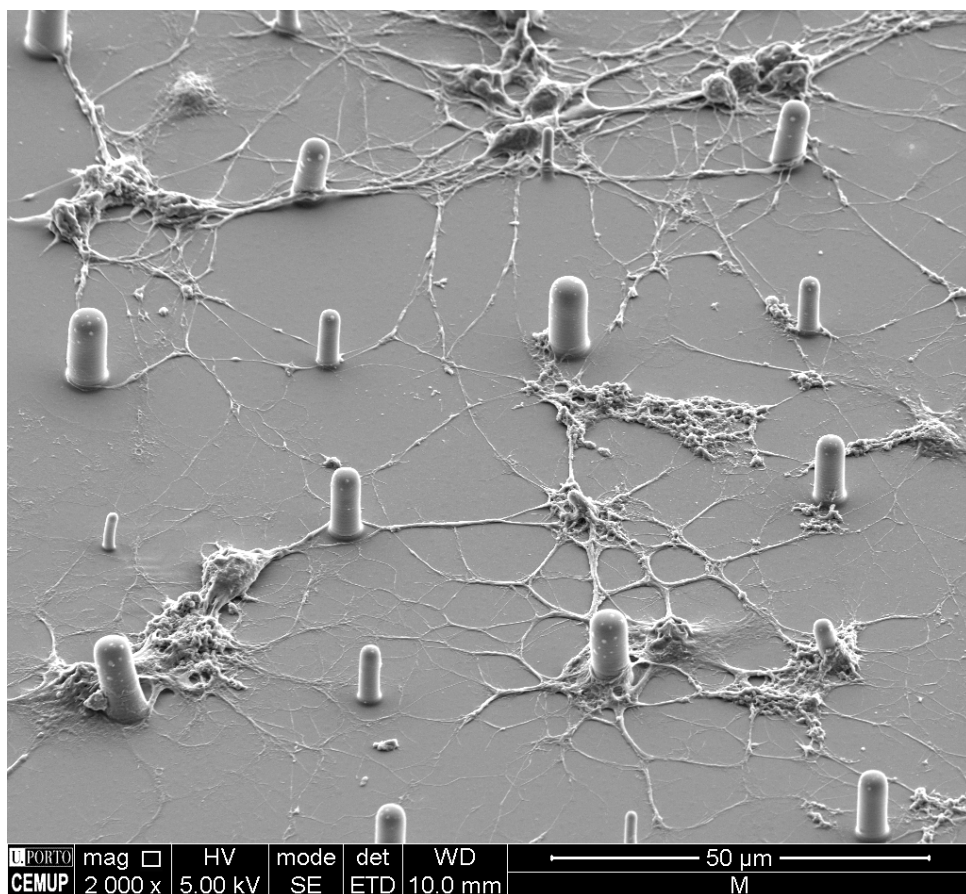
Figure 4.18: Glial cells grown on high aspect ratio pillar structures of mixed diameter. mold was ebeam structured and DRIE etched, then PDMS was cast and served as a mimic of neural structures to be wrapped and myelinated by the oligodendrocytes (Design and fabrication own work, picture and cell experiment done by Eva Carvalho, i3S - Institute for Research and Innovation in Health, Porto, Portugal)

molding. A minimal feature size of 4 µm and a structural height of 35 µm were achieved. This platform has been used to trap individual cells on a chip and electroporate them for precise gene and drug deliver applications.[17] [12]

---

[17]Microfabrication own work
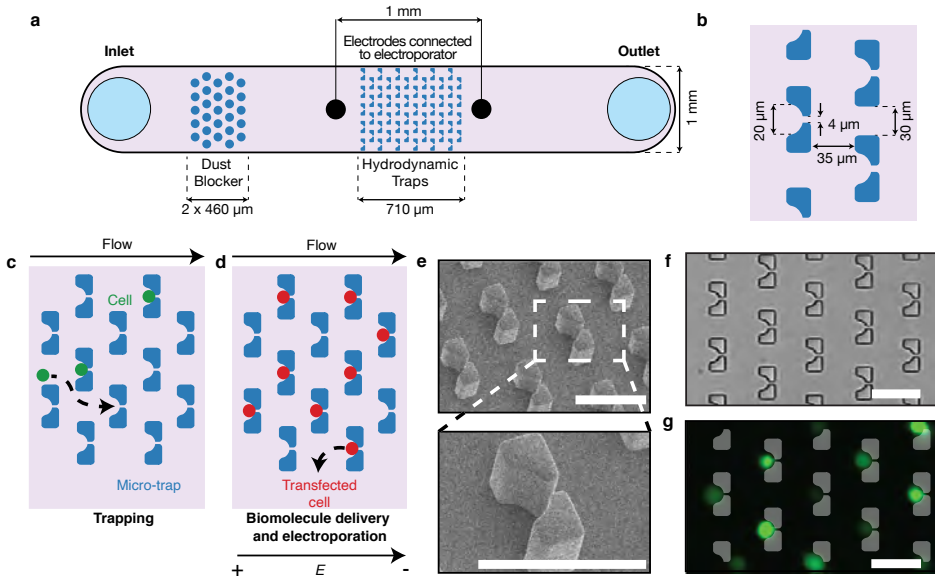
Figure 4.19: a)–d) Schematics of the single cell electroporation device manufactured using the ebeam/dry etching process. e)–g) High aspect ratio and very good resolution were achieved in creation of the microstructured mold and allow quick reproduction of PDMS microfluidic devices using the silicon/SU-8 mastermold. Channel height is 35 μm, scale bar 50 μm. Figures reprinted from collaboration Muralidharan et al. [12] licensed under CC BY-NC-ND 4.0

4.6. CONCLUSION

There are a variety of established processes available for micromanufacturing of microfluidic devices and microtopographies such as micropillar arrays. Aiming only at mold-compatible 2.5D structures, so excluding cavities, there are still many factors to consider when choosing the most advantageous technology, such as resolution, turn around time and material constraints.

For microfluidic applications, large channel heights (>30 μm) in combination with structure details in the micrometer scale will in many cases lead to a preference for the additive lithographic manufacturing as demonstrated here with SU-8 and a direct laser writer. Silicon etching techniques will require tedious hard mask processes or thick resists to achieve large heights. They are also very complex and cost-intensive machines. It is, however, combined with ebeam lithography possible to reach much

higher resolution <500 nm. It can also allow for longer lasting molds also for techniques such as hot embossing, as silicon is much tougher and there are no delaminating issues in a monolithic construction.

2PP is a very versatile process and much more a 3D technique then the previous processes. Sub-micrometer resolution is possible to achieve, but the optimization of writing parameters to the specific structure is laborious. If only a 2.5D moldable structure is desired, 2PP's advantages do rarely come into play. The writing time is naturally immense compared to the other techniques, as structures have to be build up layer by layer although the stacked layers equal in shape. Advantages can lie in using very soft materials such as hydrogels, where – especially in combination with high aspect ratios – molding would destroy smaller features and direct writing is actually a necessity.

Table 4.4: Comparative overview of discussed microfabrication processes with UV mask lithography.

Properties	Fabrication Process				
	Two-Photon Polymerization	Direct Laser Writing	near UV Mask Lithography	Deep/Extreme UV Mask Scanner	Ebeam Writing
Resolution	<1 μm	0.6 μm	1 μm[18]	<20 nm[19]	<10 nm[20]
Max. Height[21]	300 μm		2 mm[22]		<1 μm
Preparation Time	30 min[23]		~2 h		
Machine Time/4" Wafer	>6 h[24]	<1 h	<10 min		<1 h[25]
Required Skill	High	Medium		High	High
Advantages	Real 3D features	Maskless	Parallel printing		Maskless
Disadvantages	Very slow	2.5D	Mask required	Very expensive & mask required	Very expensive

[18] With some exceptions reporting 170 nm using a soft contact mask [91]

[19] Using EUV light (λ=13.5 nm) and a projection scanner with high numerical aperture [92, 93]; a brief outlook beyond EUV for the curious reader [94]

[20] A range where the resolution of classical resists (such as PMMA (poly(methyl methacrylate)), HSQ (hydrogen silsesquioxane)) becomes limiting and lower molecular mass resist is required [95]

[21] Regarding resist thickness; if combined with further processing such as dry etching, height is not limited to this value

[22] Thick resist can impede the maximum resolution.

[23] For printing in resist droplet. If spincoating of specific thickness required ~2 h

[24] Scales with volume of exposed substrate

[25] Important to minimize time consuming stage movements by optimizing the writing patterns

REFERENCES

[1] S. M. Scott and Z. Ali, *Fabrication methods for microfluidic devices: An overview,* Micromachines **12**, 319 (2021).

[2] Y. Song, X. Zhao, Q. Tian, and H. Liang, *Fundamental concepts and physics in microfluidics,* in *Microfluidics: Fundamental, Devices and Applications* (John Wiley & Sons, Ltd, 2018) Chap. 2, pp. 19–111.

[3] R. Osborne, *XXIX. An experimental Investigation of the Circumstances which determine whether the Motion of Water shall be Direct or Sinuous, and of the Law of Resistance in Parallel Channels,* Philosophical Transactions of the Royal Society of London **174**, 935 (1883).

[4] J. H. E. Cartwright, M. Feingold, and O. Piro, *An introduction to chaotic advection,* in *Mixing* (Springer US, 1999) pp. 307–342.

[5] N.-T. Nguyen, *Micromixers fundamentals, design, and fabrication* (Elsevier/William Andrew, 2012) p. 351.

[6] G. R. Wang, F. Yang, and W. Zhao, *There can be turbulence in microfluidics at low reynolds number,* Lab Chip **14**, 1452 (2014).

[7] K. Mahato, A. Srivastava, and P. Chandra, *Paper based diagnostics for personalized health care: Emerging technologies and commercial aspects,* Biosensors and Bioelectronics **96**, 246 (2017).

[8] A. B. Shrirao, Z. Fritz, E. M. Novik, G. M. Yarmush, R. S. Schloss, J. D. Zahn, and M. L. Yarmush, *Microfluidic flow cytometry: The role of microfabrication methodologies, performance and functional specification,* TECHNOLOGY **06**, 1 (2018).

[9] C.-Y. Lee, W.-T. Wang, C.-C. Liu, and L.-M. Fu, *Passive mixers in microfluidic systems: A review,* Chemical Engineering Journal **288**, 146 (2016).

[10] G. S. Jeong, S. Chung, C.-B. Kim, and S.-H. Lee, *Applications of micromixing technology,* The Analyst **135**, 460 (2010).

[11] Q. Liu, A. Muralidharan, A. Saateh, Z. Ding, P. ten Dijke, and P. E. Boukany, *A Programmable Multifunctional 3D Cancer Cell Invasion Micro Platform,* Small **18**, 2270103 (2022).

[12] A. Muralidharan, G. R. Pesch, H. Hubbe, L. Rems, M. Nouri-Goushki, and P. E. Boukany, *Microtrap array on a chip for localized electroporation and electro-gene transfection,* Bioelectrochemistry **147**, 108197 (2022).

[13] S. Halldorsson, E. Lucumi, R. Gómez-Sjöberg, and R. M. Fleming, *Advantages and challenges of microfluidic cell culture in polydimethylsiloxane devices,* Biosensors and Bioelectronics **63**, 218 (2015).

[14] M. I. Mohammed, S. Haswell, and I. Gibson, *Lab-on-a-chip or chip-in-a-lab: Challenges of commercialization lost in translation,* Procedia Technology **20**, 54 (2015).

[15] D. S. Dkhar, R. Kumari, S. J. Malode, N. P. Shetti, and P. Chandra, *Integrated lab-on-a-chip devices: Fabrication methodologies, transduction system for sensing purposes,* Journal of Pharmaceutical and Biomedical Analysis **223**, 115120 (2023).

[16] N. Convery and N. Gadegaard, *30 years of microfluidics,* Micro and Nano Engineering **2**, 76 (2019).

[17] C. Haber, *Microfluidics in commercial applications; an industry perspective,* Lab on a Chip **6**, 1118 (2006).

[18] Y. Temiz, R. D. Lovchik, G. V. Kaigala, and E. Delamarche, *Lab-on-a-chip devices: How to close and plug the lab?* Microelectronic Engineering **132**, 156 (2015).

[19] M. Estévez, E. Martínez, S. J. Yarwood, M. J. Dalby, and J. Samitier, *Adhesion and migration of cells responding to microtopography,* Journal of Biomedical Materials Research Part A **103**, 1659 (2014).

4

[20] D. Hoffman-Kim, J. A. Mitchel, and R. V. Bellamkonda, *Topography, cell response, and nerve regeneration,* Annual Review of Biomedical Engineering **12**, 203 (2010).

[21] J. B. Bergmann, D. Moatsou, U. Steiner, and B. D. Wilts, *Bio-inspired materials to control and minimise insect attachment,* Bioinspiration & Biomimetics **17**, 051001 (2022).

[22] W. Barthlott and C. Neinhuis, *Purity of the sacred lotus, or escape from contamination in biological surfaces,* Planta **202**, 1 (1997).

[23] B. Bhushan, ed., *Encyclopedia of Nanotechnology* (Springer Netherlands, Dordrecht, 2012).

[24] B. Bhushan and M. Nosonovsky, *The rose petal effect and the modes of superhydrophobicity,* Philosophical Transactions of the Royal Society A: Mathematical, Physical and Engineering Sciences **368**, 4713 (2010).

[25] W. Jo, H. S. Kang, J. Choi, J. Jung, J. Hyun, J. Kwon, I. Kim, H. Lee, and H.-T. Kim, *Light-designed shark skin-mimetic surfaces,* Nano Letters **21**, 5500 (2021).

[26] G. D. Bixler and B. Bhushan, *Fluid drag reduction with shark-skin riblet inspired microstructured surfaces,* Advanced Functional Materials **23**, 4507 (2013).

[27] B. Dean and B. Bhushan, *Shark-skin surfaces for fluid-drag reduction in turbulent flow: a review,* Philosophical Transactions of the Royal Society A: Mathematical, Physical and Engineering Sciences **368**, 4775 (2010).

[28] G. V. Lauder, D. K. Wainwright, A. G. Domel, J. C. Weaver, L. Wen, and K. Bertoldi, *Structure, biomimetics, and fluid dynamics of fish skin surfaces,* Physical Review Fluids **1**, 060502 (2016).

[29] S. N. Patek, *Biomimetics and evolution,* Science **345**, 1448 (2014).

[30] H. Chen, P. Zhang, L. Zhang, H. Liu, Y. Jiang, D. Zhang, Z. Han, and L. Jiang, *Continuous directional water transport on the peristome surface of Nepenthes alata,* Nature **532**, 85 (2016).

[31] R. B. MacKinnon, J. Oomen, and M. P. Zari, *Promises and presuppositions of biomimicry,* Biomimetics **5**, 33 (2020).

[32] O. Speck, D. Speck, R. Horn, J. Gantner, and K. P. Sedlbauer, *Biomimetic bio-inspired biomorph sustainable? An attempt to classify and clarify biology-derived technical developments,* Bioinspiration & Biomimetics **12**, 011004 (2017).

[33] W. Barthlott, M. Mail, and C. Neinhuis, *Superhydrophobic hierarchically structured surfaces in biology: evolution, structural principles and biomimetic applications,* Philosophical Transactions of the Royal Society A: Mathematical, Physical and Engineering Sciences **374**, 20160191 (2016).

[34] L. Rayleigh, *On the theory of optical images, with special reference to the microscope,* Journal of the Royal Microscopical Society **23**, 474 (1903).

[35] Rayleigh, *XXXI. Investigations in Optics, with special Reference to the Spectroscope,* The London, Edinburgh, and Dublin Philosophical Magazine and Journal of Science **8**, 261 (1879).

[36] E. Abbe, *Beiträge zur Theorie des Mikroskops und der mikroskopischen Wahrnehmung,* Archiv für Mikroskopische Anatomie **9**, 413 (1873).

[37] C. M. Sparrow, *On spectroscopic resolving power,* The Astrophysical Journal **44**, 76 (1916).

[38] Y. Jing, C. Zhang, B. Yu, D. Lin, and J. Qu, *Super-resolution microscopy: Shedding new light on in vivo imaging,* Frontiers in Chemistry **9** (2021).

4

[39] S. Pujals, N. Feiner-Gracia, P. Delcanale, I. Voets, and L. Albertazzi, *Super-resolution microscopy as a powerful tool to study complex synthetic materials,* Nature Reviews Chemistry **3**, 68 (2019).

[40] K. Prakash, B. Diederich, R. Heintzmann, and L. Schermelleh, *Super-resolution microscopy: a brief history and new avenues,* Philosophical Transactions of the Royal Society A: Mathematical, Physical and Engineering Sciences **380** (2022).

[41] D. Halliday, R. Resnick, and J. Walker, *Physik* (Wiley-VCH, 2007) p. 942.

[42] N. Erdman, D. C. Bell, and R. Reichelt, *Scanning electron microscopy,* in *Springer Handbook of Microscopy*, edited by P. W. Hawkes and J. C. H. Spence (Springer International Publishing, Cham, 2019) pp. 229–318.

[43] P. Lehmann, S. Tereschenko, and W. Xie, *Fundamental aspects of resolution and precision in vertical scanning white-light interferometry,* Surface Topography: Metrology and Properties **4**, 024004 (2016).

[44] M. L. Hair and W. Hertl, *Reactions of chlorosilanes with silica surfaces,* The Journal of Physical Chemistry **73**, 2372 (1969).

[45] S. Onclin, B. J. Ravoo, and D. N. Reinhoudt, *Gestaltung der Siliciumoxidoberfläche durch selbstorganisierte Monoschichten,* Angewandte Chemie **117**, 6438 (2005).

[46] A. Ansari, R. Trehan, C. Watson, and S. Senyo, *Increasing silicone mold longevity: a review of surface modification techniques for PDMS-PDMS double casting,* Soft Materials **19**, 388 (2020).

[47] A. Shakeri, S. Khan, and T. F. Didar, *Conventional and emerging strategies for the fabrication and functionalization of PDMS-based microfluidic devices,* Lab on a Chip **21**, 3053 (2021).

[48] F. Hua, Y. Sun, A. Gaur, M. A. Meitl, L. Bilhaut, L. Rotkina, J. Wang, P. Geil, M. Shim, J. A. Rogers, and A. Shim, *Polymer imprint lithography with molecular-scale resolution,* Nano Letters **4**, 2467 (2004).

[49] A. Piruska, I. Nikcevic, S. H. Lee, C. Ahn, W. R. Heineman, P. A. Limbach, and C. J. Seliskar, *The autofluorescence of plastic materials and chips measured under laser irradiation,* Lab on a Chip **5**, 1348 (2005).

[50] M. A. Eddings, M. A. Johnson, and B. K. Gale, *Determining the optimal PDMS–PDMS bonding technique for microfluidic devices,* Journal of Micromechanics and Microengineering **18**, 067001 (2008).

[51] A. del Campo and C. Greiner, *SU-8: a photoresist for high-aspect-ratio and 3d submicron lithography,* Journal of Micromechanics and Microengineering **17**, R81 (2007).

[52] N. Bhattacharjee, A. Urrios, S. Kang, and A. Folch, *The upcoming 3d-printing revolution in microfluidics,* Lab on a Chip **16**, 1720 (2016).

[53] Y. Ehlert, *Toward Developing an Insulator-based Dielectrophoretic Device for Continuous Sorting of Mitochondria*, mathesis, Universität Bremen (2022).

[54] Q. Liu, M. Zhao, S. Mytnyk, B. Klemm, K. Zhang, Y. Wang, D. Yan, E. Mendes, and J. H. van Esch, *Self-orienting hydrogel micro-buckets as novel cell carriers,* Angewandte Chemie International Edition **58**, 547 (2018).

[55] C. S. Chen and H. A. Pohl, *Biological dielectrophoresis: the behavior of lone cells in a nonuniform electric field,* Annals of the New York Academy of Sciences **238**, 176 (1974).

[56] R. Pethig, *Review article—dielectrophoresis: Status of the theory, technology, and applications,* Biomicrofluidics **4**, 022811 (2010).

4

[57] P.-Y. Weng, I.-A. Chen, C.-K. Yeh, P.-Y. Chen, and J.-Y. Juang, *Size-dependent dielectrophoretic crossover frequency of spherical particles,* Biomicrofluidics **10**, 011909 (2016).

[58] A. Sharaf, *Synthesis of soft polymeric pillars for simulation of neuronal axons,* Masters thesis, TU Delft (2019).

[59] W. Denk, J. H. Strickler, and W. W. Webb, *Two-photon laser scanning fluorescence microscopy,* Science **248**, 73 (1990).

[60] S. M. Kuebler, B. H. Cumpston, S. Ananthavel, S. Barlow, J. E. Ehrlich, L. L. Erskine, A. A. Heikal, D. McCord-Maughon, J. Qin, H. Roeckel, M. C. Rumi, S. R. Marder, and J. W. Perry, *Three-dimensional microfabrication using two-photon-activated chemistry,* in *Micro- and Nano-photonic Materials and Devices,* Vol. 3937, edited by J. W. Perry and A. Scherer, International Society for Optics and Photonics (SPIE, 2000) pp. 97 – 105.

[61] H.-B. Sun and S. Kawata, *Two-photon photopolymerization and 3D lithographic microfabrication,* in *NMR 3D Analysis Photopolymerization* (Springer Berlin Heidelberg, 2006) pp. 169–273.

[62] S. You, J. Li, W. Zhu, C. Yu, D. Mei, and S. Chen, *Nanoscale 3D printing of hydrogels for cellular tissue engineering,* Journal of Materials Chemistry B **6**, 2187 (2018).

[63] W. H. Teh, U. Dürig, U. Drechsler, C. G. Smith, and H.-J. Güntherodt, *Effect of low numerical-aperture femtosecond two-photon absorption on SU-8 resist for ultrahigh-aspect-ratio microstereolithography,* Journal of Applied Physics **97**, 054907 (2005), https://doi.org/10.1063/1.1856214 .

[64] W. R. Zipfel, R. M. Williams, and W. W. Webb, *Nonlinear magic: multiphoton microscopy in the biosciences,* Nature Biotechnology **21**, 1369 (2003).

[65] K. D. H. Dorkenoo, E. Sungur, H. Bulou, G. Taupier, and A. Boegli, *Monitoring the contractile properties of optically patterned liquid crystal based elastomers,* in *Advanced Elastomers - Technology, Properties and Applications* (InTech, 2012).

[66] A.-I. Bunea, N. del Castillo Iniesta, A. Droumpali, A. E. Wetzel, E. Engay, and R. Taboryski, *Micro 3D printing by two-photon polymerization: Configurations and parameters for the nanoscribe system,* Micro **1**, 164 (2021).

[67] S. D'Silva, T. Mülders, H.-J. Stock, and A. Erdmann, *Modeling the impact of shrinkage effects on photoresist development,* Journal of Micro/Nanopatterning, Materials, and Metrology **20** (2021).

[68] V. R. Manfrinato, L. Zhang, D. Su, H. Duan, R. G. Hobbs, E. A. Stach, and K. K. Berggren, *Resolution limits of electron-beam lithography toward the atomic scale,* Nano Letters **13**, 1555 (2013).

[69] V. M. Donnelly and A. Kornblit, *Plasma etching: Yesterday, today, and tomorrow,* Journal of Vacuum Science & Technology A: Vacuum, Surfaces, and Films **31**, 050825 (2013).

[70] T. Hayashi, *Recent development of si chemical dry etching technologies,* Journal of Nanomedicine & Nanotechnology **04** (2013).

[71] S. Tajima, T. Hayashi, K. Ishikawa, M. Sekine, and M. Hori, *Room-temperature si etching in NO/F_2 gases and the investigation of surface reaction mechanisms,* The Journal of Physical Chemistry C **117**, 5118 (2013).

[72] M. Blauw, *Deep anisotropic dry etching of silicon microstructures by high-density plasmas,* Ph.D. thesis, Delft University of Technology (2004).

[73] C. D. W. Wilkinson and M. Rahman, *Dry etching and sputtering,* Philosophical Transactions of the Royal Society of London. Series A: Mathematical, Physical and Engineering Sciences **362**, 125 (2003).

4

[74] M. J. Kushner, *Monte-carlo simulation of electron properties in RF parallel plate capacitively coupled discharges,* Journal of Applied Physics **54**, 4958 (1983).

[75] K. Nojiri, *Dry Etching Technology for Semiconductors* (Springer International Publishing, 2015).

[76] B. Wu, A. Kumar, and S. Pamarthy, *High aspect ratio silicon etch: A review,* Journal of Applied Physics **108**, 051101 (2010).

[77] R. Dussart, T. Tillocher, P. Lefaucheux, and M. Boufnichel, *Plasma cryogenic etching of silicon: from the early days to today's advanced technologies,* Journal of Physics D: Applied Physics **47**, 123001 (2014).

[78] L. A. Woldering, R. W. Tjerkstra, H. V. Jansen, I. D. Setija, and W. L. Vos, *Periodic arrays of deep nanopores made in silicon with reactive ion etching and deep UV lithography,* Nanotechnology **19**, 145304 (2008).

[79] A. Bagolini, P. Scauso, S. Sanguinetti, and P. Bellutti, *Silicon deep reactive ion etching with aluminum hard mask,* Materials Research Express **6**, 085913 (2019).

[80] M. D. Henry, T. R. Young, and B. Griffin, *ScAlN etch mask for highly selective silicon etching,* Journal of Vacuum Science & Technology B, Nanotechnology and Microelectronics: Materials, Processing, Measurement, and Phenomena **35**, 052001 (2017).

[81] M. Drost, S. Marschmeyer, M. Fraschke, O. Fursenko, F. Bärwolf, I. Costina, M. K. Mahadevaiah, and M. Lisker, *Etch mechanism of an Al_2O_3 hard mask in the bosch process,* Micro and Nano Engineering **14**, 100102 (2022).

[82] M. D. Henry, S. Walavalkar, A. Homyk, and A. Scherer, *Alumina etch masks for fabrication of high-aspect-ratio silicon micropillars and nanopillars,* Nanotechnology **20**, 255305 (2009).

[83] J. Dekker, K. Kolari, and R. L. Puurunen, *Inductively coupled plasma etching of amorphous Al$_2$O$_3$ and TiO$_2$ mask layers grown by atomic layer deposition,* Journal of Vacuum Science & Technology B: Microelectronics and Nanometer Structures **24**, 2350 (2006).

[84] F. Aydinoglu, F. Saffih, R. K. Dey, and B. Cui, *Chromium oxide as a hard mask material better than metallic chromium,* Journal of Vacuum Science & Technology B **35**, 06GB01 (2017), https://doi.org/10.1116/1.4998480 .

[85] S. Choi and S. Hong, *Use of hard mask for finer (<10 µm) through silicon vias (TSVs) etching,* Transactions on Electrical and Electronic Materials **16**, 312 (2015).

[86] X. Liu, J. Ge, Y. Yang, Y. Song, and T. Ren, *Feature scale simulation of PECVD of SiO$_2$ in SiH$_4$/NO$_2$ mixture,* Plasma Science and Technology **16**, 385 (2014).

[87] R. D. Mansano, P. Verdonck, and H. S. Maciel, *Anisotropic reactive ion etching in silicon, using a graphite electrode,* Sensors and Actuators A: Physical **65**, 180 (1998).

[88] L. Meng and J. Yan, *Effect of process parameters on sidewall damage in deep silicon etch,* Journal of Micromechanics and Microengineering **25**, 035024 (2015).

[89] M. J. Walker, *Comparison of Bosch and cryogenic processes for patterning high-aspect-ratio features in silicon,* in *MEMS Design, Fabrication, Characterization, and Packaging,* Vol. 4407, edited by U. F. W. Behringer and D. G. Uttamchandani, International Society for Optics and Photonics (SPIE, 2001) pp. 89 – 99.

[90] S. L. Lai, D. Johnson, and R. Westerman, *Aspect ratio dependent etching lag reduction in deep silicon etch processes,* Journal of Vacuum Science & Technology A: Vacuum, Surfaces, and Films **24**, 1283 (2006).

[91] C.-Y. Wu, H. Hsieh, and Y.-C. Lee, *Contact photolithography at sub-micrometer scale using a soft photomask,* Micromachines **10**, 547 (2019).

4

[92] R. Capelli, G. Kersteen, S. Krannich, M. Koch, L. Fischer, M. Roesch, and K. Gwosch, *AIMS EUV evolution towards high NA: challenge definition and solutions implementation,* in *Optical and EUV Nanolithography XXXV*, edited by A. Lio and M. Burkhardt (SPIE, 2022).

[93] N. Fu, , Y. Liu, X. Ma, and Z. Chen, *EUV lithography: State-of-the-art review,* Journal of Microelectronic Manufacturing **2**, 1 (2019).

[94] N. Mojarad, J. Gobrecht, and Y. Ekinci, *Beyond EUV lithography: a comparative study of efficient photoresists' performance,* Scientific Reports **5** (2015).

[95] M. S. M. Saifullah, M. Asbahi, D. C. J. Neo, Z. Mahfoud, H. R. Tan, S. T. Ha, N. Dwivedi, T. Dutta, S. bin Dolmanan, Z. Aabdin, M. Bosman, R. Ganesan, S. Tripathy, D. G. Hasko, and S. Valiyaveettil, *Patterning at the resolution limit of commercial electron beam lithography,* Nano Letters **22**, 7432 (2022).

4

5

CONCLUSION

This section concludes the findings of this thesis.

How does a self-assembled micellar nanowire platform compare to state-of-the-art polymeric nanowires?

Self-assembled micellar systems were identified as a versatile system for easy combination of different functionalities in a non-cleanroom environment. The ability to combine components of different functionalities before assembling and growth of the nanowire greatly eases the production of modified wires. Combination with dewetting techniques creates new opportunities in functional nanowire arrays. Minimal cleanroom and device usage during the process provides broader accessibility and more user-friendliness.

CHAPTER 2:

How can micellar nanowires be integrated in biological assays?

To integrate polymeric nanowires to a biological device, it is required to design the nanowire in a way that it provides at least two separate chemical functions. Both, fixation to a substrate and functional linker groups for biomolecules were integrated into bifunctional polymeric nanowires. PS-b-PEO polymer with both methacrylate and azide modifications as endgroups were synthesized and successfully assembled as nanowires. After assembly, both linker groups were active and functional. Click chemistry, as a versatile and reliable linker, does not interfere much with micelle growth and enables subsequent modification. The azide modification was characterized through NMR, FT-IR and the attachment of click chemistry compounds containing fluorophors.

Is this system compatible with common biochemical linkers?

Azide click chemistry is an established and reliable linker, compatible with a lot of commercially available biomolecules. It was successfully integrated into the nanowires and capture functionality was shown using fluorophores and microbeads. The printed nanowire arrays were additionally retrofitted with biotin using a DBCO-biotin compound: in this way, the streptavidin-biotin system – a second large group of well-established biolinkers – can also be utilized and interference of this larger molecule with self-assembly is avoided.

Can proteins be captured on this nanowire array?

Streptavidin was found to reliably bond to the biotin modified nanowires.

CHAPTER 3:

Is the array able to capture viral particles?

Bacteriophages were used as model viruses and successfully captured on the nanowires. No unspecific binding was observed on nanowires which do not contain the linker moiety.

Are their size limits to the capture of particles and cells?

Microbeads of 2.1 µm diameter were captured using the biotin-streptavidin system. To model cell capture, GUVs of mixed sizes up to ~50 µm were used. The results indicate bonding, but the connection appeared very fragile.

CHAPTER 4:

How do common microfabrication tools compare in perspective of micro-topography and microfluidic manufacturing?

A selection of microstructure platforms to handle biological samples were produced and different processes compared to each other. Choice of the best suitable production process depends on many different factors including availability of machinery, affordability, resolution requirements and time/user efforts. Based on our overview, the proper technique can be selected for a large majority of desired structures. In many cases, direct laser writing in combination with SU8 for large structural heights (>30 µm) and high aspect ratios will be the best choice. If a resolution below 5 µm is required, ebeam lithography starts to become of interest.

ACKNOWLEDGEMENTS

And once again curiosity took the lead, and to what a beautiful experience it led. Deeper understanding on so many levels and innovation. And so many people were part of this journey, supported and inspired me. With gratitude I look back on this part of the eternal journey and the people I met on the way. I especially thank my promotors Eduardo, Pouyan, Urs and Luigi, who created this wonderful project and supported me through it all. Each of you provided his unique expertise, experience, creativity and knowledge. And even more important, you care for the persons around you, you see the being and not just the function. Thank you.

I am also very grateful to all other members of our staff in ASM, PPE, Kavli nanolab and all around TU. You keep things running, you patiently educate, help, maintain, tinker with us. You provide the foundation for a never-ending stream of venturers, with all their new ideas, individual plans and needs, both technological and administrative. Thank you for all your support and the good time we shared: Jan, Rienk, Stephen, Wolter, Laura, Marcel, Veby, Els, Stephen, Duco, Kristen, Marcel, Sietse, Aleksandra, Anja, Hozanna, Erika, Charles, Arnold, Marc, Eugene, Marco and Ewan.

This project would have never happened if not for the people at Delft Global Initiative. You have managed to create an environment for true interdisciplinary and intercultural understanding. It was to me where the complexity of theoretical high tech met the complexity of a practical reality. I have learnt a great deal during our activities, and oh yes, it was also lots of fun. My gratitude to Claire, Roel, Sophie, Rezi, Lys-Anne, Jennifer, Annelies, Sophie and JC.

A major part of this journey are my fellow PhDs and postdocs in ASM and PPE. What a beautiful group of individuals, so many different backgrounds, so many stories to tell. I feel very happy to have spent this time together with you. Thank you all for the open-hearted togetherness, all the good time and support our groups shared: Benni mein chemisches Expertengremium, Gourmetkoch, Connaisseur, Coiffeur und bester Mitbewohner den man sich wünschen kann (beMidemswük), toll dass du den Weg in mein Büro gefunden hast. Und dass du uns deine liebste Nastia vorgestellt hast. Machma Beat. Elmira I miss our spontaneous philosophical sessions and excursions into the delicious Persian cuisine. Ardeshir it is always great joy talking to you, let us have another board game evening, I offer you a revanche in Siedler of Catan. Sebastién c'était un beau moment à Delft, et un mariage que je n'oublierai jamais, j'espère qu'on se reverra bientôt. Sarah and Reece, thank you for the great time together, your intuition in questions of English language details, great board games, coffee tastings and tips on polymer characterisation. Peggy, Stilikone und Heiterkeit in Person, danke für viel gemeinsames Lachen, die besten Geburtstagsparties, aber auch deine fachliche Expertise. Georgy, we had so many valuable discussions and you gave me great tips on polymer work-up, thank you. I attribute this statement to you: "A bad solvent can excel as a great non-solvent.". Aswin, thank you for the pleasant coffee pauses and for the great collaboration on the GUVs. Eva, it was a short visit in Delft for you, but we have been working together throughout this whole project, I enjoyed it a lot and still do. Hope to see you in Portugal one day. Georg, du fehlst hier, lass bald ma schnacken, vorzugsweise in einem Pub in deiner neuen Heimat! Suellen, Tobias, Irene, Benjamin, Sarah, Reece, Peggy, Anand, Alexandra, Susan, Tamar, Michelle, Cansel, Mark and Sahil: It was a fabulous time with you, in and outside of the lab. TU festivals, BBQ, after-lab-clean pizzas, Koningsnacht, artistic performances on bike racks, debating about the abundance of cream in carbonara, ice maker put to proper use, you name it! Mahdiyeh, Margherita, Pranav, Zaid, Ruben and Albert, what fun I had with you. There is always a good mood around you people. And Pranav, your dinner parties

are legendary. Yiming, Qian, Kai, Bowen, Ju, Guotai, Juncheng, Bohang, Jianan and Fan: what a great pleasure to spend time with you, thank you for all the joy, your most patient tries to teach me the correct pronunciation of Chinese words and the nice dinners, drinks and badminton sessions we had together. Angie, Matija, Jos, Emma, Giorgio, Tomasz, Fanny, Serhii, Audrey (because of you, I now prefer chocolatine over agony of chocolate): Survival run (and subsequent hot tub), beach volleyball, board game nights (sometimes also just manual reading nights), it was always lovely to do activities together. And thank you again to everybody in ASM and PPE for the cooperativeness inside the lab. On daily occasions people in our groups helped each other and everybody thrived from it.

You challenge your knowledge when you teach, and then you really learn. Thanks to my students Ahmed, Vinda, Gopal, Esmee, Shari and Niels for teaching me, and for the great time working together. Especially Ahmed, you have become a friend.

I am glad to say I love my family. Let this occasion be another nice feast for us, in a row of many more to come. My dear parents: Thank you for everything. Simply nothing of this would have happened, if not for your loving support. Liebe Geschwister, ich bin glücklich, was für ein tolles Team wir sind. Kyra, Marja en Kyrill, jullie zijn als familie voor mij geworden, mijn Nederlandse familie. Bedankt dat jullie me zo open hebben ontvangen, jullie zijn een belangrijk deel van mijn leven geworden. Zu guter Letzt mein besonderer Dank an meine Liebe Laura. Was für ein herrliches Abenteuer wir zusammen erleben, danke für deine Geduld, die viele Freude und dein offenes Herz.

All my dear friends not explicitly named: let us rather share a nice meal very soon instead of spending more time on this piece of paper. You are in my heart.

LIST OF FIGURES

LIST OF TABLES

CURRICULUM VITÆ

Hendrik Marc Konstantin HUBBE

1987   Born in Konstanz, Germany

2008–2012   B.Sc. Microsystems Engineering, University of Freiburg

Lab-on-chip for preconcentration, electrolysis and RNA ectraction of

cells. Laboratory for Sensors, Prof. Dr. G. Urban

since 2010   Lecturer for chemistry and physics, Academy of Medical Professions,

University Hospital Freiburg

2011–2012   Patent Engineer, Intellectual Property Law, University of Hagen

2012–2016   M.Sc. Microsystems Engineering, University of Freiburg

Focus on lab-on-chip, biomedical engineering and nanotechnology

Master thesis: Characterisation and integration of a lab-on-chip into a

handheld device for point-of-care diagnostics. Laboratory for Sensors,

Prof. Dr. G. Urban

2015–2017   B.Sc. Biology, University of Freiburg

Focus on cell biology, biomimetics and molecular plant physiology

Bachelor thesis: Capillary effects and wetting behaviour of biomimetic

polymer surfaces. Laboratory for Botany: Functional morphology and

bionics, Plant Biomechanics Group, Prof. Dr. T. Speck

2017-2021   PhD Candidate Chemical Engineering, TU Delft

Thesis: The role of micellar nanowires in diagnosing tropical diseases.

Advanced Soft Matter Group, Promotors: Dr. habil. E. Mendes,

Dr. P. E. Boukany, Prof. Dr. U. Staufer

LIST OF PUBLICATIONS

H. Hubbe, E. Mendes, and P.E. Boukany, *Polymeric nanowires for diagnostic applications*, Micromachines **10** (2019).

Aswin Muralidharan, Georg R. Pesch, Hendrik Hubbe, Lea Rems, Mahdiyeh Nouri-Goushki, Pouyan E. Boukany, *Microtrap array on a chip for localized electroporation and electro-gene transfection*, Bioelectrochemistry **147** (2022).

H. Hubbe, E. Mendes, P.E. Boukany, *Bifunctional micellar nanowires for biological assays,* in preparation

Eva D. Carvalho, Miguel R. G. Morais, Helena P. Ferreira, Hendrik Hubbe, Georgia Athanasopoulou, Rui Rocha, Maurizio Mattarelli, Silvia Caponi, Beatriz Custódio, Eduardo Mendes, Sofia C. Guimarães, Ana P. Pêgo, *Myelination in a dish: A micropillar array to study the mechanobiology of oligodendrocyte differentiation and myelination,* in preparation